

University of Alberta

Applications of Titanosilicate Molecular Sieve in Gas Separation

by

Meng Shi

A thesis submitted to the Faculty of Graduate Studies and Research
in partial fulfillment of the requirements for the degree of

Doctor of Philosophy

in

Chemical Engineering

Department of Chemical and Materials Engineering

©Meng Shi

Spring 2013

Edmonton, Alberta

Permission is hereby granted to the University of Alberta Libraries to reproduce single copies of this thesis and to lend or sell such copies for private, scholarly or scientific research purposes only. Where the thesis is converted to, or otherwise made available in digital form, the University of Alberta will advise potential users of the thesis of these terms.

The author reserves all other publication and other rights in association with the copyright in the thesis and, except as herein before provided, neither the thesis nor any substantial portion thereof may be printed or otherwise reproduced in any material form whatsoever without the author's prior written permission.

Abstract

Adsorption behavior of nitrogen, argon and oxygen on silver exchanged titanasilicate (Ag-ETS-10) were studied in this work. A low temperature gas chromatographic determination of relatively low concentration argon (<1%) was developed, which was applied to evaluate the production of argon free oxygen by adsorptive air separation on Ag-ETS-10. A lab-scale demonstration shows that Ag-ETS-10 is promising as an adsorbent capable of producing high purity oxygen.

A mathematic model base on mass balance proves Ag-ETS-10 bed with enhanced density possesses higher recovery yield of oxygen during adsorptive air separation. Several techniques to enhance the bed density of Ag-ETS-10 were investigated. A lab-scale demonstration was carried to verify the prediction of this correlation.

Adsorption behaviors of different hydrocarbons (methane, ethane, ethylene) on ETS-10 at high pressure were studied. Separation of binary mixture (ethylene/ethane, methane/ethane) at high pressure was investigated on ETS-10 through lab-scale demonstration. The bed selectivity was obtained from the demonstration and verified through ideal adsorbed solution theory model.

As an alternative, microwave desorption provided a faster heating rate and desorption rate, higher desorption and gas recovery and lower energy consumption compared to conductive heating. Desorption of ethylene/ethane and carbon dioxide/methane mixtures was performed by microwave heating on Na-ETS-10 were investigated.

Acknowledgement

As an International student, pursuing my Ph.D. degree in Canada, I am fortunate enough to know Prof. Steven Kuznicki, who is my supervisor and mentor. Firstly I like to express my sincere gratitude to him for his guidance, support and patience in my research in the past five and half years. Especially, I appreciate his care, help and understanding to me when I faced any difficulty in the everyday life. He has driven me to achieve my highest potential and without him none of this would have been possible.

I am also grateful to every member of my dissertation committee, Prof. Qingxia Liu, Prof. Hongbo Zeng, Prof. Zahar Hashisho, and Prof. Douglas M. Ruthven, for their valuable time, fair criticism, and helpful comments.

Special thanks to Dr. Tanya Kuznicki, Albana Zeko, and Dr. Amy Dambrowitz. Firstly, for their assistance with technical writing and manuscript development. Secondly, for their kindness of talking with me when I faced any challenge in the school.

Special thanks to Dr. James Sawada, Dr. Adolfo Avila, for their timely help and support in my research projects and thesis preparation. I sincerely thank Weizhu An, Lan Wu, Tong Qiu, Brenda Brindza and every member of our research group, for their countless assistance in every aspect during my graduate program. Without their help, I cannot smoothly graduate.

Finally, I am deeply indebted to my parents and my sister, for their love, support and encouragement during my life. Most importantly, send my gratitude to my wife Clover Mianzhen Che, for her love, understanding and patience throughout the time that she is waiting for me in China.

Table of Contents

Chapter 1. Introduction	1
1.1 Overview	2
1.2 Thesis Outline	4
1.3 Reference	10
Chapter 2. Fundamentals of Adsorption Separation	15
2.1 Titanosilicate Molecular Sieve Zeolite	16
2.1.1 Traditional zeolites	16
2.1.2 Titanosilicate ETS-10	16
2.1.3 Applications of titanosilicate ETS-10	18
2.2 Adsorption Theory	19
2.2.1 Introduction	19
2.2.2 Physical adsorption forces	20
2.2.3 Equilibrium adsorption of single gas	23
2.2.4 Equilibrium adsorption of gas mixture	30
2.2.5 Henry's Law and selectivity	32
2.2.6 Heat of adsorption	35
2.2.7 Separation mechanism	36
2.3 Adsorption Characterization	38
2.3.1 Inverse phase gas chromatography	38
2.3.2 Volumetric isotherm measurement	40
2.4 Swing Adsorption	42
2.5 Microwave Assisted Regeneration	46
2.6 References	49
Chapter 3. Production of Argon Free Oxygen by Adsorptive Air Separation on Ag-ETS-10	55
3.1 Summary	56
3.2 Introduction	57
3.3 Experimental	58
3.3.1 Sample preparation	58
3.3.2 Characterization	59
3.3.3 Gas chromatographic separation and determination of argon and oxygen in air by Ag-ETS-10	60
3.3.4 Laboratory-scale demonstration	61
3.4 Results and Discussion	63
3.5 Conclusions	73

3.6 References	74
Chapter 4. Air Separation by Silver Titanosilicate with Enhanced Density	76
4.1 Summary	77
4.2 Introduction	78
4.3 Experimental	79
4.3.1 Sample preparation	79
4.3.2 Characterization	79
4.3.3 Density evaluation	79
4.3.4 Laboratory-scale demonstration	80
4.4 Results and Discussion	80
4.4.1 Density enhancement	80
4.4.2 Breakthrough times and O ₂ recovery	83
4.4.3 Laboratory-scale demonstration	85
4.5 Conclusions	88
4.6 References	89
Chapter 5. High Pressure Adsorptive Separation of Ethylene and Ethane on Na-ETS-10	90
5.1 Summary	91
5.2 Introduction	92
5.3 Experimental	94
5.3.1 Materials synthesis	94
5.3.2 Adsorption isotherms	94
5.3.3 Breakthrough experiments	95
5.3.4 Desorption experiments	96
5.3.5 Theoretical background	97
5.4 Results and Discussion	99
5.4.1 Single-gas isotherms at high pressure	99
5.4.2 Separation of a binary ethylene/ethane mixture	104
5.5 Conclusions	108
5.6 References	109
Chapter 6. Extraction of Ethane from Natural Gas at High Pressure by Adsorption on Na-ETS-10	111
6.1 Summary	112
6.2 Introduction	113
6.3 Experimental	116
6.3.1 Material synthesis	116
6.3.2 Adsorption isotherms	116

6.3.3 Breakthrough experiments	117
6.3.4 Desorption experiments	117
6.3.5 Theoretical background	118
6.4 Results and Discussion	119
6.4.1 Single-gas isotherms at high pressure	119
6.4.2 Separation of a binary methane/ethane mixture	123
6.4.3 Separation of methane and natural gas liquids	126
6.4.4 Increase in NGL/C1 ratio with increasing column pressure	128
6.5 Conclusions	129
6.6 References	130
Chapter 7. Removal of CO₂ from a Binary Mixture of Carbon Dioxide and Methane by Na-ETS-10	132
7.1 Summary	133
7.2 Introduction	134
7.3 Experimental	136
7.3.1 Sample preparation	136
7.3.2 Characterization	136
7.3.3 Theoretical background	137
7.4 Results and Discussion	141
7.4.1 Inverse phase GC	141
7.4.2 Equilibrium isotherms	144
7.4.3 Lab-scale demonstration	145
7.4.4 Desorption	147
7.5 Conclusions	148
7.6 References	150
Chapter 8. Regeneration of Na-ETS-10 Using Microwave and Conductive Heating	152
8.1 Summary	153
8.2 Introduction	154
8.3 Experimental	156
8.3.1 Sample preparation	156
8.3.2 Adsorption-desorption experiments	157
8.4 Results and Discussion	160
8.4.1 Ethylene/ethane desorption from Na-ETS-10	160
8.4.2 Carbon dioxide/methane desorption from Na-ETS-10	166
8.5 Conclusions	171
8.6 References	173

Chapter 9. Conclusions and Recommendations	176
9.1 Conclusions	177
9.2 Recommendations	180
9.2.1 Materials aspect	180
9.2.2 Process aspect	181
9.3 References	182

List of Tables

Table 1-1.	A survey of application of natural zeolites in the purification and separation of gases	3
Table 2-1.	A survey of applications of ETS-10	19
Table 2-2.	Applications of PSA and TSA processes	46
Table 3-1.	Langmuir parameters for adsorption data in the range of 0-100 kPa at 25 °C	66
Table 3-2.	Outlet composition of the breakthrough for N ₂ , O ₂ , Ar	70
Table 3-3.	Outlet composition of the thermal desorption of the adsorbed phase gas	72
Table 4-1.	Tap density of regular ETS-10 and high density ETS-10	83
Table 4-2.	Outlet composition of the breakthrough for N ₂ , O ₂ , Ar	87
Table 5-1.	Langmuir adsorption parameters for ethylene and ethane on Na-ETS-10 material at 298 K	100
Table 5-2.	Comparison of the experimental and literature reported isosteric heats of adsorption at zero loading for Na-ETS-10 and zeolite 13X	103
Table 5-3.	Volume and composition of the extract stream (desorbed phase) for different column pressures. Adsorbent: Na-ETS-10. Temperature: 298 K	105
Table 5-4.	Observed ethylene/ethane selectivities in the extract stream at 298 K and 273 K from a Na-ETS-10 adsorption column and those predicted by Ideal Adsorbed Solution Theory, as compared to previously reported equilibrium adsorbed fractions at 280 K	107
Table 6-1.	Adsorption parameters for ethane and methane on Na-ETS-10 materials at 298 K	120

Table 6-2.	Henry's law constants for methane and ethane for Na-ETS-10 at temperatures 298 K, 323 K and 343 K and corresponding ethane/methane selectivities	122
Table 7-1.	Corrected Retention time for CH ₄ and CO ₂ on Na-ETS-10 at temperature range from 25 to 140 °C. The value in () are extrapolated through Van't Hoff Equation	142
Table 7-2.	Constrained Toth parameters for adsorption data in the range of 0-100 kPa at 25 °C	145
Table 7-3.	Comparison of IAST, and lab-scale separation demonstration at 25 °C and 100 kPa	148
Table 8-1.	Comparison of microwave and conductive heating techniques for desorbing C ₂ H ₄ /C ₂ H ₆ from Na-ETS-10	164
Table 8-2.	Summary of the desorbed gas purity measured for microwave heating and conductive heating for C ₂ H ₄ /C ₂ H ₆	164
Table 8-3.	Comparison of microwave and conductive heating techniques for desorbing CO ₂ /CH ₄ from Na-ETS-10	170
Table 8-4.	Summary of the desorbed gas purity measured for microwave heating and conductive heating for CO ₂ /CH ₄	170

List of Figures

Figure 2-1.	Framework of ETS-10, ETS-10 projections: (a) down [110] direction for polymorph B; (b) down [100] direction for polymorph A. Dark TiO ₆ octahedra, light grey SiO ₄ tetrahedra	17
Figure 2-2.	Lennard-Jones Potential	22
Figure 2-3.	The five types of adsorption isotherms, according to the BDDT classification	24
Figure 2-4.	Nitrogen, argon and oxygen adsorption isotherms at 30 °C on Ag-mordenite	33
Figure 2-5.	Inverse gas chromatography of O ₂ and N ₂ on Ag-ETS-10 at 30 °C	34
Figure 2-6.	Schematic of HPVA high-pressure volumetric adsorption analyzer	40
Figure 2-7.	General principle of the volumetric isotherm apparatus	41
Figure 2-8.	Mechanisms of PSA and TSA process	43
Figure 2-9.	Five Steps of a two-bed PSA process	44
Figure 2-10.	Schematic of TSA cycle	45
Figure 2-11.	Materials classification due to interaction with microwave	47
Figure 3-1.	Schematic of one stage process for air separation on Ag-ETS-10	61
Figure 3-2.	Schematic of desorption process	62
Figure 3-3.	A typical gas chromatography separation of N ₂ over O ₂ , Ar over O ₂ on Ag-ETS-10. Pure oxygen and argon (a), 50-50% O ₂ -Ar mixture (b), air (c) was injected into an Ag-ETS-10 column at 25 °C under a 30 mL/min flow of helium carrier gas were determined by IGC analysis	64

Figure 3-4.	Equilibrium adsorption isotherms for N ₂ , Ar, O ₂ on Ag-ETS-10 at 25 °C. P is pressure and n is capacity	65
Figure 3-5.	Gas chromatographic separation and determination of argon and oxygen in air by Ag-ETS-10. (a) pure oxygen and argon;(b) 50-50% oxygen and argon (c)95-5% oxygen and Ar (d) Enlarged GC results of 95-5% oxygen and argon	68
Figure 3-6.	Gas chromatographic determination of 0.3% argon and 99.7% oxygen in air by Ag-ETS-10 (Enlarged GC results)	68
Figure 3-7.	Air breakthrough curve on Ag-ETS-10 at ambient conditions. Compressed air (a mixture of 78% N ₂ , 21% O ₂ and 1% Ar) was introduced into a column containing 130 g of pelletized Ag-ETS-10 at a flow rate of 124 mL/min (bed volume 150 mL). Composition of the outlet gas was determined by GC analysis	69
Figure 3-8.	Outlet flow rate monitored by Agilent ADM 1000 in adsorption procedure	71
Figure 3-9.	Outlet composition analysis of the desorption procedure	72
Figure 4-1.	XRD of regular ETS-10 and ETS-10-HD	81
Figure 4-2.	SEM of regular ETS-10	82
Figure 4-3.	SEM of ETS-10-HD	82
Figure 4-4.	Air breakthrough curve on high density Ag-ETS-10 at ambient conditions. Compressed air (a mixture of 78% N ₂ , 21% O ₂ and 1% Ar) was introduced into a 150 mL column containing 175 g of pelletized high density Ag-ETS-10 with mixed granule sizes (50% 10-16 mesh size and 50% 20-50 mesh size) at a flow rate of 120 mL/min. Composition of the outlet gas was determined by GC analysis	86
Figure 4-5.	Outlet flow rate monitored by Agilent ADM 1000 in adsorption procedure for high density bed	88
Figure 5-1.	Schematic of high pressure adsorption process	95

Figure 5-2.	Schematic of the different steps involved during the adsorption cycle where PH corresponds to the high pressure step, and PL corresponds to the low pressure step	96
Figure 5-3.	Adsorption isotherms for ethylene and ethane on Na-ETS-10 at 298 K. Insert: low pressure adsorption isotherms at 0-10 kPa	100
Figure 5-4.	Adsorption isotherms of ethylene (a) and ethane (b) on Na-ETS-10 at temperatures 298 K, 323 K, 373 K, 423 K and 473 K	101
Figure 5-5.	Henry's law constants for ethylene and ethane as a function of $1000/T$ for Na-ETS-10	102
Figure 5-6.	Calculated isosteric heats of adsorption for ethylene and ethane as a function of loading for Na-ETS-10	103
Figure 5-7.	Breakthrough curves for ethylene and ethane as a function of bed volume on a fixed bed column composed of Na-ETS-10. Feed mixture: 59/41 ethylene/ethane. Feed rate: 150 sccm (298 K, 101.3 kPa). Column temperature: 298 K. Column pressure: 2,580 kPa	104
Figure 5-8.	Gas chromatography analysis of feed gas (left) and extract composition (right) under 2,580 kPa at 298 K	105
Figure 5-9.	Mole fractions of ethylene and ethane in the extract stream (closed symbols, solid line) and ethylene/ethane selectivity from a Na-ETS-10 adsorption column at 298 K (open symbols, solid line) as a function of pressure. Predicted mole fractions are based on the IAST mixture adsorption model using single gas adsorption isotherm values from ethylene and ethane on Na-ETS-10 crystals at 298 K (dotted line)	106
Figure 6-1.	Conventional NGL recovery process. Basic turbo-expander process	114
Figure 6-2.	Adsorption isotherms for methane and ethane on Na-ETS-10 at 298 K. Insert: low pressure adsorption isotherms at 0-10 kPa	120

- Figure 6-3.** Adsorption isotherms of ethane (a) and methane (b) on Na-ETS-10 at temperatures 298 K, 323 K and 343 K 122
- Figure 6-4.** Breakthrough curves for methane (C1) and ethane (C2) as a function of bed volume on a fixed bed column composed of Na-ETS-10. Feed mixture: 93/7 methane/ethane. Feed rate: 250 sccm. Column temperature: 298 K. Column pressure: 3200 kPa 123
- Figure 6-5.** Mole fractions of methane and ethane (solid lines) and ethane/methane selectivity (dotted line) in the desorbed extract stream as a function of Na-ETS-10 adsorption column operating pressure. Feed mixture: 93/7 methane/ethane. Feed rate: 250 sccm. Column temperature: 298 K 124
- Figure 6-6.** Observed mole fractions of methane and ethane in the extract stream (closed symbols, solid line) from an Na-ETS-10 adsorption column and those predicted by Ideal Adsorbed Solution Theory (dotted line), as compared to previously reported equilibrium adsorbed fractions from a 91/9 C1/C2 mixture at: (○)150 kPa, 280 K; (△)500 kPa, 280 K; (◇)150 kPa, 325 K. Predicted mole fractions are based on the IAST mixture adsorption model using single gas adsorption isotherm values from methane and ethane on NaETS-10 crystals at 298 K (dotted line) 125
- Figure 6-7.** (a): Breakthrough curves for methane (C1), ethane (C2) and propane (C3) as a function of bed volumes on a fixed bed column composed of Na-ETS-10. (b): A packed bed column composed of Na-ETS-10 producing three successive raffinate streams (A, B and C) from classified according to their outlet compositions. Feed gas composition: 90.99 CH₄: 5.60 C₂H₆: 1.63 C₃H₈: 0.69 CO₂: 0.50 N₂: 0.49 C₄H₁₀: 0.10 C₅H₁₂. Feed rate: 250 sccm. Column temperature: 298 K. Column pressure: 3200 kPa 127

Figure 6-8.	Fractions of methane (C1), ethane (C2) and propane (C3) in the desorbed extract stream following steam desorption from a fixed bed column composed of Na-ETS-10. Fractions were desorbed after the column had been exposed to ~850 bed volumes of the feed gas mixture at one of two different column pressures. Feed mixture: 90.99 CH ₄ : 5.60 C ₂ H ₆ : 1.63 C ₃ H ₈ : 0.69 CO ₂ : 0.50 N ₂ : 0.49 C ₄ H ₁₀ : 0.10 C ₅ H ₁₂ . Feed rate: 250 sccm. Column temperature: 298 K. Column pressures: 1800 or 3200 kPa	128
Figure 7-1.	A typical separation of CO ₂ and CH ₄ on Na-ETS-10 at 100 °C. A mixture of 50% CH ₄ and 50% CO ₂ was injected into a Na-ETS-10 column and retention times were determined by IGC analysis	142
Figure 7-2.	IGC analysis of methane on Na-ETS-10 at 25, 30, and 40 °C	143
Figure 7-3.	IGC analysis of Carbon dioxide on Na-ETS-10 at 100, 120, and 140 °C	143
Figure 7-4.	Arrhenius plot of the low coverage isosteric heat of adsorption for CH ₄ and CO ₂ on Na-ETS-10. CH ₄ , 23.3 kJ/mol; CO ₂ , 42.1 kJ/mol	144
Figure 7-5.	Equilibrium adsorption isotherms with Toth equation fitting for CO ₂ and CH ₄ on Na-ETS-10 at 25 °C and pressure up to 100 kPa	145
Figure 7-6.	CH ₄ /CO ₂ breakthrough curve on Na-ETS-10 at ambient Condition. Feed gas (a mixture of 10% CO ₂ and 90% CH ₄) was introduced into a column containing 120 g of pelletized Na-ETS-10 (10-20 mesh) at a flow rate of 300 mL/min (bed volume 150 mL). Column temperature 25 °C, column pressure 1 bar. Hydrocarbon content of the outlet gas was determined by GC analysis	146
Figure 7-7.	Outlet flow rate monitored by Agilent ADM 1000 in adsorption procedure	147
Figure 8-1.	Block diagram showing adsorption and regeneration of Na-ETS-10 using microwave and conductive heating	159

Figure 8-2.	Desorption of C ₂ H ₄ /C ₂ H ₆ saturated Na-ETS-10 with microwave heating and conductive heating: a) temperature; b) net power consumption; and c) desorption rate	161
Figure 8-3.	Swing capacity of Na-ETS-10 over 5 cycles remains unchanged under microwave heating and conductive heating of C ₂ H ₄ /C ₂ H ₆ at 190 °C	163
Figure 8-4.	Variation in net energy consumption over 5 cycles was insignificant during microwave heating and conductive heating of C ₂ H ₄ /C ₂ H ₆ on Na-ETS-10 at 190 °C	165
Figure 8-5.	Desorption of CO ₂ /CH ₄ saturated Na-ETS-10 with microwave heating and conductive heating: a) temperature; b) net power consumption; and c) desorption rate	167
Figure 8-6.	Swing capacity of Na-ETS-10 over 5 cycles remains unchanged under microwave heating and conductive heating of CO ₂ /CH ₄ at 190 °C	168
Figure 8-7.	Variation in net energy consumption over 5 cycles was insignificant during microwave heating and conductive heating of CO ₂ /CH ₄ on Na-ETS-10	169

Chapter 1

Introduction

1.1 Overview

Since zeolites were firstly discovered in 1756 [1], zeolite molecular sieves have been widely applied in the chemical, petrochemical and environmental industries [2-4].

The traditional zeolites are described as aluminosilicate inorganic materials possessing a three-dimensional network of AlO_4 and SiO_4 tetrahedra linked to each other by sharing the oxygen atom. Zeolites exhibits uniform pore size distribution, high surface area, high porosity, variable chemical composition, and controllable acid-base properties [5]. Because of these unique properties zeolites have found industrial uses in various fields, such as gas separation and catalytic and ion exchange applications [6-8].

Traditionally gas separation has been carried out by cryodistillation, a well-known technology operated at extreme conditions, such as low temperature and high pressure [9]. These conditions make the separation energy intensive. Adsorptive gas separation has been used as an alternative due to its low energy requirement and low equipment costs associated with the separations. Separation is achieved by using zeolite molecular sieves to preferentially partition substances from the gaseous phase onto the surface of the solid [10]. Table 1-1 shows a summary of various applications of aluminosilicate zeolites in the purification and separation of gases [6].

Although aluminosilicate zeolites have been widely applied in gas separations, several application areas still remain a challenge. Among them is the adsorptive separation for light hydrocarbons at high pressure, due to the degradation of the separation performance under these conditions for most natural adsorbents; and production of argon free oxygen from air, due to lack of positive selectivity on most zeolites for argon over oxygen. A new area of research involving the synthesis of new zeolite materials has been on-going and shows promise in overcoming the limitations of

natural zeolites.

Table 1-1. A survey of application of natural zeolites in the purification and separation of gases [6].

Application	Gas	Materials
1. Air separation	O ₂ /N ₂	Ag-MOR AgLiLSX CLI, CHA, MOR
2. Natural gas upgrading	CH ₄ /N ₂	Na, Ca-CLI Ba-ETS-4
	CH ₄ /CO ₂	K,Na,Ca-CLI CLI, MOR, ERI
3. Air pre-purification	CO ₂ , CO, NO	CHA, CLI
	H ₂ S, SO ₂	CLI
4. Gas drying	Air, hydrocarbons, H ₂ , etc.	CHA CLI, MOR
5. H ₂ , N ₂ , and rare gas purification	He, Ne, Kr, Xe	Ca-CHA
	H ₂	CHA
	N ₂	H-MOR
6. Natural gas, coal gas, biogas, etc. purification	H ₂ S, SO ₂	CLI
	SO _x	CLI, MOR, CHA
	NH ₃	PHI

In 1989, S.M. Kuznicki reported on a new class of zeolites invented at Engelhard Corporation [11]. It is a mixed octahedral/tetrahedral titanium silicate molecular sieve with a three-dimensional network of interconnecting channels [12]. The completely different physical and chemical properties of the Engelhard Titanium Silicate (ETS) give this new class of zeolites a potential advantage compared to natural zeolites especially in gas separation processes [13-20]. Among the ETS family, a large pore

zeolite ETS-10 has an average pore size of approximately 8 angstrom. This would allow most of the gas molecules (light hydrocarbons, carbon dioxide, oxygen and nitrogen) to enter into the channels and enable the separation of mixtures such as, ethylene/ethane, methane/ethane, CO₂/methane, and oxygen/nitrogen.

The work reported in this thesis has been focused on the use of ETS-10 in production of argon free oxygen [21], separation of ethylene and ethane at high pressure [22], extraction of ethane from natural gas at high pressure [23-24], and removal of carbon dioxide from natural gas [25]. Due to the difficulties of regeneration of ETS-10 after adsorption of hydrocarbons, microwave assisted regeneration as an alternative was also investigated and studied [26-27].

1.2 Thesis Outline

The purification of different components of air, such as oxygen, nitrogen, and argon, is an important industrial process [28]. Pressure Swing Adsorption (PSA) is surpassing the traditional cryogenic distillation for many air separation applications, because of its lower energy consumption [29]. Unfortunately, the oxygen product purity in an industrial PSA process is typically limited to 95% due to the presence of argon which always shows the same adsorption equilibrium properties as oxygen on most molecular sieves [30-33].

Silver exchanged zeolites such as silver mordenite [34], silver exchanged zeolite A [35], silver exchanged zeolite X [36], and silver exchanged Li-Na-LSX zeolite [37] have all been reported to show some degree of argon over oxygen selectivity. In 2003, Air Products and Chemicals Inc. reported that a vacuum and pressure swing adsorption unit using AgLiLSX adsorbent allows the production of 99% oxygen with a recovery of 15% [38].

In 2008, Kuznicki's group reported that titanium based molecular sieves, such as ETS-10, have the ability to exchange silver ions and subsequently support self-assembly of stable silver nanoparticles when heated. After such modifications, nanosilver ETS-10 exhibits unique adsorption properties, especially toward the inert gases-Ar, Kr and Xe [39]. The enhanced interaction between argon and nanosilver ETS-10 makes it possible to separate argon and oxygen, and produce high purity oxygen from air.

In chapter three, the separation performance of Ag-ETS-10 for air at ambient conditions is described. A cryogenic chromatographic method was developed to improve the quantification of O₂ and Ar in the product stream. The separation factor, breakthrough and desorption profiles of N₂, Ar, and O₂ are reported.

In chapter four, from the prediction of a mathematic model, it shows the possibility that increasing the production and recovery of high purity oxygen by enhancing Ag-ETS-10 bed density. Two methods were investigated and applied to improve the bed density of Ag-ETS-10 adsorbent, such improved adsorbents with higher density were evaluated in the same air separation lab-scale demonstration system as described in chapter three.

Ethylene produced by steam cracking and thermal decomposition of ethane must be purified prior to use in the production of plastics, rubber and films. Ethane-ethylene separation is generally achieved by cryo-distillation. The energy and equipment costs associated with ethylene purification could be significantly reduced by the development of alternative separation methods.

It has been reported that Na-ETS-10 can be used to separate a mixture of ethylene and ethane from an industrial process stream under low pressure (101 kPa) with a binary bed selectivity of 5 at 298 K [40]. However, the industrial cryogenic distillation process for ethane/ethylene separation is performed at elevated pressures (2000-2500

kPa), and the product stream is also transported at a high-pressure pipeline. Any alternative adsorptive separation technology related to ethane/ethylene separation that operates at high pressure will provide a clear advantage in reducing the energy requirements.

Chapter five describes the adsorptive separation of a binary mixture of ethane and ethylene at high pressure on Na-ETS-10 using a laboratory-scale demonstration unit. A gas mixture, with a composition similar to the one commonly found in industrial processes, was separated by adsorption on Na-ETS-10 within a packed-bed column. The separation factor, breakthrough profile and capacity for ethylene and ethane were determined. The separation performance was compared at different pressure and temperature conditions. Adsorption isotherms for ethylene and ethane at high pressures were used to calculate the mixture's adsorption equilibrium on Na-ETS-10 as a function of pressure, and to calculate the isosteric heats of adsorption as a function of loading.

Ethane, the second largest component of raw natural gas (ranging from 0.7% to 6.8% by volume), is an important source of feedstock for ethylene production via the industrial scale cracking process [41]. Annual global demand for ethylene, a precursor in the production of films, rubber and plastics, exceeds 100 million tones [42]. The recovery of natural gas liquids (NGLs), such as ethane, from natural gas was traditionally achieved by cryogenic separation method [43]. However this method has associated high-energy consumption costs. One common approach to lower the temperature of a natural gas stream is to use a turbo expansion process. In this process, refrigerants are used to cool the natural gas stream, followed by rapid gas expansion by an expansion turbine. Expanding the cooled gas produces a rapid temperature drop, which condenses out NGLs, including ethane, while methane is left in the gas phase [44]. Subsequently, the gaseous methane effluent must be recompressed to pipeline pressure, requiring further energy input.

In light of the high cost associated with the cryogenic method, there has been interest in developing alternative technologies for removing NGLs from natural gas [45-46]. Adsorptive gas separation as an alternative has been widely investigated at ambient condition, due to its low energy requirement. However, the NG feedstocks for the NGL recovery process are generally high-pressure streams, occasionally as high as 10^4 kPa. Taking this into account any potential adsorption process related to natural gas treatment should contemplate materials and engineering designs with efficient separation performance at higher pressures [46]. Working at higher pressures would also minimize the recompression work required before materials are introduced into the downstream pipeline.

In chapter six, extraction of ethane from natural gas at high pressure by adsorption on Na-ETS-10 is reported. The objective of this work was to evaluate Na-ETS-10 as an adsorbent material capable of separating C1/C2 and C1/NGL at conditions approximating natural gas pipeline pressures. Adsorption isotherms were measured for methane and ethane at high pressures and used to estimate the mixture adsorption equilibrium on Na-ETS-10 crystals as a function of pressure. The separation performance of Na-ETS-10 within packed-bed columns was analyzed based on the raffinate and extract streams produced from C1/C2 and C1/NGL feed mixtures at room temperature and high pressure (up to 5600 kPa).

The global increase in demand for energy is faced with a continuous demand for an environmentally friendly source of energy such as natural gas. The composition of natural gas varies depending on the source. Usually raw natural gas is composed mainly of methane (typically 80-95%), and impurities such as CO₂, nitrogen, and heavier hydrocarbons (C₂₊). Natural gas must be liquefied at a very low temperature before being fed to pipelines for transportation. The presence of the acidic carbon dioxide can cause pipeline corrosion and reduce transportation efficiency [47-48]. Therefore separation of carbon dioxide from methane is an important separation in the

chemical and petrochemical industries.

Many available methods exist for removal of CO₂ from natural gas in order to meet the pipeline requirements. They include adsorptive separation [49-51], chemical absorption [52-53], membrane separation [54-55], and cryogenic distillation [56]. The key to the success of adsorptive separation of carbon dioxide from natural gas is finding an adsorbent with a high CO₂ over CH₄ selectivity and a high CO₂ capacity. The pore size of ETS-10 has an average kinetic diameter of ~8 Å, which allows both CO₂ (3.3 Å) and CH₄ (3.8 Å) molecules to enter into the cages and channels of ETS-10. It is possible to separate a CO₂/CH₄ mixture on ETS-10 based on the differences in thermodynamic equilibrium between the gases [57-58].

In chapter seven, a removal of carbon dioxide from a mixture of 90% CH₄ and 10% CO₂ was demonstrated by adsorptive separation on Na-ETS-10. Adsorption of carbon dioxide and methane in Na-ETS-10 was measured by elution chromatography over a temperature range of 30-130 °C. Limiting selectivity and isosteric heat of adsorption at zero loading were obtained through these inverse-phase gas chromatography analyses. The adsorption equilibria of carbon dioxide and methane on ETS-10 were measured by a static volumetric method at 25 °C and pressure up to 100 kPa. The equilibrium isotherms were modeled using the Toth equation which was applied in the Ideal Adsorbed Solution Theory (IAST) model. IAST was used to predict the separation performance. A mixture of 10% carbon dioxide and 90% methane obtained from an industrial process stream was run through 150 mL Na-ETS-10 bed. Breakthrough data was obtained through this single bed separation system. Experimental adsorbed phase composition was investigated by water desorption and was compared with the data predicted by the IAST model.

ETS-10 is capable of adsorption and separation of hydrocarbons such as methane, ethane, and ethylene but due to their high heat of adsorption the desorption of these strongly adsorbed species becomes one of the most time and energy consuming steps

in the adsorptive separation of hydrocarbon by zeolites.

Microwave heating was first used for rapid heating of foods in the oven. Later its rapid heating capability made it popular in industrial drying as well [59-61]. The fundamental of microwave heating is the reverse of the conventional conductive heating. In a conventional conductive heating system, the thermal energy is transferred from the surface to the bulk of the materials. However, in a microwave heating system, microwave propagates through molecular interaction between the material and the electromagnetic field. This unique property makes the microwave more efficient than traditional conductive heating and attracts interest in regeneration studies [62].

The objective of chapter eight is to investigate the swing ability and energy efficiency of microwave for desorption of hydrocarbon from Na-ETS-10 in a bench scale microwave system. Desorption of single gas systems such as, methane, ethane, ethylene and carbon dioxide was evaluated first. Two gas mixtures, ethane/ethylene (C_2H_6/C_2H_4) and carbon dioxide/methane (CO_2/CH_4), commonly found in industries were separated on Na-ETS-10 in a packed bed column and were later regenerated by the microwave demonstration unit. The swing ability, energy efficiency and capacity of microwave to recover adsorbed gas were determined. At the end, the results of microwave desorption were compared with a conductive heating experiment in regenerating Na-ETS-10.

Chapter nine summarizes the key discoveries of this work. The objective of this research program is to demonstrate the production of argon free oxygen by adsorptive air separation on Ag-ETS-10; Adsorptive separation properties of titanosilicate ETS-10 and its potential applications in the petrochemical industry such as ethylene/ethane separation, extraction of ethane from natural gas, and removal of CO_2 from natural gas; Research on using microwaves in the regeneration of ETS-10 adsorbent has also been conducted and is reported in this thesis.

1.3 Reference

- [1] Cronstedt, A.F., 1756. *Academiens Handlingar Stockholm* 18, 120-130
- [2] Yang, R.T., 2003. *Adsorbents: Fundamentals and applications*. John Wiley & Sons Inc., Hoboken, New Jersey.
- [3] Degnan, T.F., 2000. *Topics in Catalysis* 13, 349-356.
- [4] Sabeha, K.O., Cheeseman, C.R., Perry, R., 1994. *Journal of Chemical Technology and Biotechnology* 59, 121-126
- [5] Breck, D.W., 1974. *Zeolite Molecular Sieves: Structure, Chemistry, and use*. John Wiley & Sons Inc., New Jersey.
- [6] Ackley, M.W., Rege, S.U., Saxena, H., 2003. *Microporous and Mesoporous Materials* 61, 25-42.
- [7] Yilmaz, B., Muller, U., 2009. *Topics in Catalysis* 52, 888-895.
- [8] Sherry, H.S., 1979. *Clay and Clay Minerals* 27, 231-237.
- [9] Geankoplis, C.J., 2003. *Transport processes and separation process principles, fourth edition*, Prentice Hall Press, New Jersey.
- [10] International Adsorption Society. <http://ias.vub.ac.be> (accessed April 11, 2012)
- [11] Kuznicki, S.M., 1989. *Large-pored crystalline titanium molecular sieve zeolites*. US Patent No. 4,853,202.
- [12] Anderson, M.W., Terasaki, O., Ohsuna, T., Philippou, A., Mackay, S.P., Ferreira, A., Rocha, J., Lidin, S., 1994. *Nature* 367, 347-351.
- [13] Krisnandi, Y.K., Southon, P.D., Adesina, A.A. Howe, R.F., 2003. *International Journal of Photoenergy* 5, 131-140.

- [14]Philippou, A., Naderi, M., Rocha, J., Anderson, M.W., 1998. *Catalysis Letters* 53, 221-224.
- [15]Lin, C.C.H., Danaie, M., Mitlin, D., Kuznicki, S.M., 2011. *Journal of Nanoscience and Nanotechnology* 11, 2537-2539.
- [16]Jeong, N.C., Lee, Y.J., Park, J.H., Lim, H., Shin, C.H., Cheong, H., Yoon, K.B., 2009. *Journal of the American Chemical Society* 131, 13080-13092.
- [17]Choi, J.H., Kim, S.D., Kwon, Y.J., Kim, W.J., 2006. *Microporous and Mesoporous Materials* 96, 157-167.
- [18]Gallo, M., Nenoff, T.M., Mitchell, M.C., 2006. *Fluid Phase Equilibria* 247, 135-142.
- [19]Kuznicki, S.M., Anson, A., Koenig, A., Kuznicki, T.M., Hastrup, T., Eyring, E.M., Hunter, D., 2007. *The Journal of Physical Chemistry C* 111, 1560-1562.
- [20]Zhao, G.X.S., Lee, J.L., Chia, P.A., 2003. *Langmuir* 19, 1977-1979.
- [21]Shi, M., Kim, J., Sawada, J.A., Lam, J., Sarabadan, S., Kuznicki, T.M., Kuznicki, S.M., 2012. *Production of argon free oxygen by adsorptive air separation on Ag-ETS-10*, accepted by *AIChE Journal*, June 19, 2012.
- [22]Shi, M., Avila, A.M., Yang, F., Kuznicki, T.M., Kuznicki, S.M., 2011. *Chemical Engineering Science* 66, 2817-2822.
- [23]Avila, A.M., Yang, F., Shi, M., Kuznicki, S.M., 2011. *Chemical Engineering Science* 66, 2991-2996.
- [24]Kuznicki, S.M., Avila, A.M., Shi, M., Strom, V.L., Herrera, P.S., 2011. *Removal of ethane from natural gas at high pressure*. Published US Patent Application No. 2011/0315012 A1.

- [25] Shi, M., Sawada, J.A., Kim, J., Kuznicki, T.M., Kuznicki, S.M., 2012. *Removal of CO₂ from a binary mixture of carbon dioxide and methane by Na-ETS-10*, in preparation.
- [26] Chowdhury, T., Shi, M., Hashisho, Z., Kuznicki, S.M., 2012. *Evaluation of controlled microwave system for desorption of hydrocarbons on titanosilicate zeolite*, in preparation.
- [27] Chowdhury, T., Shi, M., Hashisho, Z., Sawada, J.A., Kuznicki, S.M., 2012. *Regeneration of Na-ETS-10 using microwave and conductive heating*, accepted by *Chemical Engineering Science*.
- [28] Smith, A.R., Klosek, J., 2001. *Fuel Processing Technology* 70, 115-134
- [29] Yang, R.T., 1987. *Gas Separation by Adsorption Processes*, Butterworth, Stoneham, MA.
- [30] Talu, O., Li, J., Kumar, R., Mathisa, P.M., Jr, J.D.M., Schork, J.M., 1996. *Gas Separation & Purification* 10, 149-159.
- [31] Moon, I.S., Lee, D.I., Yang, J.H., Ryu, H.W., 1986. *Korean Journal of Chemical Engineering* 3, 15-21.
- [32] Jee, J.G., Lee, S.J., 2005. *Adsorption* 11, 415-420.
- [33] Zahra, M., Jafar, T., Masoud, M., 2008. *World Academy of Science, Engineering and Technology* 47, 99-103.
- [34] Wilkerson, B.E., 1990. *Master's thesis*, the Ohio State University.
- [35] Sebastian, J., Jasra, R.V., 2005. *Industrial & Engineering Chemistry Research* 44, 8014-8024.
- [36] Chiang, R.L., Whitley, R.D., Ostroski, J.E., Dee, D.P., 2002. *Argon/Oxygen Selective X-zeolite*. US Patent No. 6,432,170 B1.

- [37]Hutson, N.D., Rege, S.U., Yang, R.T., 1999. *AIChE Journal* 45, 724-734.
- [38]Dee, D.P., Chiang, R.L., Miller, E.J., Whitley, R.D., 2003. *High Purity Oxygen Production by Pressure Swing Adsorption*. US Patent No. 6,544,318 B2.
- [39]Anson, A., Kuznicki, S.M., Kuznicki, T.M., Haastrup, T., Wang, Y., Lin, C.C.H., Sawada, J.A., Eyring, E.M., Hunter, D., 2008. *Microporous Meoporous Materials* 109, 577-580.
- [40]Shi, M., Lin, C.C.H., Kuznicki, T.M., Hashisho, Z., Kuznicki, S.M., 2010. *Chemical Engineering Science* 65, 3494-3498.
- [41]Ren, T., Patel, M., Blok, K., 2006. *Energy* 31, 425-451.
- [42]Storck, W.J., 2006. *Chemical and Engineering News* 84, 59-68.
- [43]Roje, A., Jaffret, C., 1997. *Natural gas: production, processing, transport*. Editions Technip, Paris.
- [44]Chebbi, R., Al-Amoodi, N.S., Jabbar, N.M.A., Hussein, G.A., Mazroui, K.A.A., 2010. *Chemical Engineering Research and Design* 88, 779-787.
- [45]Arruebo, M., Coronas, J., Menendez, M., Santamaria, J., 2001. *Separation and Purification Technology* 25, 275-286.
- [46]Tagliabue, M., Farrusseng, D., Valencia, S., Aguado, S., Ravon, U., Rizzo, C., Corma, A., Mirodatos, C., 2009. *Chemical Engineering Journal* 155, 553-566.
- [47]Gerasimov, V.E., Peredel'skii, V.A., Lyapin, A.I., Darbinyan, R.V., Dovbish, A.L., 2004. *Chemical and Petroleum Engineering* 40, 339-343.
- [48]Cavenati, S., Grande, C.A., Rodrigues, A.E., 2006. *Energy & Fuels* 20, 2648-2659.
- [49]Kapoor, A., Yang, R.T., 1989. *Chemical Engineering Science* 44, 1723-1733.

- [50]Himeno, S., Komatsu, T., Fujita. S., 2005. *Journal of Chemical & Engineering Data* 50, 369-376.
- [51]Chaudhary, V.R., Mayadevi, S., 1996. *Zeolites* 17, 501-507.
- [52]Leal, O., Bolivar, C., Ovalles, C., Garcia, J.J., Espidel, Y., 1995. *Inorganica Chimica Acta* 240,183-189.
- [53]Gupta, H., Fan, L.S., 2002. *Industrial & Engineering Chemistry Research* 41, 4035-4042.
- [54]Sandstrom, L., Sjoberg, E., Hedlund, J., 2011. *Journal of Membrane Science* 380, 232-240.
- [55]Scholes, C.A., Stevens, G.W., Kentish, S.E., 2012. *Fuel* 96, 15-28.
- [56]Fieler, E.R., 2010. *Controlled freeze zone tower*. US Patent No. 2010/0018248 A1
- [57]Anson, A., Lin, C.C.H., Kuznicki, S.M., Sawada, J.A., 2009. *Chemical Engineering Science* 64, 3683-3687.
- [58]Kuznicki, S.M., 1991. *Large-pored crystalline titanium molecular sieve zeolites*. US Patent No. 5,011,591.
- [59]Coss, P.M., Cha, C.Y., 2000. *Journal of the Air & Waste Management Association* 50, 529-535.
- [60]Quan, X., Liu, X., Bo, L., Chen, S., Zhao, Y., Cui, X., 2004. *Water Research* 38, 4484-4490.
- [61]Kong, Y., Cha, C.Y., 1996. *Carbon* 34, 1035-1040.
- [62]Jones, D.A., Lelyveld, T.P., Mavrofidis, S.D., Kingman, S.W., Miles, N.J., 2002. *Resources, Conservation and Recycling* 34, 75-90.

Chapter 2

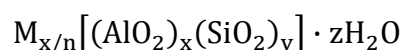
Fundamentals of Adsorptive Separation

2.1 Titanosilicate Molecular Sieve Zeolite

2.1.1 Traditional zeolites

Molecular sieve zeolites were first introduced in 1954, as commercial adsorbents for industrial separations and purifications [1]. Since then, this new class of materials has played an important role in a wide range of industrial fields. [2-4].

Zeolites are recognized as crystalline aluminosilicates of an alkali element, such as sodium, potassium, and calcium, and can be represented in terms of mole ratios of oxides as follows:

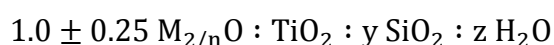


Where x and y are integral numbers and y is equal to or greater than x, n is the valence of cation M, and z is the number of water molecular in each unit cell. It possesses a three-dimensional network of AlO_4 and SiO_4 tetrahedra linked to each other by sharing the oxygen atom [5]. Due to this unique structure zeolites exhibit unique properties such as, uniform pore size distribution, high surface area, high porosity, variable chemical composition, and controllable acid-based properties [6]. These properties are the reason why zeolite materials have found industrial applications in fields, such as gas separation, ion exchange and catalysis [7-10].

2.1.2 Titanosilicate ETS-10

Due to the slow progress in the discovery of new aluminum silicate-based molecular sieves, researchers have taken various approaches to replace aluminum or silicon in zeolite synthesis to generate either new zeolite-like framework structures or to form qualitatively different active sites from the ones available in analogous aluminum

silicate based materials [11-12]. A naturally occurring alkaline titanosilicate mineral, identified as “Zorite”, was discovered in Lovozero Tundra in 1972 [13] and has been used as a model for the synthesis of novel synthetic zeolites. In 1989, a new crystalline synthetic titanium silicate molecular sieve zeolite, ETS-10, was reported by Kuznicki [14]. This new material has a definite X-ray diffraction pattern unlike other molecular sieve zeolites and can be represented by the following chemical composition:



Where M is at least one cation having a valence of n, y is from 2.5 to 25, and z is from 0 to 100. M is an alkali element, such as sodium, potassium, and y is at least 3.5 and ranges up to about 10. With the assistance of high-resolution electron microscopy, electron and powder X-ray diffraction, solid-state NMR, molecular modeling and chemical analysis, Anderson identified the structure of this new type of material

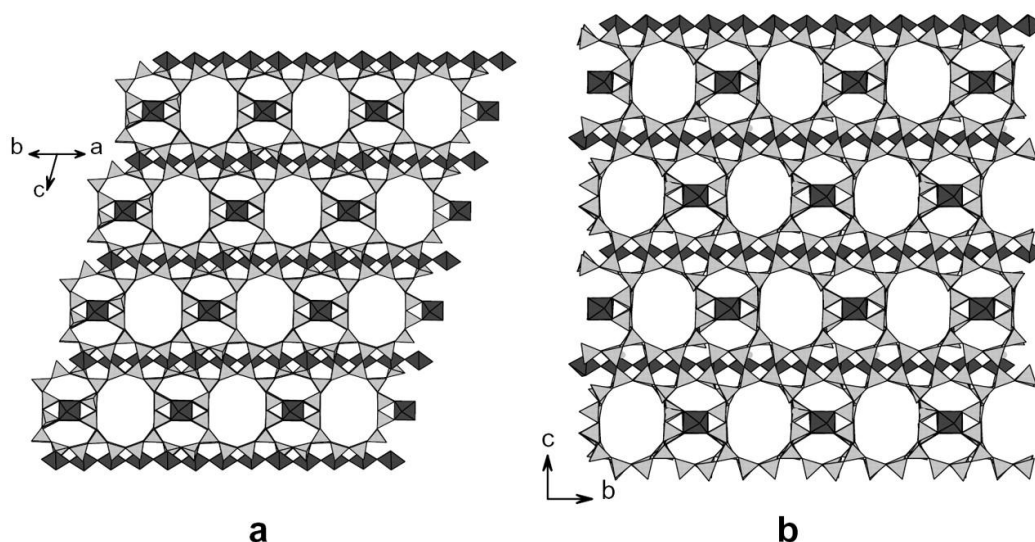


Figure 2-1. Framework of ETS-10, ETS-10 projections: (a) down [110] direction for polymorph B; (b) down [100] direction for polymorph A. Dark TiO_6 octahedra, light grey SiO_4 tetrahedra.

in 1992 [15]. The structure is shown in Figure 2-1. In ETS-10 the octahedral Ti^{4+} ions

are lined to the tetrahedral Si^{4+} ions through bridging oxygen atoms. The negative charge of these framework structures is compensated by Na^+/K^+ ions. Such structure possesses an average pore size of about 8 Angstrom units (the pore system contains a twelve-membered ring in a highly disordered structure) and the TiO_6 octahedra are not exposed at the surface of the large channels.

2.1.3 Applications of titanosilicate ETS-10

The cations M can be replaced with other cations by well-known exchange techniques. The cation candidates could be hydrogen, ammonium, or other alkaline earth metals (Mg, Ca, Ba ...). The ease of ion exchange makes ETS-10 a good candidate for water purification applications [16-19]. ETS-10 because of its basicity can be considered a zeolitic catalyst. Additionally, when it is exchanged with alkali metal cations, it has a unique catalytic function for reactions that require strong basic character, such as alcohol dehydration [20-21]. It is also reported that the alkaline earth-exchanged form of ETS-10 has a high degree of thermal stability to at least 450 °C, or higher. Such unique property will makes it useful in high temperature catalytic processes [14]. The approximately 8 Angstrom pore size makes it suitable for thermodynamic separation of mixtures which have large molecular size, such as light hydrocarbons. Table 2-1 shows the wide applications of ETS-10 in different fields

Table 2-1. A survey of applications of ETS-10.

Fields	Applications
<i>Adsorption</i>	Hydrogen/methane, hydrogen/carbon dioxide separation [26] Ethane/ethylene separation [27] Propane/propylene separation [28] Xe Capture in nuclear power plant [29]
<i>Ion exchanger</i>	Removal of heavy metal Pb^{2+} [17] Uptake of Uranium from nuclear reactor [18] Removal of Cu^{2+} , Co^{2+} , Mn^{2+} and Zn^{2+} from waste water [16] Sorption of radioactive cations $^{115}Cd^{2+}$, $^{204}Hg^{2+}$ and $^{137}Cs^{+}$ [19]
<i>Catalyst</i>	Aldol condensation of acetone [22] n-Hexane reforming reaction [23] Catalytic oxidation processes [24] Photocatalytic decomposition of acetaldehyde [25]

2.2 Adsorption Theory

2.2.1 Introduction

Adsorption is a surface phenomenon that occurs when a gas, a liquid or dissolved solids accumulates on the surface of a solid or a liquid (adsorbent), creating a molecular or atomic film (adsorbate) [30]. It is different from absorption, in which a fluid is diffused into a liquid or solid to form a solution.

Adsorption occurs in most natural physical, chemical and biological systems, and gas-phase adsorption is widely applied in purification or bulk separation. Based on the nature of the bonding between the adsorbate molecule and the solid surface, the adsorption process can be classified as physical adsorption or chemical adsorption [31]. In physical adsorption, there is a weak van der Waals attraction of the adsorbate

to the surface and the individuality of the adsorbate and adsorbent are preserved. However, chemical adsorption involves electron transfer and is essentially a chemical interaction, and such interaction is much stronger than physical adsorption.

2.2.2 *Physical adsorption force*

Adsorption happens when the total energy of the interaction is equal to the energy needed to hold the adsorbate molecule to the atoms on the adsorbent surface. The three main types of contributions to the interaction between adsorbate and adsorbent are dispersive, electrostatic and coulombic types. The latter, coulombic type, exists only on the polar surface [31-34].

The adsorbate-adsorbent potential can be written as follows:

$$\phi_{total} = \phi_D + \phi_R + \phi_P + \phi_{FD} + \phi_{FQ} \quad (2.1)$$

where ϕ_{total} is comprised of ϕ_D =dispersion energy, ϕ_R =close-range repulsive energy, ϕ_P =polarization energy (interaction between electric field and an induced dipole), ϕ_{FD} =interaction between electric field and a permanent dipole, and ϕ_{FQ} =interaction between field gradient and a quadrupole [31]. The individual contributions are discussed as follows:

Dispersion:

The dispersive force exists between any two molecules or atoms. It arises from the rapid fluctuation of electron density in each atom, inducing an electrical moment in the neighboring atom and creating an attraction between them. In the case of physical adsorption, such force always occurs between the adsorbate and the adsorbent atoms. The dispersive force was initially characterized and calculated by London, and described as:

$$\phi_D = -\frac{A}{r^6} \quad (2.2)$$

where A is the dispersion constant associated with the dipole-dipole interaction, the negative sign shows it is an attractive interaction. A can be calculated by the following Kirkwood and Muller formula:

$$A = \frac{6mc^2\alpha_i\alpha_j}{\left(\frac{\alpha_i}{\chi_i} + \frac{\alpha_j}{\chi_j}\right)} \quad (2.3)$$

where c is the speed of light, m is the mass of electron, α is the polarizability and χ is the magnetic susceptibility, i and j refer to the two atoms [32].

Repulsion:

A theoretical expression was derived for the short-range repulsive potential, which was approximated by:

$$\phi_R = +\frac{B}{r^{12}} \quad (2.4)$$

where B is an empirical constant. The dispersion and repulsion interactions form the Lennard-Jones potential. The curve is depicted in Figure 2-2. In physical adsorption, $\phi_D + \phi_R = 0$ at an equilibrium distance r_0 , which is recognized as the van der Waals radii of the interacting pair [35].

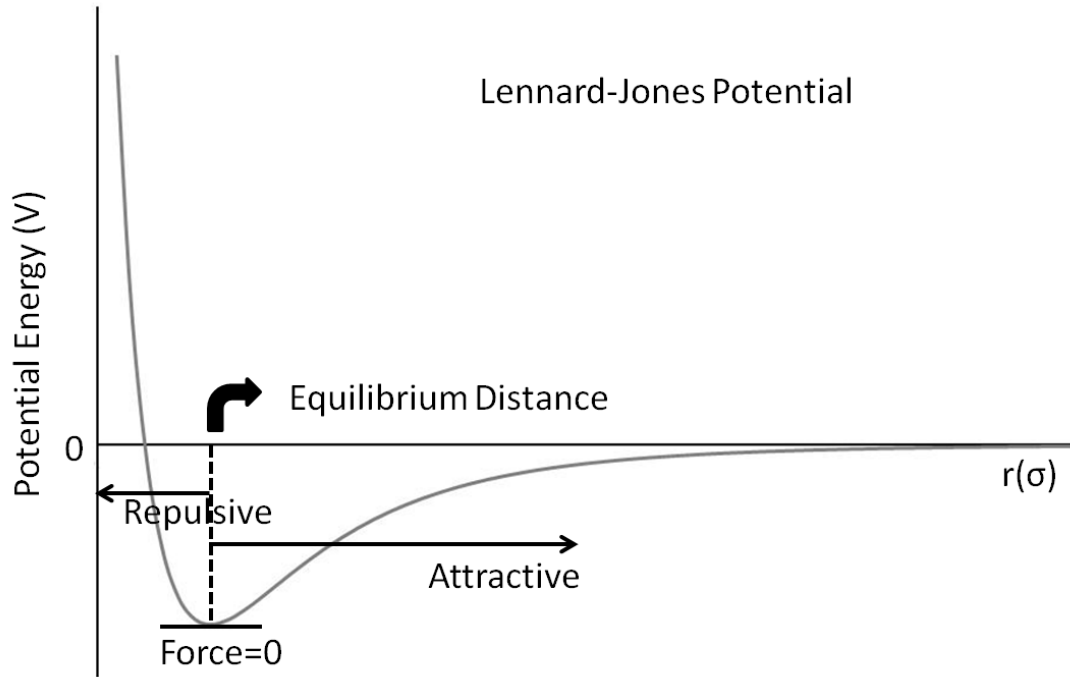


Figure 2-2. Lennard-Jones Potential

Polarization:

For a polar surface, which induces a dipole in the adsorbate molecule, the induction energy can be calculated as:

$$\phi_P = -\frac{1}{2}\alpha^2 F \quad (2.5)$$

where α is the polarizability, and F is the field strength at the center of the adsorbate [32].

Field-dipole interaction:

If the adsorbate molecule has a permanent dipole, μ , an interaction between electric field and a permanent dipole occurs. It could be approximated by [32]:

$$\phi_{FD} = -F\mu \cos \theta \quad (2.6)$$

where θ is the angle between the direction of the field and the axis of the dipole.

Field-quadrupole interaction:

If the adsorbate molecule possesses a quadrupole moment Q , an interaction can arise between the field gradient and this quadrupole moment. Such additional energy can be expressed as [32]:

$$\phi_{FQ} = \frac{1}{2} Q \dot{F} \quad (2.7)$$

where Q is the linear quadrupole moment, and \dot{F} is the electric field gradient.

The first two components ($\phi_D + \phi_R$) are effective in all adsorbate-adsorbent systems. However, the last three only arise from charges on the solid surface. For example, the contribution of ($\phi_D + \phi_R$) dominates in the case of activated carbon, while the electrostatic interactions dominate in the case of adsorbents, such as zeolites and ionic solids.

2.2.3 Equilibrium adsorption of single gas

The amount of gas which is adsorbed by a solid adsorbent depends on the equilibrium pressure, P , and the temperature, T . Such relation can be described as follows:

$$v = f(P, T) \quad (2.8)$$

where v can be expressed in cc STP/g. At a constant T , v is only a function of P , which is called an adsorption isotherm [31].

Figure 2-3 shows the BDDT classification of five types of isotherms observed to-date. Type I are characterized by a monotonic approach to a limit value conforming to a

complete monolayer surface coverage by a monolayer of adsorbed molecules. Type 2 depicts the case when first, a monolayer is formed, and then a multimolecular layer develops and becomes predominant. In Type 3, the lack of the flattish portion of the curve indicates that monolayer formation is missing, but formation of multimolecular layer still occurs. Type 4 and 5 are characteristic of capillary condensation of adsorbates in porous solids [36].

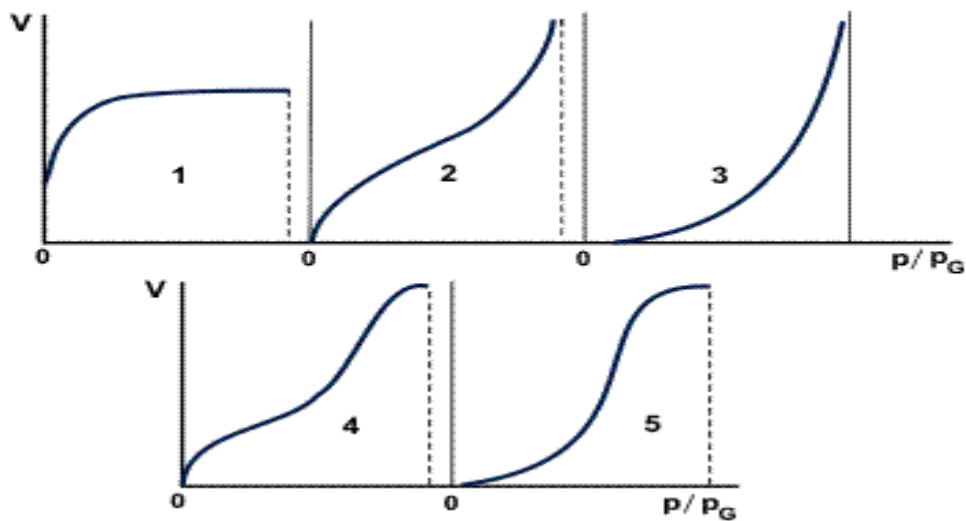


Figure 2-3. The five types of adsorption isotherms, according to the BDDT classification [37].

Here is the example of each type of adsorption isotherm [36]:

Type 1: Adsorption of nitrogen on clinoptilolite at 30 °C

Type 2: Adsorption of nitrogen on iron catalysts at -195 °C

Type 3: Adsorption of bromine on silica gel at 79 °C

Type 4: Adsorption of benzene on ferric oxide gel at 50 °C

Type 5: Adsorption of water on charcoal at 100 °C

Adsorption equilibrium information is the most important in understanding an adsorption process. Many contributions have been made in the past decade to develop

isotherm models for data correlation and design predictions for both pure component and multi-component adsorption.

Langmuir Equation

The simplest and still the most useful isotherm is the Langmuir isotherm. It was proposed by Langmuir in 1918 and is based on the concept of dynamic equilibrium that the rate of adsorption is equal to the rate of desorption [38].

Before deriving the Langmuir equation, several assumptions, listed below, should be made:

1. The surface is homogeneous (adsorption energy is constant over all the sites), and there is no interaction between neighboring adsorbates.
2. Adsorption on the surface is localized, which means the adsorbed molecule or atom is adsorbed at definite, localized sites.
3. Each site can only accommodate one molecule or atom.

Based on the kinetic theory of gas, the rate of striking the surface is given by:

$$R_s = \frac{P}{\sqrt{2\pi MR_g T}} \quad (2.9)$$

where M is the molar mass, R_g is the ideal gas constant, T is the temperature, and P is the pressure.

Allowing for the sticking coefficient α , the rate of adsorption on a bare surface can be written as:

$$R_a = \frac{\alpha P}{\sqrt{2\pi MR_g T}} \quad (2.10)$$

On an occupied surface, the rate of adsorption is equal to the rate given by (Equation 2.10) multiplied by the fraction of empty sites, which is:

$$R_a = \frac{\alpha P}{\sqrt{2\pi MR_g T}} (1 - \theta) \quad (2.11)$$

where θ is the fractional coverage.

The rate of desorption from the surface is equal to the rate, which corresponds to fully covered surface (k_d), multiplied by θ , that is:

$$R_d = k_d \theta = k_{d\infty} \exp\left(-\frac{E_d}{R_g T}\right) \theta \quad (2.12)$$

where E_d is the activation energy for desorption (equal to the heat of adsorption), and $k_{d\infty}$ is the rate constant for desorption at infinite temperature.

At dynamic equilibrium, $R_a = R_d$, we obtain the famous Langmuir equation:

$$\theta = \frac{bP}{1+bP} \quad (2.13)$$

where

$$b = \frac{\alpha \exp\left(\frac{E_d}{R_g T}\right)}{k_{d\infty} \sqrt{2\pi MR_g T}} = \frac{\alpha \exp\left(\frac{Q}{R_g T}\right)}{k_{d\infty} \sqrt{2\pi MR_g T}} = b_{\infty} \exp\left(\frac{Q}{R_g T}\right) \quad (2.14)$$

Here Q is the heat of adsorption and is also equal to the activation energy of desorption E_d . b_{∞} is the affinity constant, which can be described by:

$$b_{\infty} = \frac{\alpha}{k_{d\infty} \sqrt{2\pi MR_g T}} \quad (2.15)$$

When the pressure is very low ($bP \ll 1$), the Langmuir equation reduces to a linear type isotherm ($\theta = bP$), in which the amount of the adsorbed gas increases linearly with pressure. When pressure is sufficiently high, the amount of adsorbed gas reaches the saturation capacity ($\theta = 1$).

Toth Equation

Another popular empirical equation proposed by Toth describes well many systems with submonolayer coverage. Compared with other models, Toth model shows advantage at both low and high end of the pressure range. It can be described as [39-40]:

$$q_i = q_{i,m} \frac{b_i P}{[1+(b_i P)^t]^{1/t}} \quad (2.16)$$

where q_i is the amount of the adsorbed species i the amount of adsorbent solid, $q_{i,m}$ is the saturation adsorption capacity, b_i is the equilibrium constant or the Langmuir constant, and t is a parameter which is usually less than one.

When $t = 1$, the Toth equation reduces to the famous Langmuir equation

$$q_i = q_{i,m} \frac{b_i P}{1+b_i P} \quad (2.17)$$

As was pointed out by Do [40], t is a parameter that characterizes the system's heterogeneity. The more the parameter t deviates from unity, the more heterogeneous the system is.

Based on hundreds of verifications and comparison, the Toth equation is recommended as the first choice of isotherm fitting for adsorption of hydrocarbons, carbon dioxide, hydrogen sulfide on adsorbents such as activated carbon, and zeolites.

BET Equation

Under sub-critical conditions, multiple layers of adsorbate molecules are formed. Brunauer, Emmett and Teller (1938) were the first to develop an adsorption theory to account for multilayer adsorption [41].

Several assumptions were made by Brunauer et al. in the BET theory. They are similar to those made in Langmuir theory:

1. A flat surface has no limit to the number of layers which can be accommodated on the surface.
2. The surface is energetically homogeneous.
3. There is no interaction between the adsorbed molecules.
4. The heat of adsorption of the second and subsequent layers is the same and equal to the heat of liquefaction.
5. The ratio of the rate constants of the second and higher layers are equal to each other.

Based on these assumptions, the famous BET equation can be derived and described as following:

$$\frac{V}{V_m} = \frac{CP}{(P_0 - P) \left[1 + (C-1) \frac{P}{P_0} \right]} \quad (2.18)$$

where V is the adsorbed volume, P is the pressure in the fluid phase and P_0 is the vapor pressure.

This equation contains two fitting parameters: V_m and C . V_m is the monolayer volume, and C is an affinity constant for the adsorbate-adsorbent interaction. C can also be expressed as:

$$C = \frac{a_1 b_j}{b_1 a_j} e^{\frac{E_1 - E_L}{R_g T}} \quad (2.19)$$

where R_g is the ideal gas constant, T is the temperature, E_1 is the interaction energy between the solid and the adsorbate molecule in the first layer, E_L is the heat of liquefaction, a and b are both the rate constant, 1 and j indicate the number of layers from the surface.

Once the monolayer volume V_m is known, given the area occupied by one molecule, the surface area of the solid can be calculated. Due to this unique property of BET model, BET equation is extensively applied in porous solids surface area measurements.

To determine V_m , equation 2.18 can be expressed as follows:

$$\frac{P}{V(P_0 - P)} = \frac{1}{V_m C} + \left(\frac{C-1}{V_m C}\right) \frac{P}{P_0} \quad (2.20)$$

A plot of $\frac{P}{V(P_0 - P)}$ against $\frac{P}{P_0}$ would give a straight line with a slope s and y-intercept i , where:

$$s = \frac{C-1}{V_m C} \quad (2.21)$$

$$i = \frac{1}{V_m C} \quad (2.22)$$

$$V_m = 1/(s + i) \quad (2.23)$$

Once V_m is obtained, the surface area can be calculated by:

$$A = V_m N_A a_m \quad (2.24)$$

Where N_A is the Avogadro constant and a_m is the molecule's projected area.

2.2.4 *Equilibrium adsorption of gas mixture*

In the previous section, it is mentioned that the adsorption isotherm for single gas is very important for understanding and investigation of the adsorption process. However, in the real world, most adsorption systems usually involve more than one component. It is necessary to develop a method for predicting the adsorption equilibria of a gas mixture from the known adsorption isotherms of the pure components. Approaches such as extended Langmuir equation, the ideal adsorbed solution theory, the real adsorption solution theory, the vacancy solution theory and the potential theory have been proposed [40]. Detailed introduction of ideal adsorbed solution theory will be presented here.

Ideal adsorbed solution Theory (IAST) is the basis of solution thermodynamics. The mixed adsorbates are treated as a solution in equilibrium with the gas phase, and the adsorbed mixture is also treated as a two-dimensional phase [42].

IAST can be expressed as an analogue of Raoult's law for vapor-liquid equilibrium:

$$P y_i = P_i^0(\pi) x_i \quad (\text{constant } T) \quad (2.25)$$

where P is the total pressure of the gas-phase mixture, y_i is the composition of the component i in the gas phase, x_i is the composition of component i in the adsorbed phase, and $P_i^0(\pi)$ is the pure component hypothetical pressure which yields the same spreading pressure as that of the mixture.

From the Gibbs isotherm, the spreading pressure π can be calculated based on its

pure isotherm.

$$\pi_i = \frac{RT}{A} \int_0^{P_i^0} \frac{n_i^0(P)}{P} dP \quad (\text{constant } T) \quad (2.26)$$

Where $n_i^0(P)$ is the adsorption isotherm for pure component i , A is the area, R is the ideal gas constant, and T is the temperature.

The basic assumption of IAST is that the spreading pressures are equal for all components at the adsorption equilibrium, which is:

$$\pi_1 = \pi_2 = \dots = \pi_N \quad (2.27)$$

For a binary system, the IAST model consists of the following set of equations.

$$Py_1 = P_1^0(\pi)x_1 \quad (2.28)$$

$$Py_2 = P_2^0(\pi)x_2 \quad (2.29)$$

$$x_1 + x_2 = 1 \quad (2.30)$$

$$y_1 + y_2 = 1 \quad (2.31)$$

$$\int_0^{P_1^0} \frac{n_1^0(P)}{P} dP = \int_0^{P_2^0} \frac{n_2^0(P)}{P} dP \quad (2.32)$$

$$\frac{1}{n_t} = \frac{x_1}{n_1^0(P_1^0)} + \frac{x_2}{n_2^0(P_2^0)} \quad (2.33)$$

If the Langmuir isotherm is substituted, equation 2.32 can be written as:

$$q_{m1} \int_0^{P_1^0} \frac{b_1}{1+b_1P} dP = q_{m2} \int_0^{P_2^0} \frac{b_2}{1+b_2P} dP \quad (2.34)$$

And it could be analytically solved as:

$$q_{m1} \ln (1 + b_1 P_1^0) = q_{m2} \ln (1 + b_2 P_2^0) \quad (2.35)$$

2.2.5 Henry's law and selectivity

At very low pressure, the Langmuir equation reduces to:

$$\theta \left(= \frac{q}{q_m} \right) = bP \quad , \quad q = KP \quad (2.36)$$

$$K = q_m b = q_m b_\infty \exp \left(\frac{Q}{R_g T} \right) \quad (2.37)$$

$$K \propto \exp \left(\frac{Q}{R_g T} \right) \quad (2.38)$$

in which, the adsorption q is proportional to the pressure. It is known as Henry's law, and K here is known as Henry's law constant. All isotherms should reduce to the Henry's law form at extreme dilute condition. Such relation can be illustrated by classical isotherms of N₂, Ar, and O₂ on Ag-Mordenite as shown in Figure 2-4.

For a given adsorbent, the relative strength of adsorption of different adsorbate molecules depends on the relative magnitudes of the polarizability, dipole moment, and quadrupole moment of each. Selectivity is widely used to reflect the difference between the relative strength of adsorption.

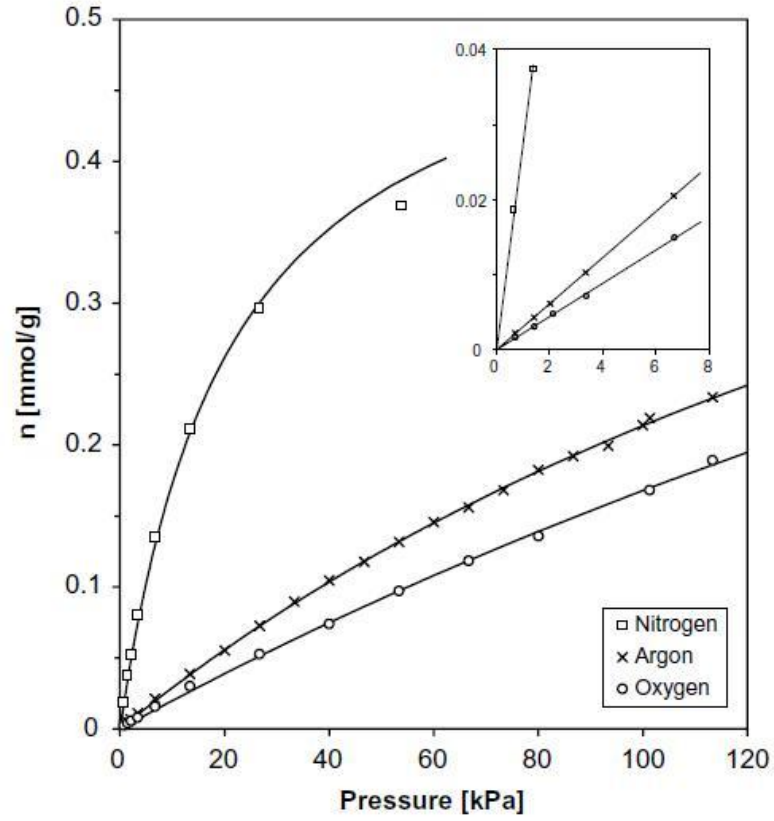


Figure 2-4. Nitrogen, argon and oxygen adsorption isotherms at 30 °C on Ag-mordenite [43].

Figure 2-4 shows typical adsorption isotherms of nitrogen, argon, and oxygen on silver mordenite at ambient condition. It can be seen that the isotherms reduce into a linear shape at the zero pressure zone. The selectivity of A over B in the Henry's law region (or at zero loading), α , is defined as the ratio of the Henry's law constant of A and B, which is exactly the ratio of slopes of the isotherm at low pressure.

$$\alpha_B^A = \frac{K_A}{K_B} \quad (2.39)$$

so,

$$\alpha_B^A \propto \exp\left(\frac{Q_A - Q_B}{R_g T}\right) \quad (2.40)$$

Such limiting selectivity could also be predicted by inverse-phase gas chromatography (IGC). For a given IGC chromatograph as in Figure 2-5, α can be defined as:

$$\alpha_B^A = \frac{t_A - t_o}{t_B - t_o} \quad (2.41)$$

Where t_A and t_B are the retention times of component A and B, while t_o is the dead time.

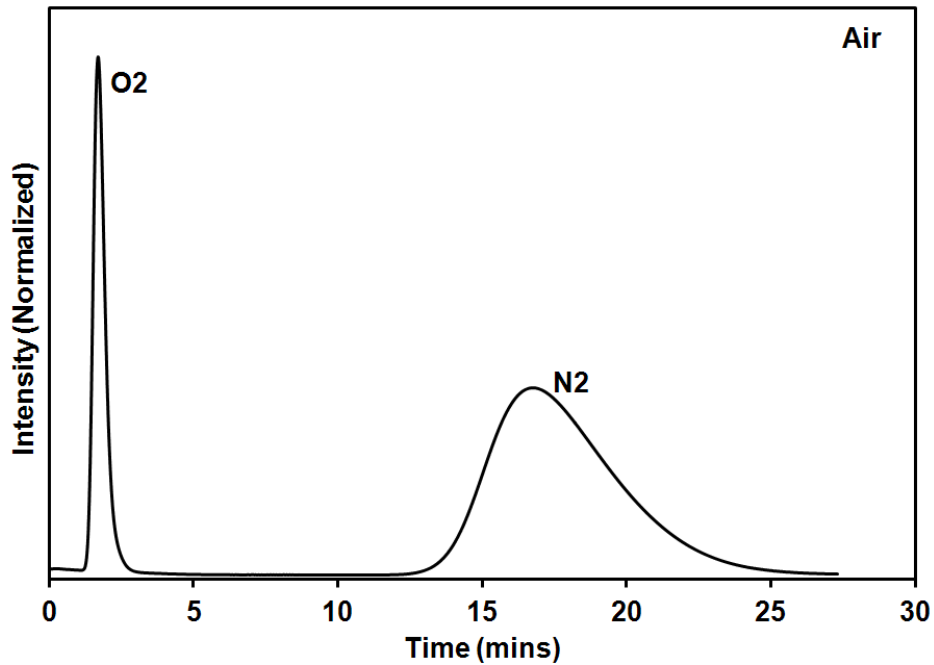


Figure 2-5. Inverse gas chromatography of O₂ and N₂ on Ag-ETS-10 at 30 °C [44].

In a two-component mixture system, the relative selectivity or separation factor can be obtained from the equilibrium gas phase composition and the composition of the adsorbed phase. The separation factor α for A over B can be defined by the following equation:

$$\alpha = \frac{y_A/y_B}{x_A/x_B} \quad (2.42)$$

Where y_A and y_B are the compositions of the adsorbed phase for A and B respectively and x_A and x_B are the gas phase composition.

2.2.6 Heat of adsorption

Since $G \equiv H - T$, when the temperature T is constant, we obtain the following thermodynamics equation:

$$\Delta G = \Delta H - T\Delta S \quad (2.43)$$

During the adsorption, molecules in the adsorbed phase are more ordered than in the gas phase (a decrease in the degree of freedom), so $\Delta S < 0$. Physical adsorption, in order to be a spontaneous thermodynamics process must have a negative ΔG . From the thermodynamics equation, we can demonstrate that physical adsorption processes are exothermic ($\Delta H < 0$), ie, they release heat [45-46].

The knowledge of the energetics of the gas adsorption process is critical because it helps to understand the binding behavior of a gas to the adsorbent. The relevant heat of adsorption of a gas is called “isosteric heat of adsorption” which is defined by the Clausius-Clapeyron relationship [46]:

$$q_{st} = RT^2 \left(\frac{\partial \ln P}{\partial T} \right)_n \quad (2.44)$$

This equation can be used to calculate q_{st} as a function of n and T for pure gas adsorption from the experimentally measured isotherms of the gas at different temperatures. A plot of $\ln P$ against $1/T$ at constant n yields a straight line with a slope equal to $\frac{q_{st}}{R}$ for pure gas adsorption.

Application of equation 2.44 to the Henry’s law region for a pure gas yield:

$$q^* = -RT^2 \left[\frac{d \ln K(T)}{dT} \right] \quad (2.45)$$

where q^* is the isosteric heat of adsorption at zero loading. Equation 2.45 can be integrated in the equation below.

$$K(T) = a \cdot \exp \left(\frac{q^*}{RT} \right) \quad (2.46)$$

where a is the integration constant. This equation is the same as the one obtained previously (equation 2.38).

2.2.7 Separation mechanism

Adsorptive separation is based on three distinct mechanisms: equilibrium, steric, and kinetic mechanisms [31]. The following is a brief explanation of these mechanisms.

Thermodynamic equilibrium effect

Selectivity results from differences in the adsorption strengths and is driven by the laws of electrostatics and thermodynamics. The controlling factors of the adsorption are adsorbate polarizability and the charge exposure of the sieve sites.

An example of thermodynamic equilibrium separation is the separation of ethylene and ethane by the titanosilicate ETS-10 [47]. The pore size of ETS-10 has an average kinetic diameter of 8 Å, which is larger than the molecular diameters of both ethylene and ethane (4.163 Å and 4.443 Å, respectively). Since both species may enter into the crystalline lattice, separation of ethylene and ethane by ETS-10 would be based on equilibrium competitive adsorption.

Steric effect

The selectivity of molecular exclusion (steric separation) results from differences in molecular/pore size and can be quasi-equilibrium. The steric effect is driven by the molecular sieving property of zeolites.

In the case of steric separation, only small and properly shaped molecules can diffuse into the adsorbent, whereas other molecules are completely excluded. This mechanism is unique to zeolitic materials since these materials possess uniform aperture size in their crystalline structure.

The application of zeolite 3A on ethanol drying is a good example of steric separation adsorption [48]. The water molecule is smaller than 3 Å, while the ethanol molecule is larger than 3 Å. The pore size of titanosilicate ETS-4 (3~5 Å) can be tuned by ion exchange and barium-exchanged ETS-4 was applied on nitrogen (3.6 Å) and methane (3.8 Å) separation. Such separation also, proved to be based on the steric mechanism [49].

Kinetic effect

Kinetic separation results from differences in the adsorption rates and transition. In such separation systems, the adsorbent possessing a distribution of pore sizes will allow different gases to diffuse at different rates while completely avoiding exclusion of any of the gases in the mixture.

For example, carbon molecular sieve (CMS) is used for nitrogen production from air [50]. Such a kinetic separation is achieved due to the difference between the kinetic diameters of nitrogen and oxygen, which making oxygen have a relatively higher diffusivity. Recently, Lee reported that separation of propene and propane could be accomplished by metal-organic frameworks (MOF) based on a kinetic separation mechanism [51]. The controlling diffusion rates in such plate-shaped crystals was achieved by tuning of the pore apertures and crystallite aspect ratios.

2.3 Adsorption Characterization

2.3.1 Inverse gas chromatography (IGC)

Inverse-phase gas chromatography (IGC) is a materials characterization technique that is used for the determination of sorption properties of gases. Traditional gas chromatography (GC) is an analytical technique. In traditional GC, the mobile phase is a carrier gas, such as helium, and the stationary phase is some solid adsorbent inside metal tubing (called “standard column”). Such a standard column is used to separate and characterize several gases (or vapors). However, in IGC, the roles of the stationary (solid) and mobile (gas) phases are inverted. A single gas (or vapor) is injected into a column packed with the solid sample under investigation.

During an IGC experiment, a pulse or constant concentration of gas is injected down the column at a fixed carrier gas flow rate. The retention behavior of the pulse or concentration front is then measured by a detector, such as a thermal conductivity detector (TCD). Such experiment is typically carried out at infinite dilution where only small amounts of the probe molecule are injected. It is also called Henry’s law region. In this infinite dilute condition, probe-probe interaction is negligible and only probe-solid interactions are considered. A fundamental property measured by IGC is known as the retention volume, V_N , which reflects how strongly the probe molecule interacts with the solid. Many other properties can be derived from V_N , such as, the Henry constant, the limiting selectivity, and the heat of adsorption. The retention volume V_N is obtained from the retention time using the following equation [52]:

$$V_N = F \cdot (t_R - t_o) \cdot j \cdot \left(1 - \frac{p_w}{p_o}\right) \cdot \frac{T}{T_R} \quad (2.47)$$

Where j is derived by

$$j = \left(\frac{3}{2}\right) \left[\frac{\left(\frac{p_i}{p_o}\right)^2 - 1}{\left(\frac{p_i}{p_o}\right)^3 - 1} \right] \quad (2.48)$$

F is the carrier gas flow rate, t_R is the retention time, t_o is the dead time (retention time for a non-interaction probe), p_i and p_o are the column inlet and outlet pressures, p_w is the water vapor pressure at room temperature T_R , and T are the column temperatures.

The retention time per gram of an adsorbent (specific retention volume, V_m) is given by:

$$V_m = V_N/m \quad (2.49)$$

where m is the weight of the adsorbent packed in the column. Because the IGC experiment occurs in the Henry's law region, by using the ideal gas law, V_m can be converted to the initial slope of K (Henry constant) of the isotherm:

$$K = V_m/RT \quad (2.50)$$

where R is the ideal gas constant, and T is the GC column temperature.

The selectivity of A over B at zero loading can be obtained by:

$$\alpha_B^A = \frac{K_A}{K_B} = \frac{V_m(A)}{V_m(B)} = \frac{t_A - t_o}{t_B - t_o} \quad (2.51)$$

The heat of adsorption of A at zero loading can be derived by:

$$q_A^* = R \left[\frac{d \ln K}{d \left(\frac{1}{T}\right)} \right] = R \left[\frac{d \ln \left(\frac{V_m}{T}\right)}{d \left(\frac{1}{T}\right)} \right] = R \left[\frac{d \ln(t_A - t_o)}{d \left(\frac{1}{T}\right)} \right] \quad (2.52)$$

Both of these two properties are related to the retention volume and the retention time.

2.3.2 Volumetric isotherm measurement

The adsorption isotherm is generally determined by one of two methods. The first method, the gravimetric method measures the amount of gas or vapor adsorbed by weighing the sample in a closed system on a balance. The second method, the volumetric method, determines the quantity of gas present in the system by measurement of the volume of the adsorbed gas [53]. Below is a description of the second method which was frequently used in this dissertation.

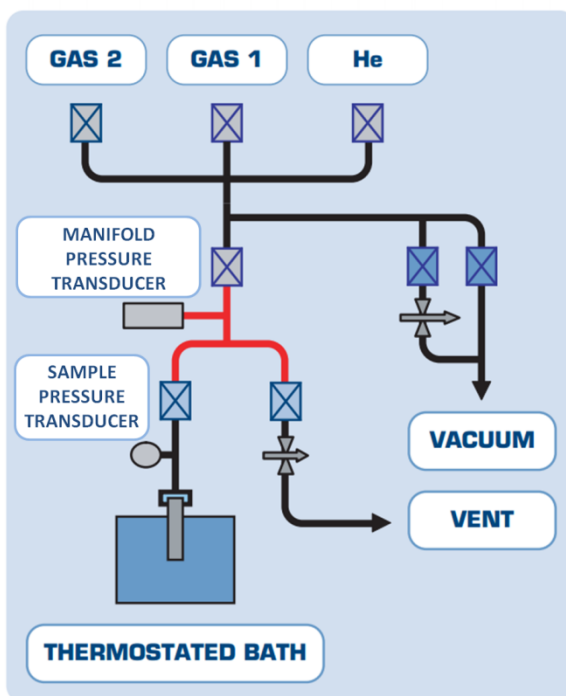


Figure 2-6. Schematic of HPVA high-pressure volumetric adsorption analyzer [54].

Figure 2-6 simply shows a System Schematic of HPVA high pressure volumetric adsorption analyzer, from which we can see that a classical volumetric set-up is usually made up of 5 important parts: a manifold, a pressure transducer, a vacuum

system, a constant temperature bath, and an activation unit. The general principle of the volumetric method is illustrated in Figure 2-7. The volumetric technique consists of introducing (dosing) a known amount of gas (adsorbate) into the chamber containing the sample to be analyzed. When the sample reaches equilibrium with the adsorbate gas, the initial and final equilibrium pressures are recorded. This data is then used to calculate the volume of the gas adsorbed by the sample. This process is repeated at given pressure intervals until the maximum pre-selected pressure is reached. Each of the resulting equilibrium points (volume adsorbed and equilibrium pressure) is then plotted to generate an isotherm.

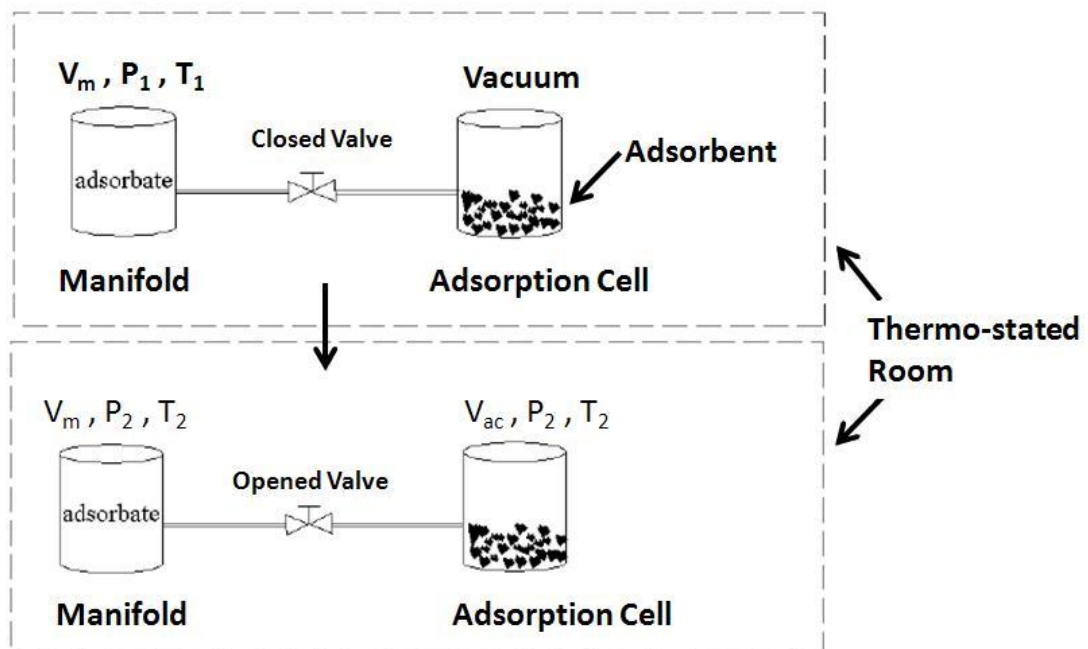


Figure 2-7. General principle of the volumetric isotherm apparatus [53].

The volumes of both manifold and adsorption cell (V_m, V_{ac}) are known. Each measurement of the total quantity of gas admitted into the system (n_1), and of the amount of gas remaining in the gas phase (V_m and V_{ac}) at the adsorption equilibrium (n_2) is determined by the real gas equation of state before and after adsorption. The amount adsorbed is calculated by a mass balance on the gas phase before and after adsorption.

The calculations are given by equation 2.53 to 2.55:

$$n_1 = \frac{V_m}{v_a(T_1, P_1)} \quad (2.53)$$

$$n_2 = \frac{V_m + V_{ac}}{v_a(T_2, P_2)} \quad (2.54)$$

$$n_{ads} = \frac{n_1 - n_2}{m_{sample}} \quad (2.55)$$

Where: n_1 is the adsorbate mole number in the manifold before the adsorption, n_2 is the adsorbate mole number remaining in the gas phase after the adsorption, P_1 is the pressure in the manifold before the adsorption, P_2 is the equilibrium pressure in both manifold and adsorption cell after the adsorption, $T_1 = T_2$ is the experimental temperature of this thermo-stated environment, $v_a(T, P)$ is the molar volume of the adsorbate in the gas phase at temperature T and pressure P , and it is calculated by real gas equation of state, m_{sample} is the mass of the outgassed adsorbent, and n_{ads} is the adsorbed mole number per unit of mass of the outgassed adsorbent.

2.4 Pressure/Temperature Swing Adsorption

Desorption, contrary to adsorption, is thermodynamically favored at low pressure and high temperature. Figure 2-8 shows how the adsorbent loading is reduced by either a pressure reduction (pressure swing) or by an increase in temperature (temperature swing) [55].

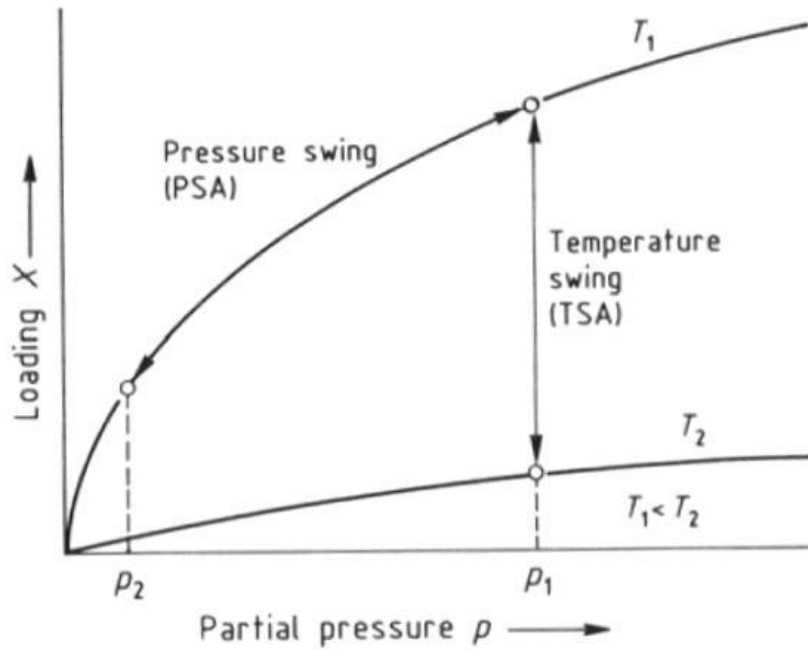


Figure 2-8. Mechanisms of PSA and TSA process

Based on these mechanisms, we define pressure swing adsorption (PSA) and temperature swing adsorption (TSA), two of the most commonly used adsorption processes for gas separation.

In a typical pressure swing adsorption cycle, each bed goes through the following five basic steps: (I) pressurization, (II) adsorption, (III) concurrent blowdown, (VI) countercurrent blowdown, and (V) purge. Usually two or more interconnected beds are operated so that a continuous feed and products are possible. Figure 2-9 shows a two-bed PSA system for continuous bulk separation of air [56-57].

In step I, bed one is pressurized to the feed pressure by the feed (or by the blowdown gases, which are the least adsorbed gases from the other bed). In step II, the high pressure feed flows through bed one while a portion of the effluent O₂ product is used to purge bed two at reduced pressure. Step III, concurrent blowdown, is used to recover the O₂ remained in the voids and to allow time for N₂ to desorb in the bed. Steps IV and V are both operated countercurrent to the feed direction to produce N₂ and provide a clean bed for the next cycle. The performance of a PSA process is

determined by three interrelated sets of results: product purity, product recovery, and productivity.

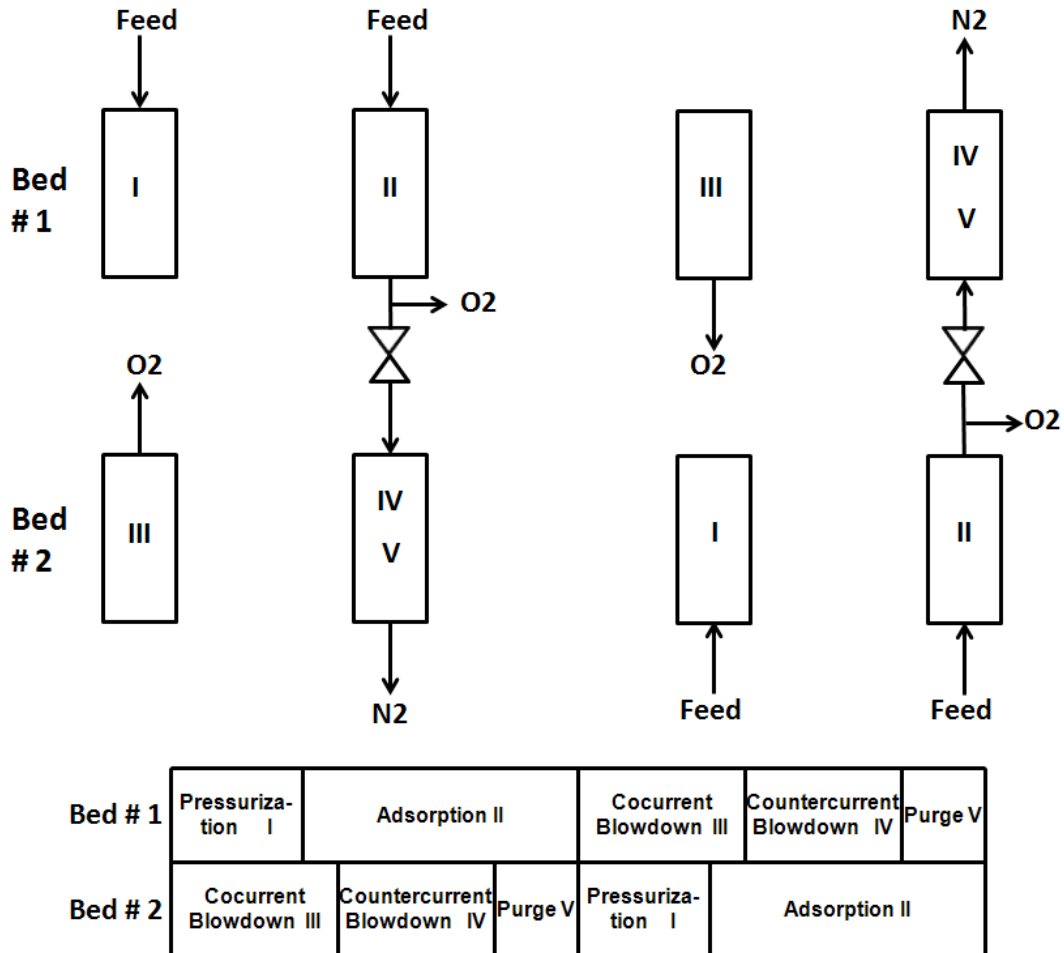


Figure 2-9. Five Steps of a two-bed PSA process.

Figure 2-10 is a schematic representation of the TSA (temperature swing adsorption) process [34]. For a given partial pressure of the adsorbate in the gas phase, an increase in temperature leads to a decrease in the quantity adsorbed. If the partial pressure remains constant at P_1 , increasing the temperature from T_1 to T_2 will decrease the equilibrium loading from X_1 to X_2 . A relatively modest increase in temperature can affect a relatively large decrease in loading. It is therefore generally possible to desorb any components provided that the temperature is high enough. In a TSA process cycle, two steps occur during regeneration: heating and purging. Heating provides energy to

raise the temperature of the system, desorb the adsorbed gas, and make up for heat losses. Passage of a hot purged gas or steam through the bed to sweep out the desorbed components is always used in conjunction with the increase in temperature.

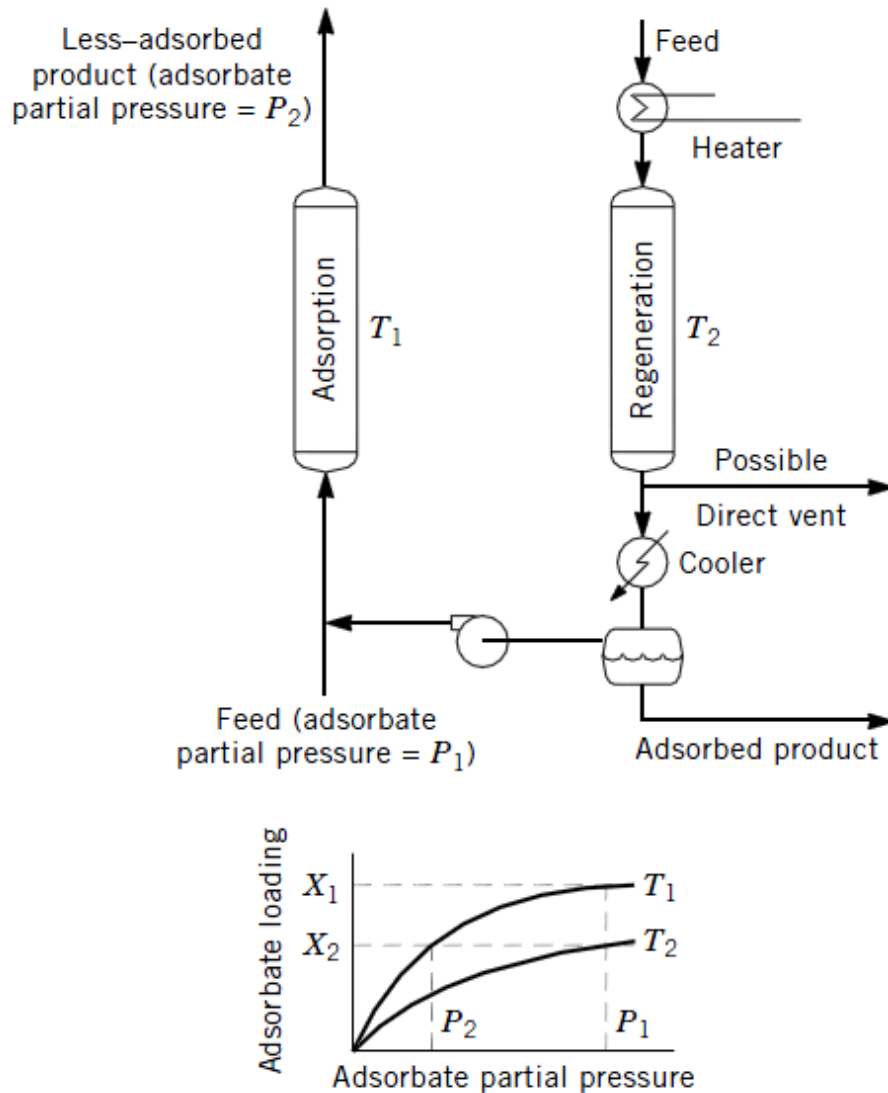


Figure 2-10. Schematic of TSA cycle

The use of the pressure swing adsorption process has seen tremendous growth during the last decades mainly due to its simplicity and low operating costs. Its principal application is for bulk separations where contaminants are present at high concentration. Major applications have been the recovery of high purity hydrogen from raw gas, such as synthesis gases from steam reforming, partial oxidation or gasification processes, as well as refinery off-gases, ethylene off-gas, coke oven gas,

methanol and ammonia purge-gases as well as the generation of nitrogen and oxygen. In addition, it has gained significance for the bulk removal of carbon dioxide in direct reduction plants in the iron-making industry [58].

The principal application of TSA is for separations in which contaminants are present at low concentration, i.e., drying compressed air and natural gas, as well as carbon dioxide stripping from air. Table 2-2 is a summary of applications for PSA and TSA.

Table 2-2. Applications of PSA and TSA processes.

Process	Adsorbent	Applications
<i>PSA</i>	CMS	Nitrogen Generation [59]
	AgLiLSX	Oxygen Generation [60]
	Zeolite 5A	Hydrogen/CO ₂ [61]
	Ba-ETS-4	Methane/Nitrogen[62]
<i>TSA</i>	Zeolite 13X	CO ₂ Capture [63]
	ZrO ₂ -based oxides	Removal of NO _x [64]
	Activated Carbon	Removal of VOC from air [65]
	Co-ZSM-5	SO ₂ removal from flue gases [66]

2.5 Microwave Assisted Regeneration

Microwaves refer to the electromagnetic waves between 300 MHz and 300 GHz, with a corresponding wavelength between 1 m and 1 mm. The waves obey the laws of optics and so can be transmitted, absorbed and reflected by a material. According to the interaction with the microwaves, materials could be classified into three groups: conductors (metals and alloys), insulators (glasses, ceramics, and Teflon) and absorbers (aqueous solution and polar solvent). According to the illustration in Figure 2-11, conductors are materials on which microwaves are reflected and cannot

penetrate; insulators are materials which are substantially transparent to the microwaves; and absorbers are materials which absorb microwave radiation, direct energy transfer, and are termed as dielectrics [67-69].

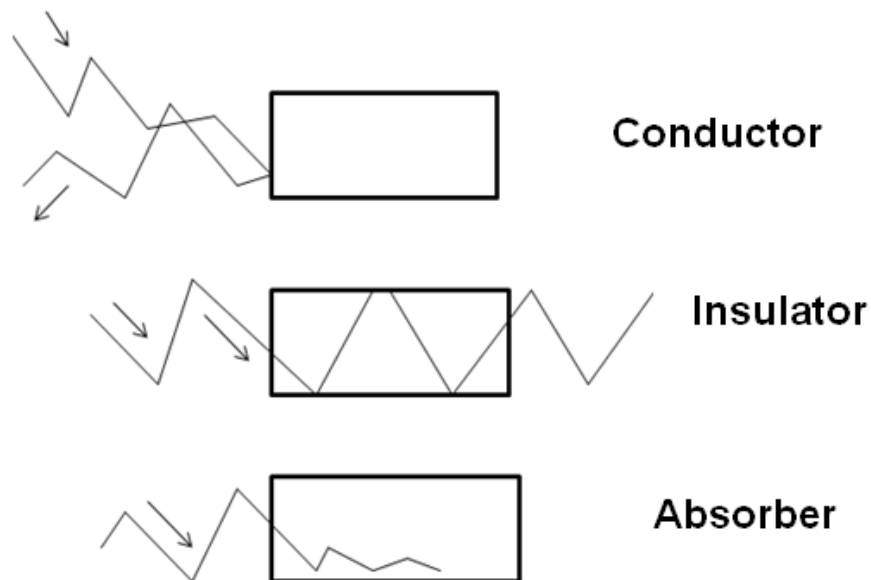


Figure 2-11. Materials classification due to interaction with microwave

When microwaves are applied to the dielectric materials with an oscillating electric field, the dipoles within the materials will attempt to realign themselves and flip around the applied field. This dipole movement generates friction inside dielectric materials and the internal energy is dissipated as heat. Molecules with a symmetric charge distribution are non-polar, have a very small dipole moment, and exhibit limited absorption of microwaves. In contrast, water and a wide range of organic compounds are polar and since they have charge asymmetry they have large dipole moments and absorb microwave energy [70].

Although microwave heating was initially used for rapid heating of food, its unique selectivity and fast heating rate proved to be useful in other applications such as industrial drying [68-69]. In a conventional thermal regeneration process, the thermal

energy is transferred from the surface to the bulk of the material. Such heating conduction and/or convection can easily establish a temperature gradient in the material until conditions of steady state are reached. By contrast, in the microwave heating process, heat is produced internally within the material instead of originating from external sources, and the energy is directly transferred to the adsorbate molecules in the interfacial region where it is needed. Consequently, microwave heating makes it possible to regenerate adsorbents very rapidly and efficiently.

2.6 References

- [1] Rabo, J.A., Schoonover, M.W., 2001. *Applied Catalysis A: General* 222, 261-275.
- [2] Flanigen, E.M., 1980. *Pure & Appl. Chem.* 52, 2191-2211.
- [3] Bhatia, S., 1989. *Zeolite Catalysts: Principle and Applications*. CRC Press, Boca Raton, Florida.
- [4] Barrer, R.M., 1978. *Zeolites and Clay Minerals as Sorbents and Molecular Sieves*. Academic Press
- [5] Baerlocher, Ch., McCusker, L.B., Olson, D.H., 2007. *Atlas of Zeolite Framework Types, 6th Edition*. Elsevier Science.
- [6] Breck, D.W., 1974. *Zeolite Molecular Sieves: Structure, Chemistry, and use*. John Wiley & Sons Inc., New Jersey.
- [7] Ackley, M.W., Rege, S.U., Saxena, H., 2003. *Microporous and Mesoporous Materials* 61, 25-42.
- [8] Dyer, A., 1988. *An Introduction to Zeolite Molecular Sieves*. John Wiley and Sons Inc., New York.
- [9] Robinson, S.M., Arnold, W.D., Byers, C.H., 2004. *AIChE Journal* 40, 2045-2054.
- [10] Curkovic, L., Cerjan-Stefanovic, S., Filipan, T., 1997. *Water Research* 31, 1379-1382.
- [11] Szostak, R., 1989. *Molecular Sieves: Principles of Synthesis and Identification*. Blackie Academic & Professional, London, UK.
- [12] Davis, M.E., Lobo, R.F., 1992. *Chemistry of Materials* 4, 756-768.
- [13] Mer'kov, A.N., Bussen, I.V., Goyko, Ye.A., Kul'chitskaya, Ye.A., Men'shikov, Yu.P., Nedorezova, A.P., 1973. *International Geology Review* 15, 1087-1094.

- [14]Kuznicki, S.M., 1989. *Large-pored crystalline titanium molecular sieve zeolites*.
US Patent No. 4,853,202.
- [15]Anderson, M.W., Terasaki, O., Ohsuna, T., Philippou, A., Mackay, S.P., Ferreira, A., Rocha, J., Lidin, S., 1994. *Nature* 367, 347-351.
- [16]Choi, J.H., Kim, S.D., Kwon, Y.J., Kim, W.J., 2006. *Microporous and Mesoporous Materials* 96, 157-167.
- [17]Zhao, G.X.S., Lee, J.L., Chia, P.A., 2003. *Langmuir* 19, 1977-1979.
- [18]Al-Attar, L., Dyer, A., Blackburn, R., 2004. *Journal of Radioanalytical and Nuclear Chemistry* 246, 451-455.
- [19]Pavel, C.C., Popa, K., Bilba, N., Cecal, A., Cozma, D., Pui, A., 2003. *Journal of Radioanalytical and Nuclear Chemistry* 258, 243-248.
- [20]Dorskocil, E.J., 2004. *Microporous and Mesoporous Materials* 76, 177-183.
- [21]Gervasini, A., Picciau, C., Auroux, A., 2000. *Microporous and Mesoporous Materials* 35, 457-469.
- [22]Philippou, A., Anderson, M.W., 2000. *Journal of Catalysis* 189, 395-400.
- [23]Philippou, A., Naderi, M., Pervaiz, N., Rocha, J., Anderson, M.W., 1998. *Journal of Catalysis* 178, 174-181.
- [24]Nash, M.J., Lobo, R.F., Doren, D.J., 2009. *Applied Catalysis B: Environmental* 88, 232-239.
- [25]Uma, S., Rodrigues, S., Martyanov, I.N., Klabunde, K.J., 2004. *Microporous and Mesoporous Materials* 67, 181-187.
- [26]Gallo, M., Nenoff, T.M., Mitchell, M.C., 2006. *Fluid Phase Equilibria* 247, 135-142.

- [27] Anson, A., Lin, C.C.H., Kuznicki, T.M., Kuznicki, S.M., 2010. *Chemical Engineering Science* 65, 807-811.
- [28] Tiscornia, I., Irusta, S., Tellez, C., Coronas, J., Santamaria, J., 2008. *Journal of Membrane Science* 311, 326-335.
- [29] Kuznicki, S.M., Anson, A., Koenig, A., Kuznicki, T.M., Haastrup, T., Eyring, E.M., Hunter, D., 2007. *The Journal of Physical Chemistry C* 111, 1560-1562.
- [30] Wikipedia. <http://en.wikipedia.org/wiki/Adsorption> (accessed April 16, 2012)
- [31] Yang, R.T., 1987. *Gas Separation by Adsorption Processes*, Butterworth, Stoneham, MA.
- [32] Yang, R.T., 2003. *Adsorbents: Fundamentals and Applications*. John Wiley & Sons, Inc., Hoboken, New Jersey.
- [33] Ruthven, D.M., 2001. *Adsorption, Fundamentals*. *Kirk-Othmer Encyclopedia of Chemical Technology*, 582-617.
- [34] Yon, C.M., Sherman, J.D., 2003. *Adsorption, Gas Separation*. *Kirk-Othmer Encyclopedia of Chemical Technology*, 617-663.
- [35] http://chemwiki.ucdavis.edu/Physical_Chemistry/Quantum_Mechanics/Intermolecular_Forces/Lennard-Jones_Potential (accessed April 16, 2012)
- [36] Brunauer, S., Deming, L.S., Deming, W.E., Teller, E., 1940. *Journal of the American Chemical Society* 62, 1723-1732.
- [37] <http://www.thermopedia.com/content/292/> (accessed April 16, 2012)
- [38] Langmuir, I., 1918. *Journal of the American Chemical Society* 40, 1361-1403.
- [39] Toth, J., 2002. *Adsorption: Theory, Modelling, and Analysis*. Marcel Dekker, New York.

- [40]Do, D.D., 1998. *Adsorption Analysis: Equilibria and Kinetics*. Imperial College Press, London.
- [41]Brunauer, S., Emmett, P.H., Teller, E., 1938. *Journal of the American Chemical Society* 60, 309-319.
- [42]Myers, A.L., Prausnitz, J.M., 1965. *AIChE Journal* 11, 121-127.
- [43]Anson, A., Kuznicki, S.M., Kuznicki, T.M., Haastrup, T., Wang, Y., Lin, C.C.H., Sawada, J.A., Eyring, E.M., Hunter, D., 2008. *Microporous Meoporous Materials* 109, 577-580.
- [44]Shi, M., Kim, J., Sawada, J.A., Lam, J., Sarabadan, S., Kuznicki, T.M., Kuznicki, S.M., 2012. *Production of argon free oxygen by adsorptive air separation on Ag-ETS-10*, reviewed by *AIChE Journal*.
- [45]Myers, A.L., 2004. "Thermodynamics of Adsorption", Chapter 21 in *Chemical Thermodynamics for Industry*. Royal Society of Chemistry, Cambridge, UK.
- [46]Myers, A.L., 2002. *AIChE Journal* 48, 145-160.
- [47]Shi, M., Avila, A.M., Yang, F., Kuznicki, T.M., Kuznicki, S.M., 2011. *Chemical Engineering Science* 66, 2817-2822.
- [48]Fornoff, L.L., 1981. *Process for dehydrating ethanol and for the production of gasohol therefore*. US Patent No. 4,273,621.
- [49]Kuznicki, S.M., Bell, V.A., Nair, S., Hillhouse, H.W., Jacobinas, R.M., Braunbarth, C.M., Toby, B.H., Tsapatsis, M., 2001. *Nature* 412, 720-724.
- [50]Chen, Y.D., Yang, R.T., Uawithya, P., 1994. *AIChE Journal* 40, 577-585.
- [51]Lee, C.Y., Bae, Y.S., Jeong, N.C., Farha, O.K., Sarjeant, A.A., Stern, C.L., Nickias, P., Snurr, R.Q., Hupp, J.T., Nguyen, S.T., 2011. *Journal of the American Chemical Society* 133, 5228-5231.

- [52] Choudary, V.N., Jasra, R.V., Bhat, T.S.G., 1993. *Industrial & Engineering Chemistry Research* 32, 548-552.
- [53] Belmabkhout, Y., Frere, M., Weireld, G.D., 2004. *Measurement Science and Technology* 15, 848-858.
- [54] <http://www.micromeritics.com/Repository/Files/HPVA.pdf> (accessed April 16, 2012)
- [55] Bart, H., Gemmingen, U.V., 2005. *Adsorption. Ullmann's Encyclopedia of Industrial Chemistry*, 549-620.
- [56] Bhadra, S.J., 2007. *Methane-nitrogen separation by pressure swing adsorption*. M.Sc. Thesis, National University of Singapore.
- [57] Ruthven, D.M., Farooq, S., Knaebel, K.S., 1993. *Pressure Swing Adsorption*. Wiley-VCH.
- [58] http://www.linde-engineering.com/en/process_plants/adsorption_plants/index.html (accessed April 17, 2012)
- [59] Schulte-Schulze-Berndt, A., Krabiell, K., 1993. *Gas Separation & Purification* 7, 253-257.
- [60] Santos, J.C., Cruz, P., Regala, T., Magalhaes, F.D., Mendes, A., 2007. *Industrial & Engineering Chemistry Research* 46, 591-599.
- [61] Kim, W., Yang, J., Han, S., Cho, C., Lee, C., Lee, H., 1995. *Korean Journal of Chemical Engineering* 12, 503-511.
- [62] Butwell, K.F., Dolan, W.B., Kuznicki, S.M., 2001. *Selective removal of nitrogen from natural gas by pressure swing adsorption*. US Patent No. 6, 315, 817 B1.
- [63] Merel, J., Clause, M., Meunier, F., 2006. *Environmental Progress* 25, 327-333.

- [64]Machida, M., Yoshii, A., Kijima, T., 2000. *International Journal of Inorganic Materials* 2, 413-417.
- [65]Hwang, K.S., Choi, D.K., Gong, S.Y., Cho, S.Y., 1997. *Chemical Engineering Science* 52, 1111-1123.
- [66]Yukuhiro, T., Saburo, N., Hidetomo, N., Jun, I., Nobuyuki, O., Shigeo, U., 2001. *Kagaku Kogaku Ronbunshu* 27, 314-318.
- [67]Bradshaw, S.M., Wyk, E.J., Swardt, J.B., 1998. *The Journal of the South African Institute of Mining and Metallurgy* 07/08, 201-212.
- [68]Yuen, F.K., Hameed, B.H., 2009. *Advances in Colloid and Interface Science* 149, 19-27.
- [69]Jones, D.A., Lelyveld, T.P., Mavrofidis, S.D., Kingman, S.W., Miles, N.J., 2002. *Resources, Conservation and Recycling* 34, 75-90.
- [70]Hashisho, Z., 2007. *Microwave swing adsorption for the capture and recovery, or destruction for a more sustainable use of organic vapors*. Ph.D. Dissertation, University of Illinois at Urbana-Champaign.

Chapter 3

Production of Argon Free Oxygen by Adsorptive Air Separation on Ag-ETS-10

A version of this chapter has been published. Reproduced with permission from Shi, M., Kim, J., Sawada, J.A., Lam, J., Sarabadan, S., Kuznicki, T.M., Kuznicki, S.M. 2012, *AIChE J.* DOI:10.1002/aic.13879.

3.1 Summary

The purification of different components of air, such as oxygen, nitrogen, and argon, is an important industrial process. Pressure Swing Adsorption (PSA) is surpassing the traditional cryogenic distillation for many air separation applications, because of its lower energy consumption. Unfortunately, the oxygen product purity in an industrial PSA process is typically limited to 95% due to the presence of argon which always shows the same adsorption equilibrium properties as oxygen on most molecular sieves. Recent work investigating the adsorption of nitrogen, oxygen and argon on the surface of silver-exchanged Engelhard Titanosilicate-10 (ETS-10), indicates that this molecular sieve is promising as an adsorbent capable of producing high purity oxygen. In this work high purity oxygen (99+%) was generated using a bed of Ag-ETS-10 granules to separate air (78% N₂, 21% O₂, 1% Ar) at 25 °C and 100 kPa, with an O₂ recovery rate greater than 30%.

3.2 Introduction

The purification of different gases in air, such as nitrogen, oxygen and argon, is an important industrial process. Applications such as welding and cutting processes, plasma chemistry and laboratory applications require oxygen purity greater than 99%. Cryogenic air separation technology has long been used for producing high purity oxygen and nitrogen for industrial and medical applications [1], and is currently the most efficient technology when very large quantities of gas are required. The energetics and complexity of cryogenic distillation plants do not lend themselves well to point-of-use or on-demand high purity O₂ applications. PSA separation of O₂ is well suited to applications where intermittent, on-demand requirements cannot be met using bottled gas or liquid O₂ delivery. Current PSA systems cannot deliver greater than 95% O₂ due to limitations in conventional air separation adsorbents.

An air separation pressure swing adsorption (PSA) process uses zeolites as adsorbents, as they preferentially adsorb nitrogen to oxygen. The recovery of O₂ depends strongly on the adsorbent selected. Zeolites A and X have been used commercially as adsorbents for air separation [3-6]. A number of studies have investigated utilization of various zeolites such as Zeolite 5A and Zeolite 13X as adsorbents in PSA processes [4, 6]. In all the cases, the oxygen product purity is limited to 95% due to the presence of argon which has almost identical adsorption equilibrium properties as oxygen.

Another option to separate Ar from O₂ is by non-equilibrium methods. Another type of adsorbent, carbon molecular sieves (CMS), with a kinetic selectivity of oxygen over argon has been investigated and employed for production of purified oxygen and argon [7-11]. Ba-RPZ-3, a titanosilicate molecular sieve, was found to favor oxygen based on the sieving properties of the adsorbent and the difference in size between O₂ molecules and Ar atoms [12]. A two step experimental study was reported by Hayashi et al. where direct air feed using Ca-X zeolite was used in the first step, producing 95%

of oxygen and 5% of argon, and CMS is used in the second step to remove argon [13]. In both these studies, the O₂ is generated as the low pressure product and will require re-compression adding cost and complexity to the process.

The earliest report of remarkable selectivity of Ag exchanged zeolite X for the atmospheric gases was firstly pointed out by Harry Habgood fifty years ago [16]. After that, the unusual preference of silver mordenite for Ar over O₂ was also noted by Boniface in 1983[14]. Silver exchanged zeolite A [15], and silver exchanged Li-Na-LSX zeolite [17] have all been reported to show some degree of argon over oxygen selectivity. In 2003, Air Products and Chemicals Inc. reported that a vacuum and pressure swing adsorption unit using AgLiLSX adsorbent allows the production of 99% oxygen with a recovery of 15% [18].

In 2008, Kuznicki's group demonstrated that silver exchanged ETS-10, a mixed coordination titanosilicate molecular sieve, has an adsorptive selectivity for argon over oxygen [19]. The selectivity, reached 1.49 in Henry's region, is the highest selectivity reported to date for a silver-exchanged sieve.

This paper describes the adsorptive separation performance of Ag-ETS-10 for air at ambient condition on Ag-ETS-10 using a laboratory-scale demonstration unit. An adapted chromatographic method was developed to improve the quantification of O₂ and Ar in the product stream. The separation factor, breakthrough and desorption profiles are reported.

3.3 Experimental

3.3.1 Sample preparation

Na-ETS-10 was synthesized using conventional hydrothermal synthesis [20]. Preparation involved thoroughly mixing 50 g of sodium silicate (28.8% SiO₂, 9.14%

Na₂O, Fisher), 3.2 g of sodium hydroxide (97+% NaOH, Fisher), 3.8 g of KF (anhydrous, Fisher), 4 g of HCl (1 M), and 16.3 g of TiCl₃ solution (Fisher), stirring the mixture in a Waring blender for 1 h, and then transferring the reactants to a 125 cm³ sealed, teflon-lined autoclave (PARR Instruments) and heating at 215 °C for 64 h. The material was then thoroughly washed with de-ionized water, and dried in oven at 100 °C. The ETS-10 adsorbent was ion exchanged by adding 5 g of ETS-10 to 10 g of silver nitrate (Fisher, USP) in 50 g of deionized water. The mixture was heated to 80 °C for 1 h. The silver exchanged material was filtered, washed with deionized water and the exchanged procedure was repeated two more times (for a total of three exchanges). The silver exchanged ETS-10 was dried at 80 °C in air. Ag-ETS-10 materials were pelletized by mixing 6 g of the molecular sieve with 2.5 g of Ludox HS-40 colloidal silica (Aldrich). The mixture was homogenized using a mortar and pestle and compressed in a pellet press at 69,000 kPa for 3 min. The resulting cakes were crushed and sieved to obtain particles (sieve size between 0.85-1.68 mm). The pelletized, crushed and sieved materials were used in both gas chromatographic and column separation experiments.

3.3.2 Characterization

Inverse-phase gas chromatography (IGC) analysis was performed on a Varian 3800 gas chromatograph (GC) equipped with a thermal conductivity detector (TCD). Test adsorbents were packed into 10-inch copper columns with OD of 6.35 mm. The columns were filled with 4 g pelletized adsorbent (sieve size between 0.368-1.04 mm), which was activated at 200 °C for 10 h under a helium flow of 30 cm³/min. Analysis gases (Ar, O₂, 50/50 mixture of O₂-Ar, and air) were introduced by 1 cm³ pulse injections into the column at 30 °C.

Low pressure adsorption isotherms (up to 100 kPa) for nitrogen, oxygen and argon on crystalline adsorbent powders were measured volumetrically at 25 °C using an AUTOSORB-1-MP from Quantachrome Instruments (Boynton Beach, FL). No binders or diluents were added to the adsorbent samples. Samples were activated at

200 °C for 10 h under vacuum (<0.00005 kPa). Experimental isotherms were fitted to the Langmuir adsorption isotherm (Eq. 3.1):

$$\frac{q_i}{q_{i,m}} = \frac{b_i P_i}{1 + b_i P_i} \quad (3.1)$$

with the standard deviations (σ Eq.3.2):

$$\sigma = \sqrt{\frac{\sum(n_{exp} - n_{calc})^2}{N-2}} \quad (3.2)$$

where q_i is the amount adsorbed on the solid, P_i represents the pressure in the gas phase, $q_{i,m}$ is the saturation or maximum adsorption capacity, and b_i is the Langmuir (equilibrium) constant. n_{exp} is the experimentally measured adsorption at pressure P , n_{calc} is the adsorption calculated from the Langmuir equation at the same pressure. N is the number of measured experimental points. The Henry's Law constants $K_i = q_{i,m} b_i$, for each component were used to calculate the limiting selectivity of A over B (α Eq.3.3):

$$\alpha = \frac{K_A}{K_B} \quad (3.3)$$

3.3.3 Gas chromatographic separation and determination of argon and oxygen in air by Ag-ETS-10

Traditional chromatographic packings do not resolve the O₂ and Ar elution peaks very well and a significant amount of overlap between the two components is typical. As this work aims to generate O₂ of purity greater than 99.5%, the quantification of minor amounts of Ar was necessary. A chromatographic method that enhances the resolution between the two elution peaks was developed for this work.

A Varian 3800 gas chromatograph (GC) equipped with a thermal conductivity detector (TCD) was adapted to operate at cryogenic temperature. The method used Ag-ETS-10 granules packed into 50.8 cm copper columns having an OD of 6.35 mm. The columns were filled with 8 g pelletized adsorbent (sieve size between 0.368-1.04 mm), which was activated at 200 °C for 10 h under a helium flow of 30 cm³/min. After activation, the 50.8 cm column was dipped in an ethanol and dry ice solution which maintains the column at a temperature close to -78 °C. Analysis gases (Ar, O₂, 50/50 mixture of O₂-Ar, and 95/5 O₂-Ar) were introduced by 1 cm³ pulse injections into the column.

3.3.4 Laboratory-scale demonstration

Laboratory-scale demonstration is illustrated in Figure 3-1. Breakthrough experiments were performed using 130 g samples of pelletized, crushed, and sieved test adsorbents. The adsorbent was packed into a 150 cm³ cylindrical stainless steel chamber with an inner diameter of 20 mm and a length of 450 mm. The columns packed with adsorbent pellets were activated at 200 °C for 10 h under 100 cm³/min of helium flow.

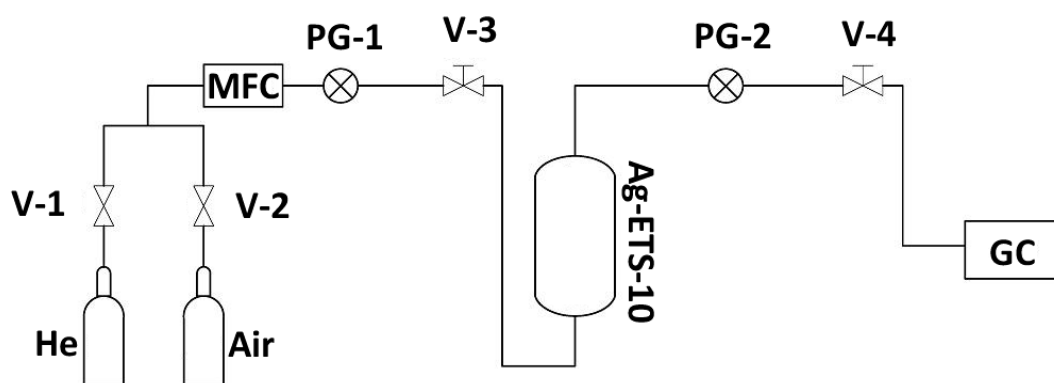


Figure 3-1. Schematic of one stage process for air separation on Ag-ETS-10.

The breakthrough experiments were run by conditioning the bed at 100 kPa with helium to purge any adsorbed gas from the system. The column temperature was maintained at 25 °C using a water jacket around the bed coupled to a circulating water bath. Dry, compressed air was introduced into the fixed-bed column at a flow rate of 126 cm³/min and the outlet gas composition was analyzed every 1.08 min using the adapted Varian 3800 gas chromatograph (GC) as described as above. N₂ breakthrough was analyzed with the column at ambient condition, while the Ar and O₂ composition of the gas stream was analyzed at -78 °C.

To analyze the solid-phase composition of the gas mixture, a desorption experiment was carried out on the bed. Figure 3-2 shows the schematics of desorption experiment. After 40 min of adsorption, system reaches equilibrium when the gas-phase outlet concentration is equal to the inlet gas concentration. GC analysis of the outlet composition was used to confirm that equilibrium was reached.

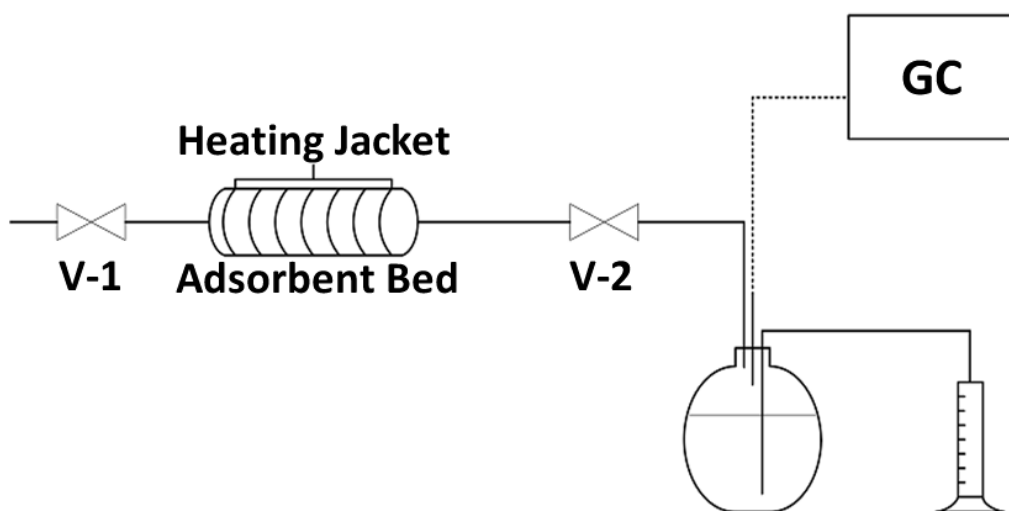


Figure 3-2. Schematic of desorption process.

Once equilibrium is reached, the inlet of the bed is isolated and the bed is heated via a heating jacket until its internal temperature reaches 200 °C. Heating the bed greatly reduces its adsorption capacity and forces the expanded gas downstream into the gas collector where it displaces a volume of water equal to the volume of collected outlet gas. Samples were taken from the outlet stream and analyzed by GC. After gas stopped flowing to the collector, the collected gas was sampled and analyzed by GC.

The gas collected includes both the adsorbed gas and the gas in the free space, but since the dead volume of the system is small compared to the amount of gas adsorbed, the collected gas should closely reflect the solid-phase composition of the bed.

3.4 Results and discussion

Figure 3-3 shows the results of IGC analysis of the separation of pure oxygen and argon, a mixture of 50%-50% oxygen and argon, and air on Ag-ETS-10 at 25 °C. The retention time for pure argon is larger than pure oxygen, indicating a preferred interaction between argon and Ag-ETS-10. This preference was also reflected in the analysis results for the 50-50% Ar-O₂ mixture. IGC analysis of the mixture shows that two peaks were present, and the greater degree of overlap between the O₂ and Ar peaks (compared to the pure components) suggests that the two species are competing for some of the same adsorption sites in the material. Similar to other reported silver-exchange sieves, Ag-ETS-10 has a strong affinity for N₂ which allows it to efficiently remove N₂ from an air stream. The IGC results demonstrate that Ag-ETS-10 can effectively separate the various components in air with a limiting selectivity (α) of 12.88 for N₂ over O₂, and of 1.41 for Ar over O₂.

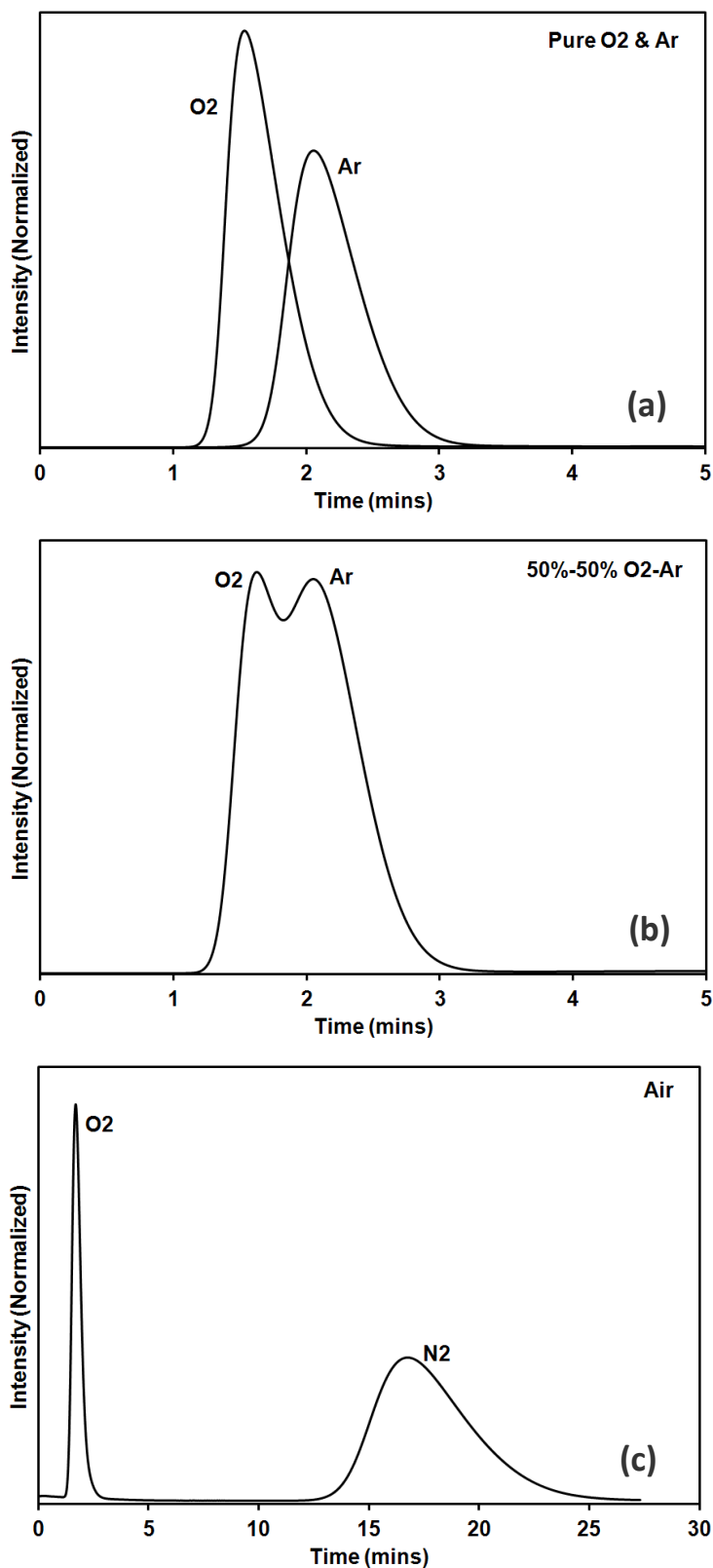


Figure 3-3. A typical gas chromatography separation of N₂ over O₂, Ar over O₂ on Ag-ETS-10. Pure oxygen and argon (a), 50-50% O₂-Ar mixture (b), air (c) was injected into an Ag-ETS-10 column at 25 °C under a 30 cm³/min flow of helium carrier gas were determined by IGC analysis.

The selectivities of Ag-ETS-10 for N₂/O₂ and Ar/O₂ may also be calculated through the pure component adsorption isotherms; Figure 3-4 shows adsorption isotherms at 25 °C in pressure range of 0-100 kPa for N₂, O₂ and Ar on Ag-ETS-10 together with the calculated Langmuir fits. The parameters of these Langmuir isotherms are listed in Table 3-1. Limiting selectivities of N₂ over O₂ (N₂ over Ar, Ar over O₂) at zero pressure can also be predicted by the Langmuir isotherms. These values are also presented in Table 3-1. The values calculated from the isotherm fits demonstrate that Ag-ETS-10 has a higher selectivity for argon over oxygen compared to other silver-exchanged sieves and has a strong preference for nitrogen over oxygen at zero pressure. The IGC and adsorption data are consistent in their estimation of adsorption selectivity and suggest that Ag-ETS-10, as a single adsorbent, can effectively and simultaneously remove N₂ and Ar from an air stream.

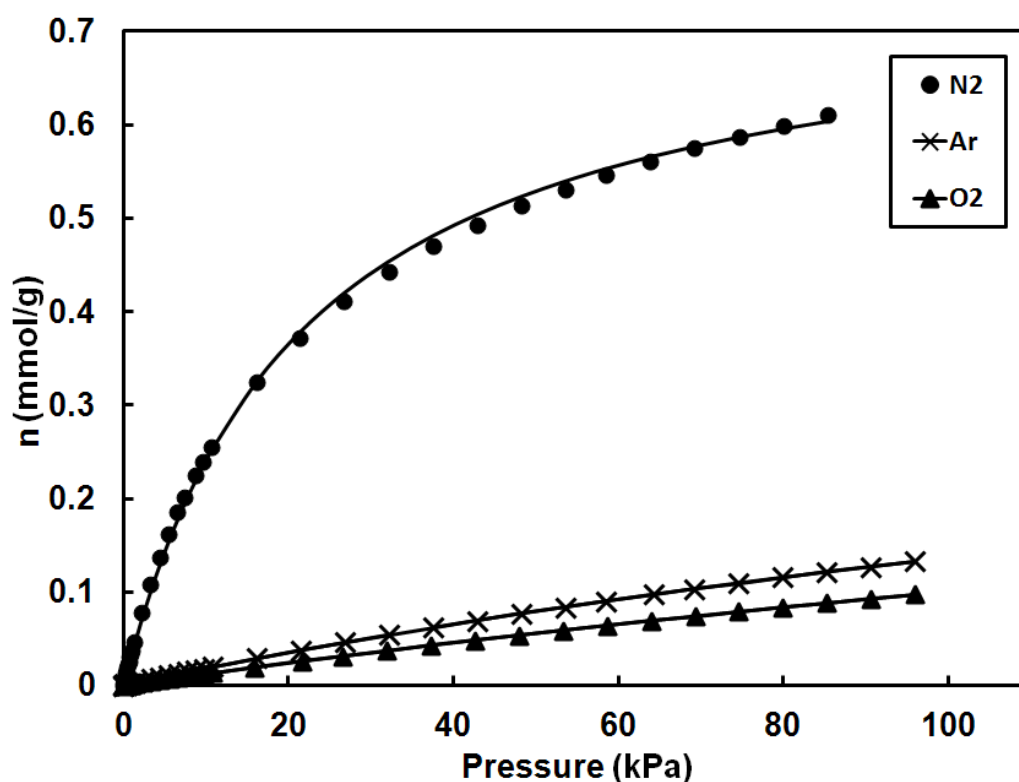
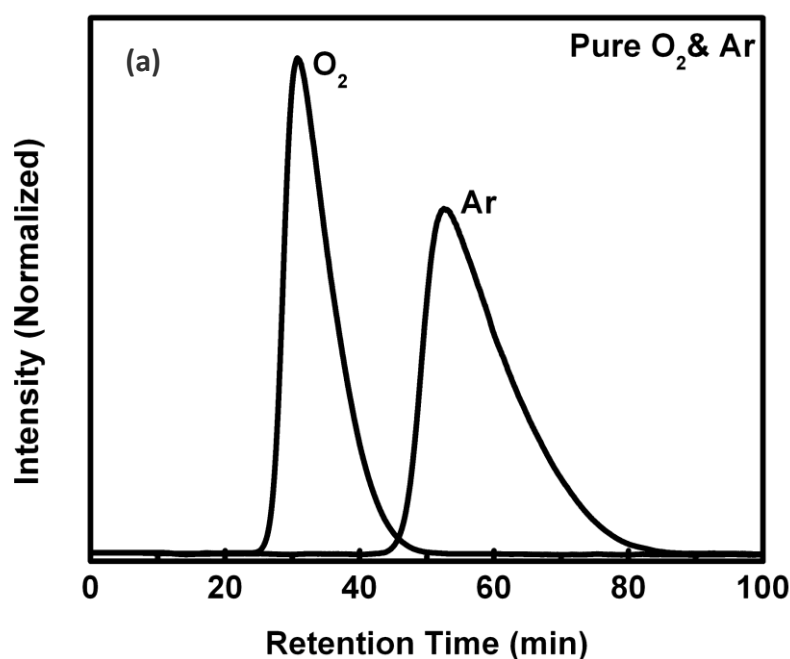


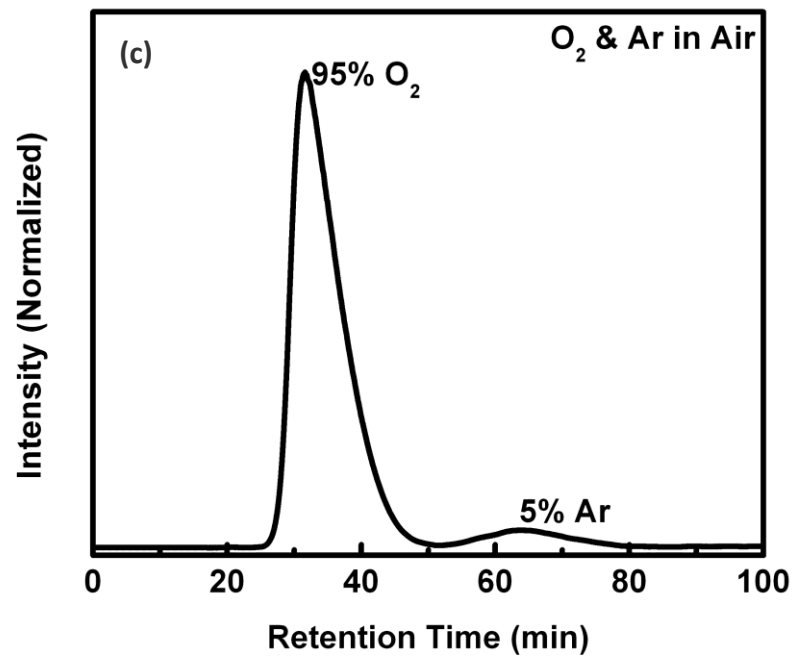
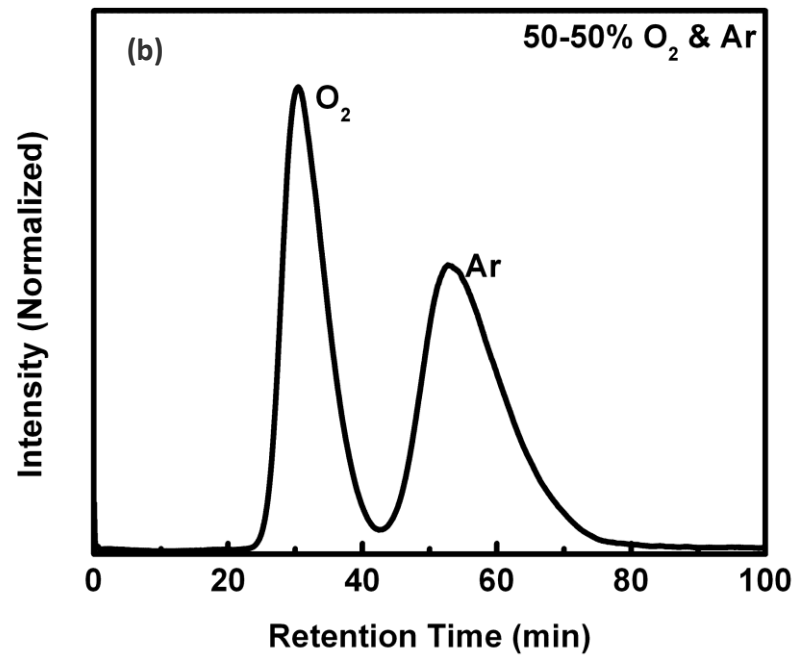
Figure 3-4. Equilibrium adsorption isotherms for N₂, Ar, O₂ on Ag-ETS-10 at 25 °C. P is pressure and n is capacity.

Table 3-1. Langmuir parameters for adsorption data in the range of 0-100 kPa at 25 °C.

Adsorbate	Langmuir isotherm parameters			Selectivity
	$q_{i,m}$ (mmol g ⁻¹)	b_i (kPa ⁻¹)	K_i (mmol kPa ⁻¹ g ⁻¹)	
N ₂	0.7545	0.0471	0.0355	$\alpha(N_2/O_2)=28$
Ar	0.4856	0.0039	0.0019	$\alpha(N_2/Ar)=18.7$
O ₂	0.4844	0.0026	0.0013	$\alpha(Ar/O_2)=1.5$

Figure 3-5 shows the results of GC analysis of the separation of pure oxygen and argon, a mixture of 50%-50% oxygen and argon, and of 95-5% O₂-Ar on Ag-ETS-10 at -78 °C. It demonstrates that the modified GC can quantitatively analyze Ar-O₂ mixture which contains low levels of argon. Figure 3-6 shows a plot of a mixture that is 99.7% O₂ with 0.3% Ar. It can be seen in the plot that the Ar peak remains well-resolved even at this level of purity. From this result we estimate our detection threshold for Ar to be about 0.1% and thus our Ar-free oxygen has a purity of better than 99.9%.





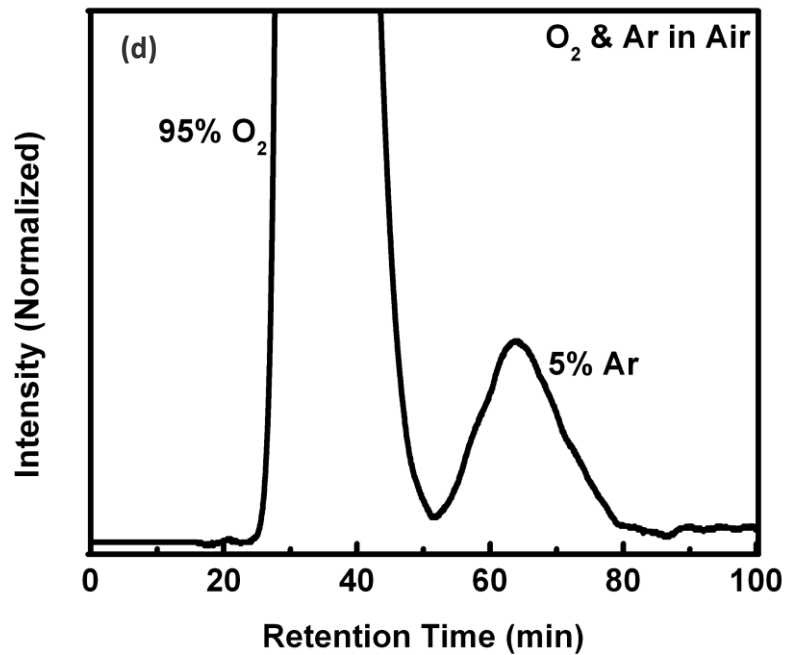


Figure 3-5. Gas chromatographic separation and determination of argon and oxygen in air by Ag-ETS-10. (a) pure oxygen and argon; (b) 50-50% oxygen and argon (c) 95-5% oxygen and Ar (d) Enlarged GC results of 95-5% oxygen and argon

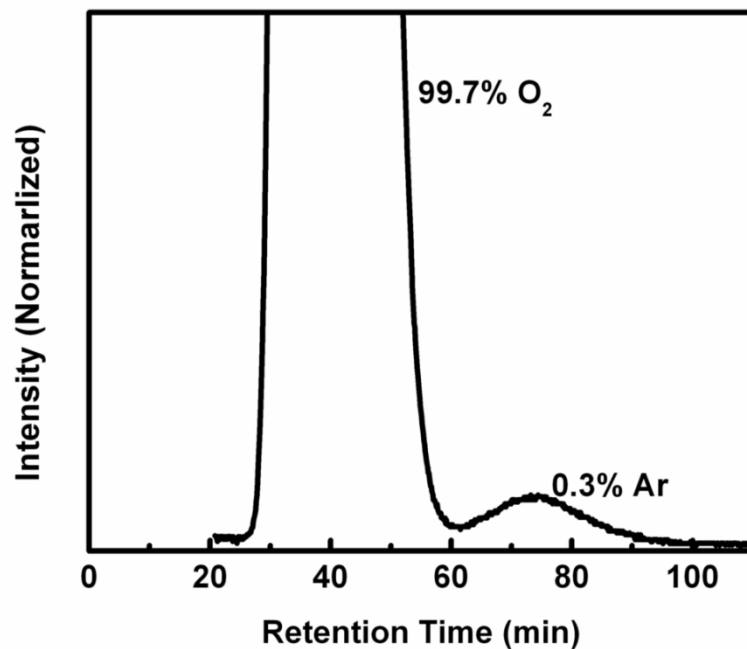


Figure 3-6. Gas chromatographic determination of 0.3% argon and 99.7% oxygen in air by Ag-ETS-10 (Enlarged GC results)

Figure 3-7 depicts a breakthrough curve for air on Ag-ETS-10 at 25 °C and 100 kPa which is represented in Table 3-2 as outlet concentration versus time. With a continuous flow of feed gas (78% N₂, 21% O₂ and 1% Ar) at 124 mL/min, an argon-free oxygen product was detected at 9 min (O₂ breakthrough). The bed continued to produce high purity oxygen stream (>98% O₂) for 2 min. During this period, a total of 86.8 mL of high purity (99+%) O₂ can be produced. At 13.5 min, the nitrogen front started to breakthrough. After 17 min of continuous flow in total, the concentration of N₂, O₂, and Ar in the outlet gas begins to reflect the inlet (feed gas) composition, indicating that the Ag-ETS-10 adsorbent has reached saturation.

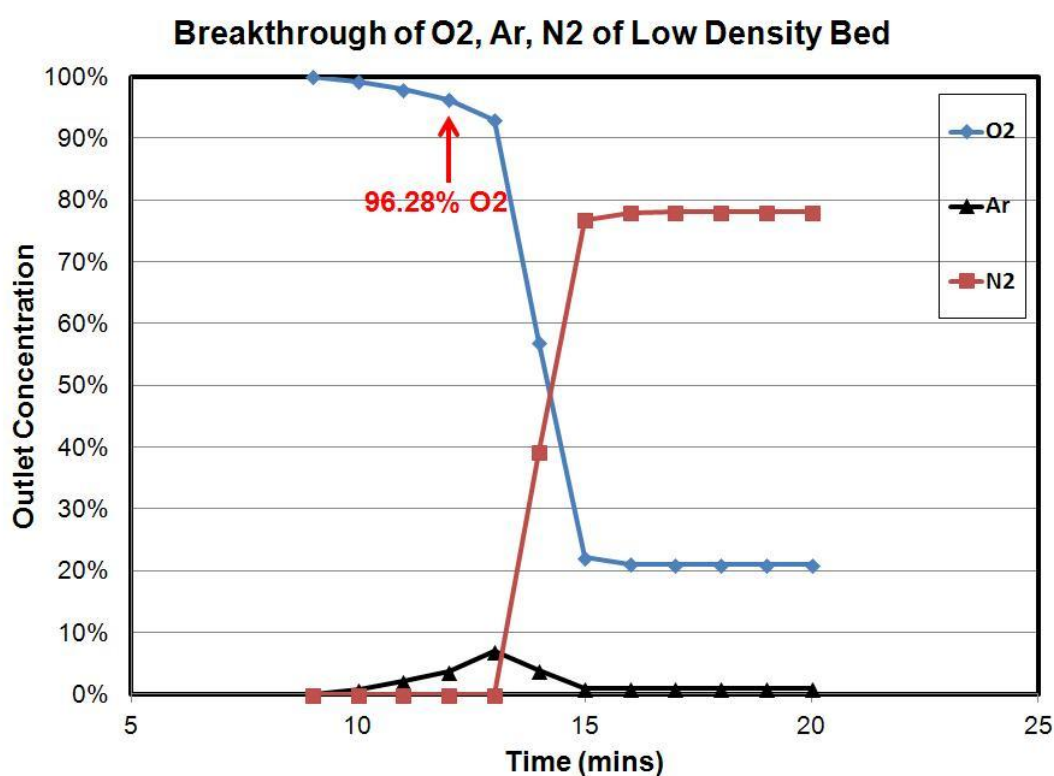


Figure 3-7. Air breakthrough curve on Ag-ETS-10 at ambient conditions. Compressed air (a mixture of 78% N₂, 21% O₂ and 1% Ar) was introduced into a column containing 130 g of pelletized Ag-ETS-10 at a flow rate of 124 mL/min (bed volume 150 mL). Composition of the outlet gas was determined by GC analysis.

Table 3-2. Outlet composition of the breakthrough for N₂, O₂, Ar

Time (min)	Outlet Concentration(%)		
	N₂	O₂	Ar
Feed in	78.08	20.95	0.97
0-8	0	0	0.00
9	0	100.00	0.00
10	0	99.20	0.80
11	0	97.90	2.10
12	0	96.28	3.72
13	0	93.00	7.00
14	39.31	56.86	3.83
15	76.83	22.13	1.04
16	78	21.05	0.95
17	78.09	20.97	0.94
18	78.09	20.97	0.94
19	78.09	20.97	0.94
20	78.09	20.97	0.94

Figure 3-8 shows the outlet gas flow rate monitored by an Agilent ADM 1000. Combined with the breakthrough information of oxygen, argon and nitrogen, it also illustrates that helium from the dead volume came out at the first 9 min. High purity of oxygen product came out since that. Nitrogen started to breakthrough at 13.5 min. The two step-changes exactly match the breakthrough of oxygen and nitrogen, which are the two main components of air. Integrating the flow measured between the O₂ and Ar breakthrough events, 88 mL of 99+% O₂ was generated.

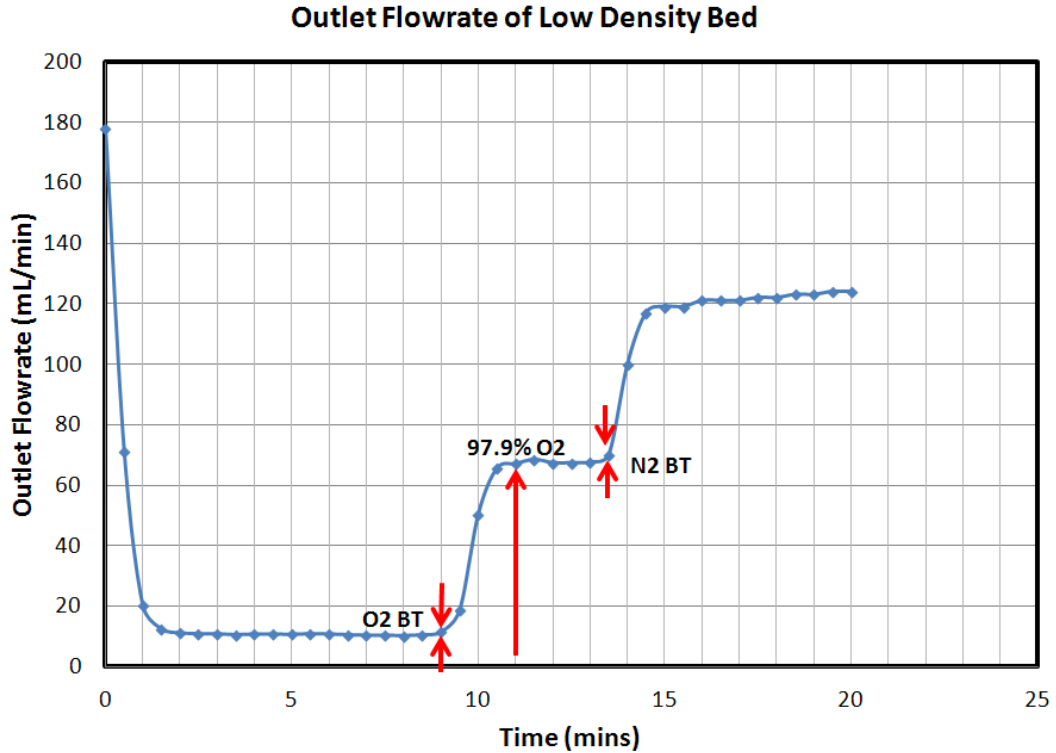


Figure 3-8. Outlet flow rate monitored by Agilent ADM 1000 in adsorption procedure.

Recovery rate of oxygen could be calculated as:

$$\text{Recovery rate of oxygen} = \frac{\text{volume of produced oxygen}}{\text{Feed in air} \times 21\%}$$

Given the feed flow rate of 124 mL/min, 86.77 mL of 99+% oxygen, the recovery rate of oxygen is 30.29%. Based on the information collected, it should be possible to recover pure oxygen using a PSA containing Ag-ETS-10 as the sole adsorbent.

Thermal desorption was applied after the adsorption was allowed to last for one hour (which was used to make sure the system reached equilibrium for all components). Figure 3-9 shows the outlet gas composition during the thermal desorption procedure and Table 3-3 helps to illustrate the concentration values of the outlet of desorption.

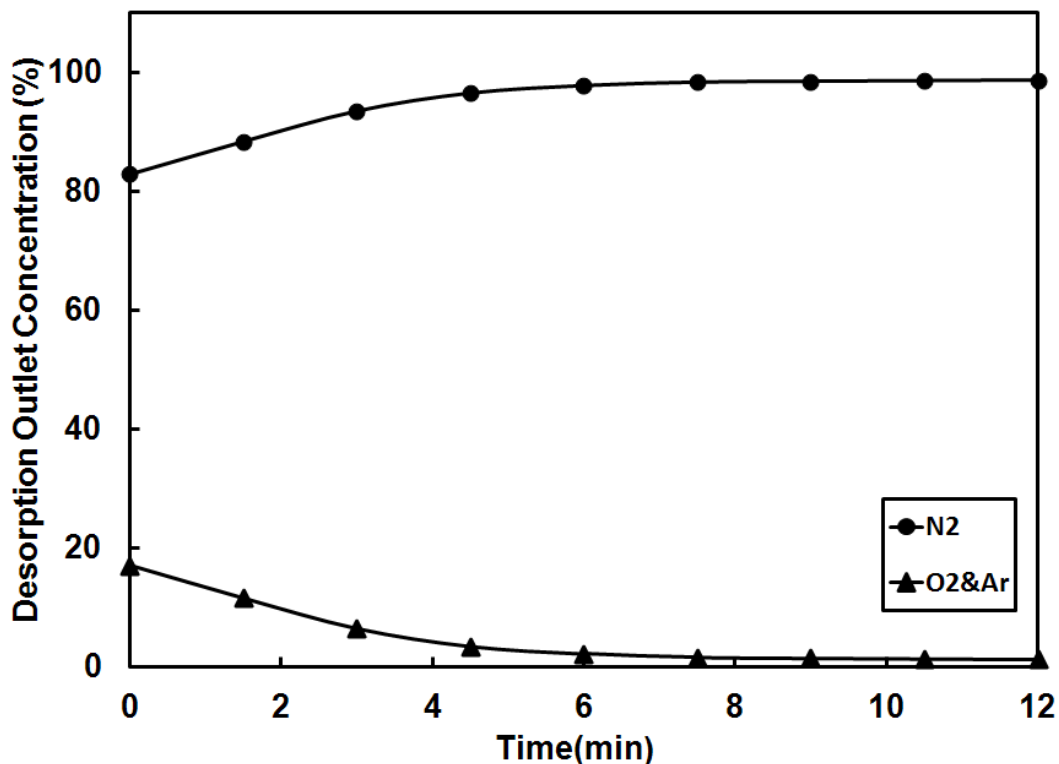


Figure 3-9. Outlet composition analysis of the desorption procedure.

Table 3-3. Outlet composition of the thermal desorption of the adsorbed phase gas

Time (min)	Outlet Concentration (%)	
	N ₂	O ₂ & Ar
0	82.95	17.05
1.5	88.43	11.57
3	93.52	6.48
4.5	96.52	3.48
6	97.77	2.23
7.5	98.36	1.64
9	98.5	1.5
10.5	98.61	1.39
12	98.7	1.30

We can observe that the outlet gas composition was mostly concentrated above 90% N₂. At the end, we can obtain 1200 mL desorbed gas from the Ag-ETS-10 bed. The concentration for the adsorbed phase is 94% N₂, 6% of mixture of O₂ and Ar. We can

approximately calculate the bed selectivity of N₂/O₂ based on the equation here (Eq. 3.4):

$$S_{N_2/O_2} = \frac{X_{N_2}Y_{O_2}}{X_{O_2}Y_{N_2}} \quad (3.4)$$

where X_{N_2} , X_{O_2} are the adsorbed phase concentration of N₂ and O₂, Y_{N_2} , Y_{O_2} are the N₂ and O₂ concentration in air. Bed selectivity of N₂ over O₂ on Ag-ETS-10 at ambient condition is 4.16.

The multicomponent breakthrough demonstration suggests that Ag-ETS-10 would be a very strong candidate as adsorbent for a PSA process to produce high-purity oxygen at ambient temperature.

3.5 Conclusions

Adsorption measurements demonstrate that Ag-ETS-10 is selective for argon over oxygen and nitrogen over oxygen. In this work, 86.77 mL of high purity (99+%) oxygen was produced over a 150 mL bed of 130 g Ag-ETS-10 granules using compressed air at 100 kPa and 25 °C, with an O₂ recovery rate greater than 30%. This suggests that Ag-ETS-10 could be an effective adsorbent in a PSA system designed for generating high purity O₂.

3.6 References

- [1] Smith, A.R., Klosek, J., 2001. *Fuel Processing Technology* 70, 115-134
- [2] Yang, R.T., 1987. *Gas Separation by Adsorption Processes*, Butterworth, Stoneham, MA.
- [3] Talu, O., Li, J., Kumar, R., Mathisa, P.M., Jr, J.D.M., Schork, J.M., 1996. *Gas Separation & Purification* 10, 149-159.
- [4] Moon, I.S., Lee, D.I., Yang, J.H., Ryu, H.W., 1986. *Korean Journal of Chemical Engineering* 3, 15-21.
- [5] Jee, J.G., Lee, S.J., 2005. *Adsorption* 11, 415-420.
- [6] Zahra, M., Jafar, T., Masoud, M., 2008. *World Academy of Science, Engineering and Technology* 47, 99-103.
- [7] Reid, C.R., O'koye, I.P., Thomas, K.M., 1998. *Langmuir* 14, 2415-2425.
- [8] Tan, J.S., Ani, F.N., 2004. *Separation & Purification Technology* 35, 47-54.
- [9] Jee, J.G., Lee, S.J., Lee, C.H., 2004. *Korean Journal of Chemical Engineering* 21, 1183-1192.
- [10] Rutherford, S.W., Coons, J.E., 2005. *Journal of Colloid and Interface Science* 284, 432-439.
- [11] Jee, J.G., Kim, M.B., Lee, C.H., 2005. *Chemical Engineering Science* 60, 869-882.
- [12] Anson, A., Kuznicki, S.M., Kuznicki, T.M., Dunn, B.C., Eyring, E.M., Hunter, D.B., 2009. *Separation Science & Technology* 44, 1604-1620.
- [13] Hayashi, S., Kawai, M., Kaneko, T., 1996. *Gas Separation & Purification* 10, 19-23.

- [14]Boniface, H.A., 1983. *Ph.D thesis*, the University of New Brunswick, Fredericton, Canada
- [15]Sebastian, J., Jasra, R.V., 2005. *Industrial & Engineering Chemistry Research* 44, 8014-8024.
- [16]Habgood, H.W., 1964. *Canadian Journal of Chemistry* 42, 2340-2350.
- [17]Hutson, N.D., Rege, S.U., Yang, R.T., 1999. *AIChE Journal* 45, 724-734.
- [18]Dee, D.P., Chiang, R.L., Miller, E.J., Whitley, R.D., 2003. *High Purity Oxygen Production by Pressure Swing Adsorption*. US Patent No. 6,544,318 B2.
- [19]Anson, A., Kuznicki, S.M., Kuznicki, T.M., Haastrup, T., Wang, Y., Lin, C.C.H., Sawada, J.A., Eyring, E.M., Hunter, D., 2008. *Microporous Meoporous Materials* 109, 577-580.
- [20]Kuznicki, S.M., 1991. *Large-Pored Crystalline Titanium Molecular Sieve Zeolites*. US Patent No. 5, 011, 591.

Chapter 4

Air Separation by Silver Titanosilicate with Enhanced Density

A version of this chapter was submitted to Sep. Purif. Technol. Reproduced with permission from Shi, M., Avila, A.M., Wu, L., Sawada, J.A., Kuznicki, T.M., Kuznicki, S.M., 2012.

4.1 Summary

Previously, we reported that Ag-ETS-10 can be used to separate air, and produce argon free oxygen. High purity oxygen (99+%) was generated using a bed of Ag-ETS-10 granules to separate air (78% N₂, 21% O₂, 1% Ar) at 25 °C and 100 kPa, with an O₂ recovery larger than 30%. In this study, a higher recovery was achieved by increasing the bulk density of the adsorbent material and thus the adsorbent packing efficiency within the bed enhanced. The packing efficiency was further increased through mixing different large and small size particles. A lab scale demonstration was carried out to demonstrate that Ag-ETS-10 with enhanced bed density can produce high purity oxygen (99+%) by adsorptive air separation (78% N₂, 21% O₂, 1% Ar), with an O₂ recovery approaching 40%.

4.2 Introduction

In Chapter three, adsorption analysis, such as, equilibrium isotherm and inverse phase gas chromatography, showed that silver exchanged titanosilicate has an adsorptive selectivity for both nitrogen over oxygen, and argon over oxygen. Furthermore, a 150 mL bed packed with 130 g of regular Ag-ETS-10 was tested in a lab-scale air separation demonstration system. High purity oxygen (99+%) was generated at ambient condition and with an oxygen recovery rate greater than 30%.

High purity O₂ recovery from air can be enhanced as Ar/O₂ adsorption selectivity values are larger. Also, O₂ recovery can be enhanced by improving the packing efficiency of the adsorbent material within the bed. The as-synthesized ETS-10 further cation-exchanged to generate Ag-ETS-10 has a tap density of 0.78 g/mL. The density of ETS-10 crystals is 2.5 g/mL. Thus, higher tap density could be achieved through a more favorable ETS-10 crystal morphology as an outcome of the optimization of synthesis conditions. It is reported that multi-size sphere packing can decrease the bed voidage[1-2]. The density of adsorbent bed could also be enhanced by packing different size granules. It is encouraging to investigate the correlation between the enhanced bed density and the production and the recovery of the product.

This work deals with the optimization of high purity O₂ recovery from air by using an enhanced ETS-10 material with higher tap density. The production and recovery yield of oxygen using this more compact material were evaluated and compared with those results obtained with a regular lower density bed. A mathematical expression for the O₂ recovery from air was developed based on integral mass balances in the adsorbent column.

4.3 Experimental

4.3.1 Sample preparation

Both regular ETS-10 (ETS-10-R) and high density ETS-10 (ETS-10-HD) were synthesized using conventional hydrothermal synthesis. The regular ETS-10 with low density was synthesized as reported by Kuznicki [3]. The later one with high density was prepared following the recipe reported by Lan by change of the synthetic conditions (2012) [4], such as temperature and time. The as-synthesized ETS-10-HD was Ag⁺- exchanged by adding 5 g of as-synthesized adsorbent to 10 g of silver nitrate (Fisher, USP) in 50 g of deionized water. The mixture was heated to 80 °C for 1 h. The silver exchanged material was filtered, washed with deionized water and the exchanged procedure was repeated two more times (for a total of three exchanges). The silver exchanged ETS-10-HD was dried at 80 °C in air.

4.3.2 Characterization

Phase identification of the as-synthesized sodium titanate was conducted by X-ray powder diffraction analysis (XRD) using a Rigaku Geigerflex 2173 with a vertical goniometer equipped with a graphite monochromator for filtration of K- β wavelengths. Scanning electron microscopy (SEM) was performed on a Hitachi S2700 equipped with an X-ray EDS detector. Oxygen, argon, and nitrogen composition analysis was performed on a modified Varian 3800 gas chromatography (GC) equipped with a thermal conductivity detector (TCD), which was reported by Shi.

4.3.3 Density evaluation

Powder samples (Regular ETS-10, ETS-10-HD, Ag-ETS-10-R, and Ag-ETS-10-HD), were pelletized by using a mortar and pestle and compressed in a pellet press at 69,000 kPa for 3 min. The resulting cakes were crushed and sieved to obtain particles

(sieve size between 20-50 mesh and 10-16 mesh). Mixed packing was achieved by mixing 50% 20-50 mesh size granules and 50% 10-16 mesh size granules through a rotation machine. The determination of tap density for powder and the pelletized, crushed and sieved materials followed the ISO standardization [5].

4.3.4 Laboratory-scale demonstration

Laboratory-scale demonstration is illustrated in chapter three. Breakthrough experiments were performed for high density adsorbent bed. The adsorbent was packed into a 150 mL cylindrical stainless steel chamber with an inner diameter of 20 mm and a length of 450 mm. The columns packed with adsorbent pellets were activated at 200 °C for 10 h under 100 mL/min of helium flow.

The breakthrough experiments were run by conditioning the bed at 100 kPa with helium to purge any adsorbed gas from the system. The column temperature was maintained at 25 °C using a heating jacket around the bed coupled to a circulating water bath. Dry, compressed air was introduced into the fixed-bed column at a flow rate of 120 mL/min and the outlet gas composition was analyzed every 1 min using the adapted Varian 3800 gas chromatograph (GC) as described above. Outlet gas flow rate monitored by an Agilent ADM 1000. The Agilent flow meter was calibrated using a Bronkhorst mini CORI-FLOW™ to allow the measured volumetric flow rates to be accurately converted to standard conditions.

4.4 Results and discussion

4.4.1 Density enhancement

Figure 4-1 shows the XRD pattern of the high density ETS-10 (Na-10-HD) is identical to the pattern of low density ETS-10 (Na-10-LD), both conforming to the pattern reported by Kuznicki [3], This is an indication that although the density of

Na-10-HD was enhanced, it still has the unique zeolitic structure as classical ETS-10.

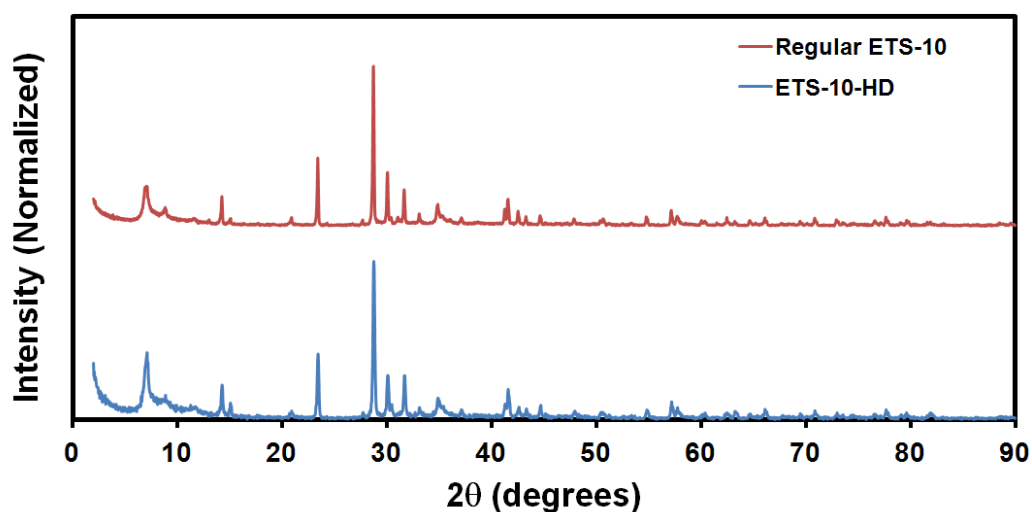


Figure 4-1. XRD of regular ETS-10 and ETS-10-HD.

SEM analysis (Fig.4-2 and 4-3) show the morphology of both Na-10-HD and Na-10-LD. Typically, ETS-10 crystals obtained in the present study resembled truncated bi-pyramids with square basal plane shared by the two pyramids [6-7]. Here, both Na-10-LD and Na-10-HD have such feature as described above, however, the as-synthesized low density ETS-10 is more cubic in shape and with some defects on the surface. The crystal of high density ETS-10 is more flat and with perfect surface. We assume the difference in tap density is due to the difference of morphology. Both XRD and SEM show that the new synthesized Na-10-HD possesses the reported ETS-10 structure.

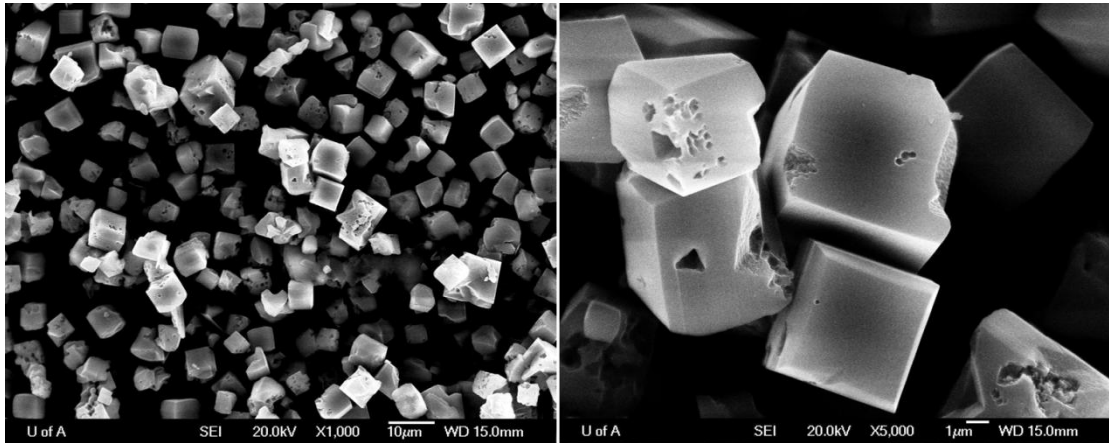


Figure 4-2. SEM of regular ETS-10.

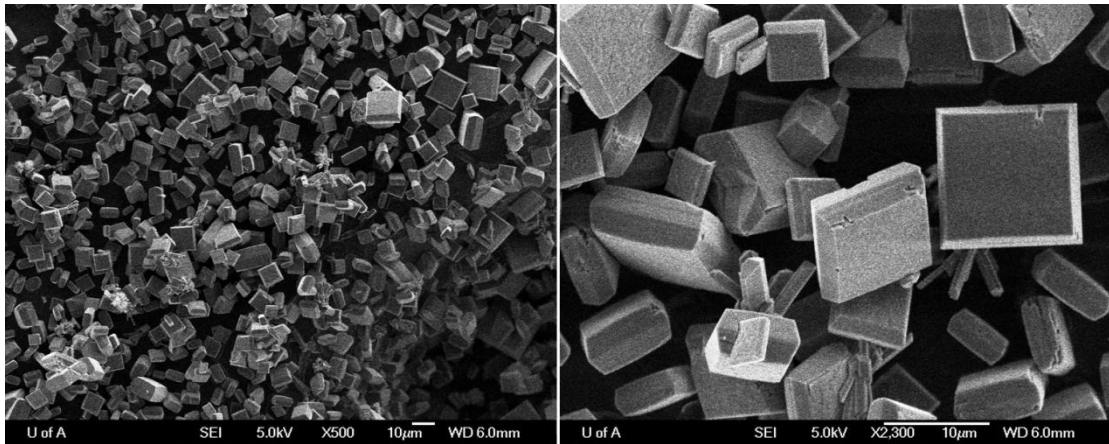


Figure 4-3. SEM of ETS-10-HD.

The table 4-1 shows the comparison of tap density for regular ETS-10, high density ETS-10, regular Ag-ETS-10 and high density Ag-ETS-10 in different forms, such as, powder, 10-16 mesh size particles, 20-50 mesh size particles, and mixed size granules. The data indicated that ETS-10 density could be enhanced through the new synthesis method, and could also be increased by mixed packing. A 150 mL adsorbent bed can pack 130 g low density Ag-ETS-10 with 10-16 mesh size. At the same time 175 g high density Ag-ETS-10 with different size granules (50% 10-16 mesh size mixed with 50% 20-50 mesh size) could be packed in the same volume. These two

improvements result in a 34.6wt% more packing of Ag-ETS-10 in a fixed volume.

Table 4-1. Tap density of regular ETS-10 and high density ETS-10

	Powder (Tap Density)	10-16 mesh particles Tap Density	20-50 mesh particles (Tap Density)	Mixed particle (Tap Density)	Adsorbent in 150 mL Bed
ETS-10-R	0.78 g/mL	0.712 g/mL	0.736 g/mL	0.85 g/mL	-
ETS-10-HD	0.95 g/mL	0.87	0.88	1.01 g/mL	-
Ag-ETS-10-R	1.0 g/mL	0.931	0.953	1.121	130 g
Ag-ETS-10-HD	1.23 g/mL	1.18	1.2	1.45 g/mL	175 g

4.4.2 Breakthrough times and O₂ recovery

Mass balance of the bed could be expressed as:

$$\int_0^{\infty} (F_{in,j} - F_{out,j}) dt = q_{Ar}^* \rho_b V_b + C_{Ar} V_b \epsilon_b \quad (4.1)$$

From equation 4.1, the mean residence time or mean breakthrough time (also known as stoichiometric breakthrough time) is expressed as:

$$t_{bk} = \int_0^{\infty} \left(1 - \frac{F_{out,j}}{F_{in,j}}\right) dt = \frac{L}{v_{int}} \left(\frac{q_j^* \rho_b}{C_j \epsilon_b} + 1 \right) \quad (4.2)$$

Considering that the mass transfer zone in the ternary mixture breakthrough travels as a shock wave, the mass balance for each component can be expressed as:

$$F_{in,j} \times t_{BT,j} = q_j^* \rho_b V_b + C_j V_b \epsilon_b; \quad j = N_2, O_2 \text{ and } Ar \quad (4.3)$$

O₂ can also be expressed as:

$$\int_0^{t_{BT,O_2}} F_{in,O_2} dt + \int_{t_{BT,O_2}}^{t_{BT,Ar}} F_{in,O_2} dt - \int_0^{t_{BT,O_2}} F_{out,O_2} dt - \int_{t_{BT,O_2}}^{t_{BT,Ar}} F_{out,O_2} dt$$

$$= q_{O_2}^* \rho_b V_b + C_{O_2} V_b \epsilon_b$$
(4.4)

$$F_{in,O_2} \times t_{BT,Ar} - \int_{t_{BT,O_2}}^{t_{BT,Ar}} F_{out,O_2} dt = q_{O_2}^* \rho_b V_b + C_{O_2} V_b \epsilon_b$$
(4.5)

$$\int_{t_{BT,O_2}}^{t_{BT,Ar}} F_{out,O_2} dt = F_{in,O_2} \times t_{BT,Ar} - F_{in,O_2} \times t_{BT,O_2} = F_{in,O_2} \times (t_{BT,Ar} - t_{BT,O_2})$$
(4.6)

So the recovery of O₂ can be expressed as:

$$Rec\% = \frac{\int_{t_{BT,O_2}}^{t_{BT,Ar}} F_{out,O_2} dt}{F_{in,O_2} \times t_{BT,Ar}} = \frac{F_{in,O_2} \times (t_{BT,Ar} - t_{BT,O_2})}{F_{in,O_2} \times t_{BT,Ar}} = 1 - \frac{t_{BT,O_2}}{t_{BT,Ar}}$$
(4.7)

Breakthrough time can be calculated as:

$$t_{BT,Ar} = \frac{q_{Ar}^* \rho_b V_b + C_{Ar} V_b \epsilon_b}{F_{in,Ar}} = \frac{L}{v_{int}} \left(\frac{q_{Ar}^* \rho_b}{C_{Ar} \epsilon_b} + 1 \right)$$
(4.8)

The relation between bed density ρ_b and voidage ϵ_b can be expressed as:

$$\frac{\rho_b}{1 - \epsilon_b} = Constant = A$$
(4.9)

$$Rec\% = 1 - \frac{t_{BT,O_2}}{t_{BT,Ar}} = 1 - \frac{\frac{q_{O_2}^* \rho_b}{C_{O_2} \epsilon_b} + 1}{\frac{q_{Ar}^* \rho_b}{C_{Ar} \epsilon_b} + 1} \quad (4.10)$$

Which can simplified as:

$$Rec\% = \frac{\frac{q_{Ar}^*}{C_{Ar}} - \frac{q_{O_2}^*}{C_{O_2}}}{\frac{q_{Ar}^*}{C_{Ar}} + \frac{\epsilon_b}{\rho_b}} \quad (4.11)$$

As we know q_{Ar}^* , $q_{O_2}^*$, C_{Ar} , C_{O_2} are constant.

Assuming the same affinity for both materials, the recovery of O_2 could expressed as:

$$Rec\% = \frac{M}{N + \frac{\epsilon_b}{\rho_b}} \quad (M, N \text{ are constant}) \quad (4.12)$$

$$Rec\% = \frac{M}{N + \frac{\epsilon_b}{A \times (1 - \epsilon_b)}} = \frac{M}{N + \frac{1}{A \times (\frac{1}{\epsilon_b} - 1)}} \quad (4.13)$$

It demonstrates that, when the bed voidage is decreasing, which means the bed density increases, the recovery of O_2 increases.

4.4.3 Lab-scale demonstration

Figure 4-4 depicts a breakthrough curve for air on 175 g of high density Ag-ETS-10 at 25 °C and 100 kPa which is represented in Table 4-2 as outlet concentration versus time. With a continuous flow of air at 120 mL/min, an argon-free oxygen product was detected at 16 min. The bed continued to produce high purity oxygen stream balanced

with relatively low level of argon (<1.9% Ar) for 3 min. During these three minutes, a total of 186.25 mL of high purity (99+%) O₂ was produced. At 23 min, the nitrogen front started to breakthrough. At 32 min, the concentration of N₂, O₂, and Ar in the outlet gas begins to reflect the inlet (feed gas) composition, indicating that the Ag-ETS-10 adsorbent has reached saturation.

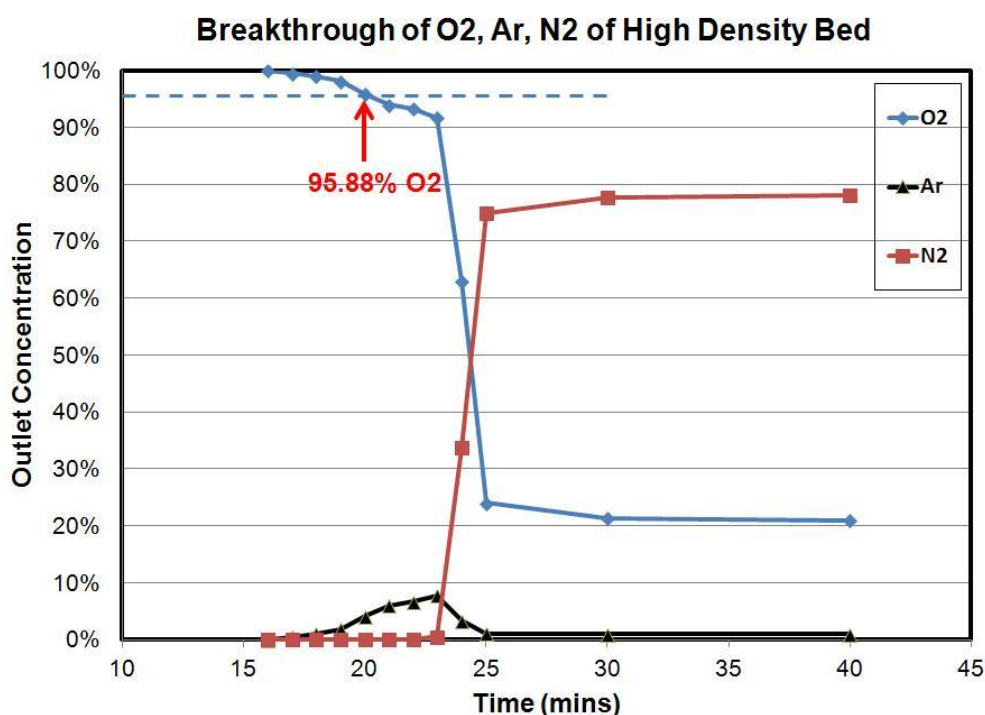


Figure 4-4. Air breakthrough curve on high density Ag-ETS-10 at ambient conditions. Compressed air (a mixture of 78% N₂, 21% O₂ and 1% Ar) was introduced into a 150 mL column containing 175 g of pelletized high density Ag-ETS-10 with mixed granule sizes (50% 10-16 mesh size and 50% 20-50 mesh size) at a flow rate of 120 mL/min. Composition of the outlet gas was determined by GC analysis.

Table 4-2. Outlet composition of the breakthrough for N₂, O₂, Ar

Time (min)	Outlet Concentration(%)		
	N ₂	O ₂	Ar
Feed in	78.08	20.95	0.97
0-15	0	0	0.00
16	0.00	99.99	N/A
17	0.00	99.50	0.50
18	0.00	99.00	1.00
19	0.00	98.10	1.90
20	0.00	95.88	4.12
21	0.00	93.98	6.02
22	0.00	93.30	6.7
23	0.57	91.63	7.8
24	33.72	62.97	3.31
25	74.88	24.04	1.08
30	77.67	21.37	0.96
40	78.10	20.96	0.94

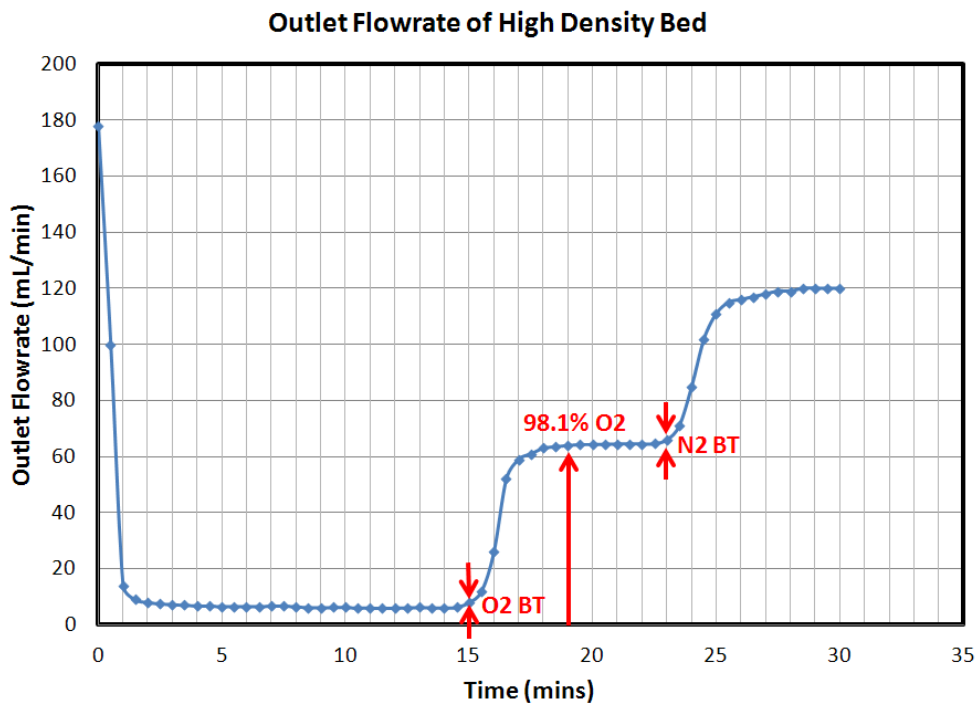


Figure 4-5. Outlet flow rate monitored by Agilent ADM 1000 in adsorption procedure for high density bed.

Figure 4-5 shows the outlet gas flow rate for the high density bed. Combined with the breakthrough information of oxygen, argon and nitrogen, it also illustrates that helium from the dead volume came out at the first 15 min. High purity of oxygen product came out after that. Nitrogen started to breakthrough at 23 min. The two step-changes exactly match the breakthrough of O₂ and N₂, which are the two main component of air (21% O₂ and 78% N₂). Integrating the flow measured between the O₂ and Ar breakthrough events, 190 mL of 99+% O₂ was generated.

Given the feed flow rate of 120 mL/min, and 186.25 mL of 99+% oxygen, the recovery rate of oxygen is 38.89%. In chapter three, it shows Ag-ETS-10 with lower bed density possesses an oxygen recovery rate of 30% under the same experiment conditions (same temperature, pressure, bed volume, and feed in flow rate). Compared with the recovery rate we obtained in this high density bed, we can conclude that by using the same silver exchanged titanosilicate materials, the bed with higher density could produce more high purity (99%+) oxygen in one step process. In addition the recovery of oxygen was increase from 30% to almost 40%, which matches the prediction from the mathematic modeling. Enhanced bed density will help increase the recovery of oxygen.

4.5 Conclusions

In this work, we demonstrated that new synthesized high density ETS-10 and mix packing enhanced the Ag-ETS-10 bed density by 34.6%. A mathematical model predicted that enhanced bed density would help increase the recovery of oxygen during air separation. In a lab-scale demonstration and comparison, 186.25 mL of high purity (99+%) oxygen was produced over a 150 mL bed of high density Ag-ETS-10 granules using compressed air at 100 kPa and 25 °C, with an O₂ recovery rate approaching to 40%. Both the production and recovery was improved by

enhanced bed density. This suggests that high density Ag-ETS-10 can improve the performance of argon free oxygen production by adsorptive air separation.

4.6 References

- [1] Abdel-Dawad, Y.A., Abdullah, W.S., 2002. *Construction and Building Materials* 16, 495-508.
- [2] Yamada, S., Kanno, J., Miyauchi, M., 2011. *Information Processing Society of Japan Online Transactions* 4, 126-133.
- [3] Kuznicki, S.M., 1991. *Large-Pored Crystalline Titanium Molecular Sieve Zeolites*. US Patent No. 5, 011, 591.
- [4] Wu, L., Kuznicki, S.M., 2012. *New Synthesis of Enhanced Density Titanosilicate-10*, in preparation.
- [5] Determination of Tap Density. <http://www.iso.org> (accessed October 1, 2012)
- [6] Anderson, M.W., Terasaki, O., Ohsuna, T., Philippou, A., Mackay, S.P., Ferreira, A., Rocha, J., Lidin, S., 1994. *Nature* 367, 347-351.
- [7] Ji, Z., Yilmaz, B., Warzywoda, J., Sacco, A., 2005. *Microporous and Mesoporous Materials* 81, 1-10.

Chapter 5

High Pressure Adsorptive Separation of Ethylene and Ethane on Na-ETS-10

A version of this chapter has been published. Reproduced with permission from Shi, M., Avila, A.M., Yang, F., Kuznicki, T.M., Kuznicki, S.M., 2011. *Chemical Engineering Science* 66, 2817-2822.

5.1 Summary

Previously, we reported that Na-ETS-10 can be used to separate a mixture of ethylene and ethane from an industrial process stream under low pressure (101 kPa) with a binary bed selectivity of 5 at 298 K and 101.3 kPa. In this study, we show that selectivity improves considerably under high pressure conditions. Na-ETS-10 was used as a packed bed adsorbent to separate an ethylene/ethane 59/41 mixture over a pressure range of 101-2,580 kPa and at two different temperatures (273 and 298 K). At these pressures, pure ethane gas raffinate streams prior to ethylene breakthrough are obtained. The extract phase obtained following desorption from the packed bed column contained up to 94% ethylene. The separation performance improved as adsorption column pressures increased. The ethylene/ethane bed selectivity achieved at 298 K and 2,580 kPa was ~11, more than double the previously reported selectivity under low pressure.

5.2 Introduction

Ethylene is an important commodity petrochemical used mostly as a raw material in the manufacture of polymers such as polyethylene, polyester, polyvinyl chloride, polystyrene as well as fibers and other organic chemicals. It has replaced acetylene as the most important building block in industrial organic chemistry [1]. According to a report by Global Industry Analysts, the world ethylene market will reach 160 million tons by 2015 [2]. One of the most important methods of manufacturing ethylene is steam cracking and thermal decomposition of ethane [3]. In a typical ethylene plant, the separation of ethylene and ethane is a key stage in the whole production chain. The ethylene and ethane separation process is mostly carried out by cryogenic distillation at high pressure and low temperature and requires high energy supply [4]. Therefore an effective ethylene and ethane separation method that could reduce the energy and equipment costs is desirable.

Adsorptive separation is an alternative method to cryogenic distillation and is more sustainable because of low energy costs and capital investment [3]. The key to the success of the adsorptive separation of ethylene and ethane mixtures is finding an effective adsorbent.

In the adsorptive separation of olefin/paraffin mixtures, zeolite 13X has often been considered the primary adsorbent for the separation. Miltenburg tested the separation of ethane/ethylene mixtures working with CuCl/NaX at 358K and 200 kPa [5]. The use of zeolite 13X in the separation of propane/propylene mixtures has also been reported in several articles from Delft's and Porto's research groups [5-8]. Uniformly these studies have been conducted at relatively low pressures (less than 200 kPa) and not at high pressures (typically 2000+ kPa) where ethane and ethylene are separated industrially.

Engelhard Titanosilicate-10 (ETS-10) is a large-pored, mixed octahedral/tetrahedral titanium silicate molecular sieve with a three-dimensional network of interconnecting channels [9, 10]. The pore size of ETS-10 has an average kinetic diameter of ~ 8 Å, which is larger than the molecular diameter of either C_2H_4 or C_2H_6 (4.163 and 4.443 Å, respectively) [11]. As a result both species may enter the crystalline lattice, and ethylene/ethane separation selectivity on ETS-10 would be based on equilibrium competitive adsorption.

A number of studies, including modeling predictions, suggest that ETS-10-type materials especially Na-ETS-10, have great potential as adsorbents for ethylene/ethane separations [12]. Other studies have shown that the characteristics of the ethylene and ethane adsorption on ETS-10-type materials can be manipulated by cation exchange [4, 13]. More recently, it was reported that the adsorption separation of a binary mixture of ethylene and ethane using Na-ETS-10 at 298 K and 101.3 kPa, can achieve a bed selectivity of approximately 5 [14].

However, the industrial cryogenic distillation process for ethane/ethylene separation is performed at elevated pressures (2000-2500 kPa). Hence, any alternative adsorption technology related to ethane/ethylene separation should contemplate materials and engineering designs that allow efficient separation at higher pressures. Working at high pressures would also minimize re-compression work and provide clear advantages in reducing the energy requirements.

This work describes the adsorptive separation performance of a binary mixture of C_2H_4 and C_2H_6 at high pressure on Na-ETS-10 using a laboratory-scale demonstration unit. A gas mixture, with composition commonly found in industrial processes, was separated by adsorption on Na-ETS-10 within a packed-bed column. The separation factor, breakthrough profile and capacity for C_2H_4 and C_2H_6 were determined. The separation performance was compared at different pressure and temperature conditions. Adsorption isotherms were measured for ethylene and ethane at high

pressures and used to estimate the mixture adsorption equilibrium on Na-ETS-10 crystals as a function of pressure, and to estimate the isosteric heats of adsorption as a function of loading.

5.3 Experimental

5.3.1 Material Synthesis

Na-ETS-10 was synthesized hydrothermally as reported by Kuznicki [9]. A typical sample preparation involved thoroughly mixing 50 g of sodium silicate (28.8% SiO₂, 9.14% Na₂O, Fisher), 3.2 g of sodium hydroxide (97+% NaOH, Fisher), 3.8 g of KF (anhydrous, Fisher), 4 g of HCl (1M), and 16.3 g of TiCl₃ solution (Fisher). The mixture was stirred in a blender for 1 h, and then reacted in a 125 mL sealed autoclave (PARR Instruments) at 488 K for 64 h. The resulting material was thoroughly washed with de-ionized water, and dried at 373 K. The Na-ETS-10 materials were pelletized by mixing 6.0 g of the molecular sieves (equilibrated at 373 K) with 2.5 g of Ludox HS-40 colloidal silica (Aldrich). The mixture was homogenized using a mortar and pestle and compressed in a pellet press to 10,000 psi for 3 minutes. The resulting cakes were crushed and sieved to obtain 20-50 mesh particles. The pelletized, crushed and sieved materials were used in the column separation experiments.

5.3.2 Adsorption Isotherms

The ethane and ethylene adsorption isotherms on Na-ETS-10 at high pressures (0-1800 kPa) were measured at 298, 323, 373, 423 and 473 K with an HPVA-100 High Pressure Volumetric Analyzer adsorption unit from VTI instruments (Hialeah, FL) using a static volumetric method. Low pressure isotherms (up to 10 kPa) were obtained at 298 K with an Autosorb-1MP volumetric system from Quantachrome Instruments (Boynton Beach, FL). Prior to adsorption tests Na-ETS-10 materials in crystalline powder form (with no added binders or diluents) were dried at 523 K for 12 h under a vacuum of greater than 10⁻⁴ Torr.

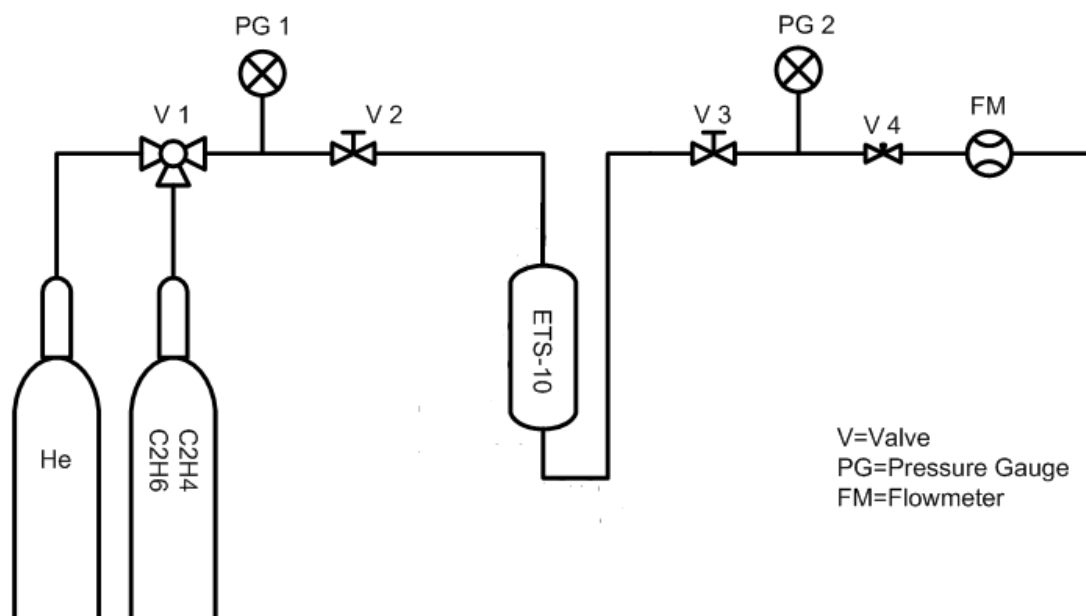


Figure 5-1. Schematic of high pressure adsorption process.

5.3.3 Breakthrough Experiments

Laboratory-scale demonstration is illustrated in Figure 5-1. Breakthrough experiments were performed using 28 g samples of pelletized, ground and sieved test adsorbent. The adsorbent was packed into a 50 mL cylindrical stainless steel chamber with an outer diameter of 38 mm and a length of 95 mm. Following adsorbent loading, columns were activated at 473 K for 10 h under 30 mL/min of helium flow. The feed gas mixture composition was: a binary ethylene/ethane mixture (59% C₂H₄: 41% C₂H₆). The gas mixture was prepared by Praxair to mimic the process gas composition at the inlet of the C₂ splitter tower in an ethylene plant. The feed mixture was introduced into the fixed-bed column at a flow rate of 150 mL/min (298 K, 101.3 kPa). The column pressure was 2580 kPa and column temperature was maintained at 298 K. Outlet gas composition was analyzed using a Varian 3800 gas chromatograph (GC) equipped with an HAYESEP Q column and a thermal conductivity detector. The adsorbed phase was extracted by steam desorption as described below and analyzed by GC.

5.3.4 Desorption Experiments

Figure 5-2 is a schematic representation of the pressure steps during one cycle. The first step involves the pressurization with He. The second (“adsorption”) step involves passing of the ethane/ethylene mixture at a constant high pressure through the Na-ETS-10 bed. The third step is the co-current depressurization (down to ambient pressure) of the column. The fourth step is co-current steam desorption followed by He purge under ambient pressure.

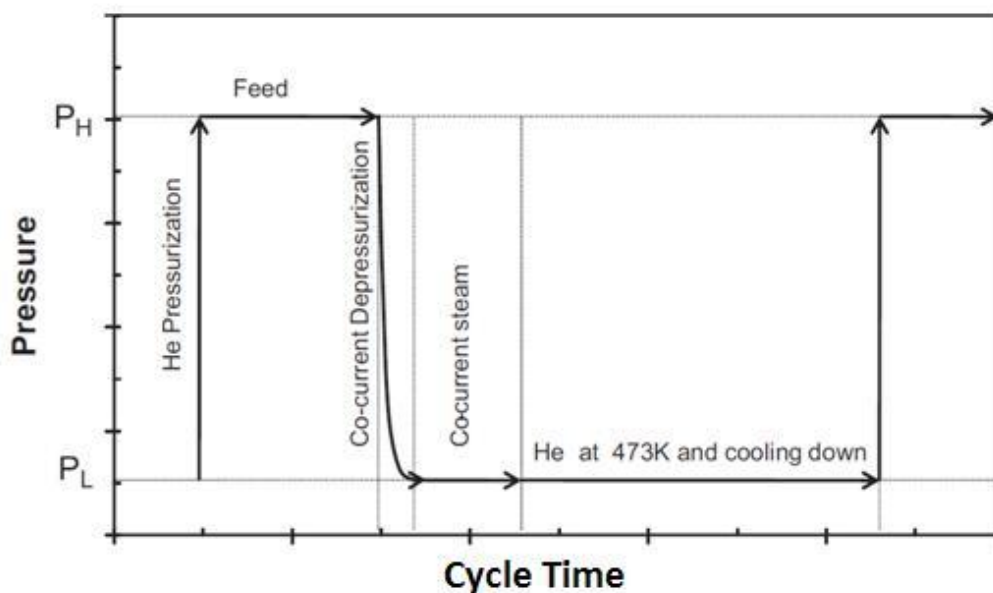


Figure 5-2. Schematic of the different steps involved during the adsorption cycle where P_H corresponds to the high pressure step, and P_L corresponds to the low pressure step.

The steam desorption was performed according to the method described by Shi [14]. When the adsorbent within the column approached equilibrium with the feed gas mixture, the column pressure was released against ambient pressure. Next, steam at 473 K was passed over the adsorbent bed and the gas desorbed from the adsorbent (the adsorbed phase) flowed into a downstream flask, displacing a volume of water

equal to the volume of outlet gas. Outlet gas was sampled and analyzed by GC and, after desorption was complete, the sorbent was thermally re-activated at 473 K for 10 h prior to initiation of further adsorption/desorption cycles.

5.3.5 Theoretical Background

Experimental isotherms were fitted to the Langmuir adsorption isotherm (Eq. 5.1):

$$\frac{q_i}{q_{i,m}} = \frac{b_i P_i}{1 + b_i P_i} \quad (5.1)$$

For each hydrocarbon, q_i is the amount adsorbed on the solid, P_i represents the pressure in the gas phase, $q_{i,m}$ is the saturation or maximum adsorption capacity, and b_i is the Langmuir (equilibrium) constant. The Henry's Law constants $K_i = q_{i,m} b_i$, for each hydrocarbon were used to calculate the limiting ethylene/ethane selectivity (α , Eq. 5.2):

$$\alpha = \frac{K_{C_2H_4}}{K_{C_2H_6}} \quad (5.2)$$

The isosteric heats of adsorption $Q_{st,i}$ (absolute values of the differential enthalpies of adsorption ΔH_i) were calculated from the Van't Hoff equation [15, 16]. The values of $Q_{st,i}$ at different adsorbed loadings were estimated from the isobars obtained from the set of experimental adsorption isotherms:

$$Q_{st,i} = -\Delta H_i = -R \left[\frac{\partial \ln P_i}{\partial (1/T)} \right]_{\theta_i} \quad (5.3)$$

where $\theta_i = q_i/q_{i,m(298\text{ K})}$ is the loading and $q_{i,m(298\text{ K})}$ is the saturation or maximum adsorption capacity at 298 K. The isosteric heats at zero loading were estimated as follows [16]:

$$\Delta H_{i,0} = \lim_{P_i \rightarrow 0} \Delta H_i = -R \left[\frac{d \ln K_i}{d(1/T)} \right] \quad (5.4)$$

The Ideal Adsorbed Solution Theory (IAST) was used to estimate binary isotherms based on single component data [17]. Analogous to Raoult's law for vapour-liquid equilibrium, the IAST equation can be expressed as (Eq. 5.5):

$$P y_i = x_i P_i^*(\pi) \quad i = 1, 2, \dots, n \quad (5.5)$$

where x_i is the mole fraction in the adsorbed phase is (Eq. 5.6)

$$x_i = \frac{\theta_i}{\sum_1^n \theta_i} \quad (5.6)$$

and $P_i^*(\pi)$ is the sorption pressure for each pure component, which yields the same spreading pressure, π , as that of the mixture. The Gibbs adsorption isotherm [18] defines the spreading pressure as:

$$\frac{\pi A}{RT} = \int_0^{P_i^*} \frac{q_{i,m} \theta_{i,pure}(P)}{P} dP \quad (5.7)$$

The observed ethylene/ethane separation selectivity for Na-ETS-10 was defined in terms of the extract composition and the feed mixture fractions (Eq. 5.8):

$$S = \frac{X_{Et}}{X_E} / \frac{Y_{Et}}{Y_E} \quad (5.8)$$

where X_{Et} , X_E and Y_{Et} , Y_E are the mole fractions of ethylene (Et) and ethane (E) in the extract and feed gas, respectively.

5.4 Results and discussion

5.4.1 Single-gas isotherms at high pressure

In order to investigate the suitability of Na-ETS-10 as an adsorbent for the separation of ethylene from ethane in industrial streams, single gas adsorption isotherms should include a pressure range that is far from diluted conditions. In Figure 5-3 we show single gas adsorption isotherms of C₂H₄ and C₂H₆ on Na-ETS-10 crystals at 298 K and a pressure range up to 1800 kPa. The C₂H₄ isotherm is more rectangular indicating that C₂H₄ is adsorbed stronger than C₂H₆ on Na-ETS-10. Both single isotherms approach saturation at pressures above 600 kPa, although the saturation capacity is higher for ethylene than ethane.

The adsorption data were fitted with a Langmuir model and the adsorption parameters are shown in Table 5-1. The corresponding Henry's law constant (K_i) was estimated based on the high pressure data, and the selectivity for ethylene/ethane was determined to be $\alpha = 8.1$, which matches the selectivity estimated from low pressure isotherms (0-10 kPa).

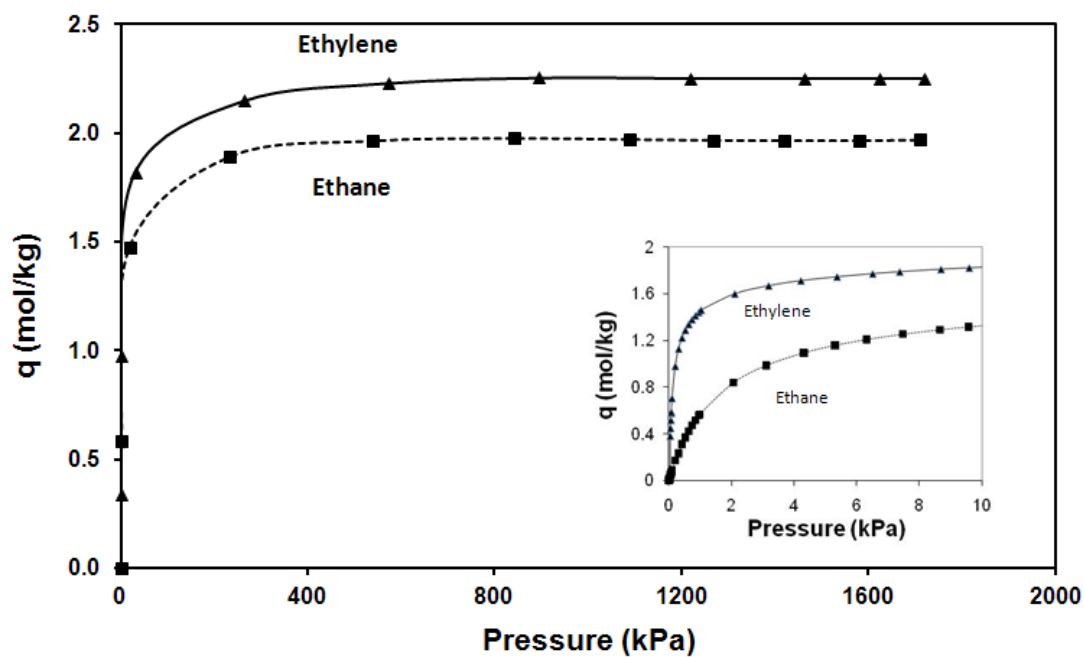


Figure 5-3. Adsorption isotherms for ethylene and ethane on Na-ETS-10 at 298K .
 Insert: low pressure adsorption isotherms at 0-10 kPa.

Table 5-1. Langmuir adsorption parameters for ethylene and ethane on Na-ETS-10 material at 298 K

Gas	$q_{i,m}$ (mol/kg)	b_i (kPa ⁻¹)	K_i (mmol/g kPa)	$\alpha_{C_2H_4}^{C_2H_6}$ (0-1800 kPa)	$\alpha_{C_2H_4}^{C_2H_6}$ (0-10 kPa)
C ₂ H ₄	2.22	1.60	3.55	-	-
C ₂ H ₆	1.95	0.22	0.44	8.1	8.1

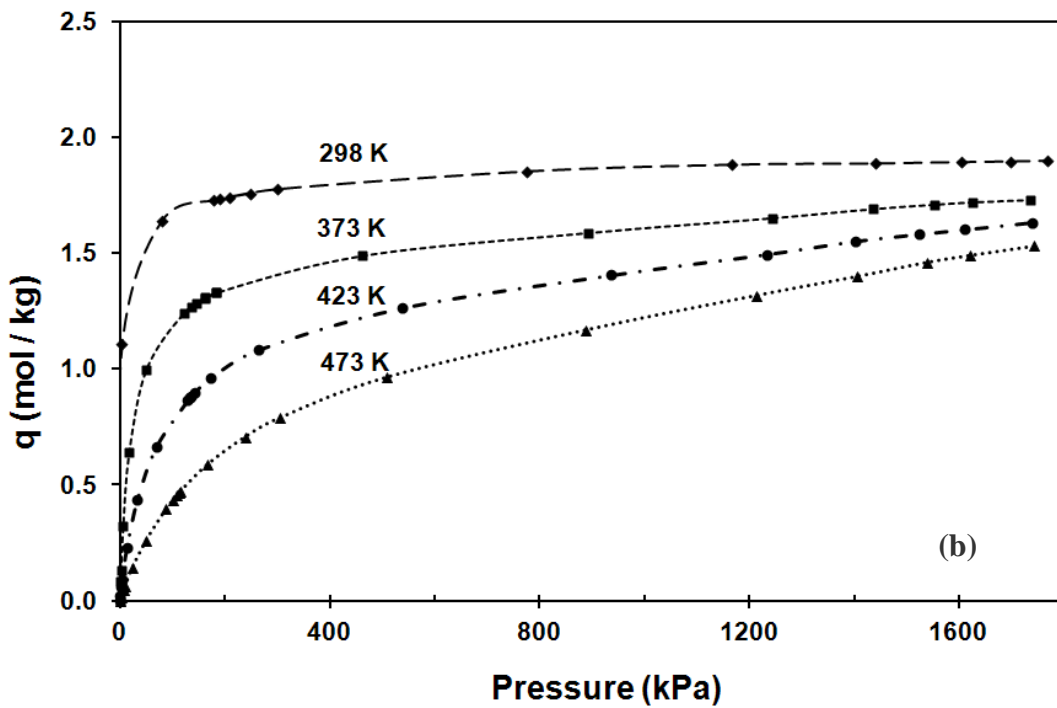
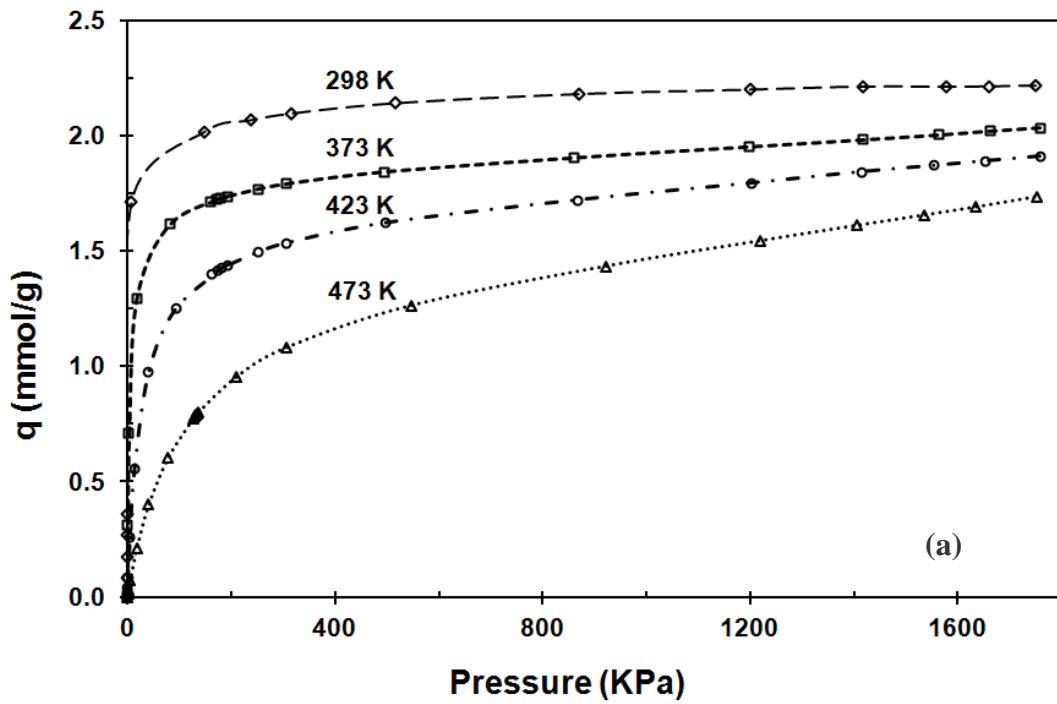


Figure 5-4. Adsorption isotherms of ethylene (a) and ethane (b) on Na-ETS-10 at temperatures 298 K, 323 K, 373 K, 423 K and 473 K.

Figure 5-4 presents the adsorption isotherms for ethane and ethylene at elevated temperatures: 298 K, 323 K, 373 K, 423 K and 473 K. The Henry's law constants were evaluated using a Langmuir model that fits each isotherm. The values of the Henry's constants (K_i) can be plotted as a function of $1000/T$ (as shown in Figure 5-5) to calculate the adsorption heats at zero loading based on Eq. 4.4. These values are shown in Table 5-2 along with those reported in the literature for Na-ETS-10 and zeolite 13X. Na-ETS-10 shows a higher adsorption affinity than zeolite 13X for these hydrocarbons, especially for ethylene.

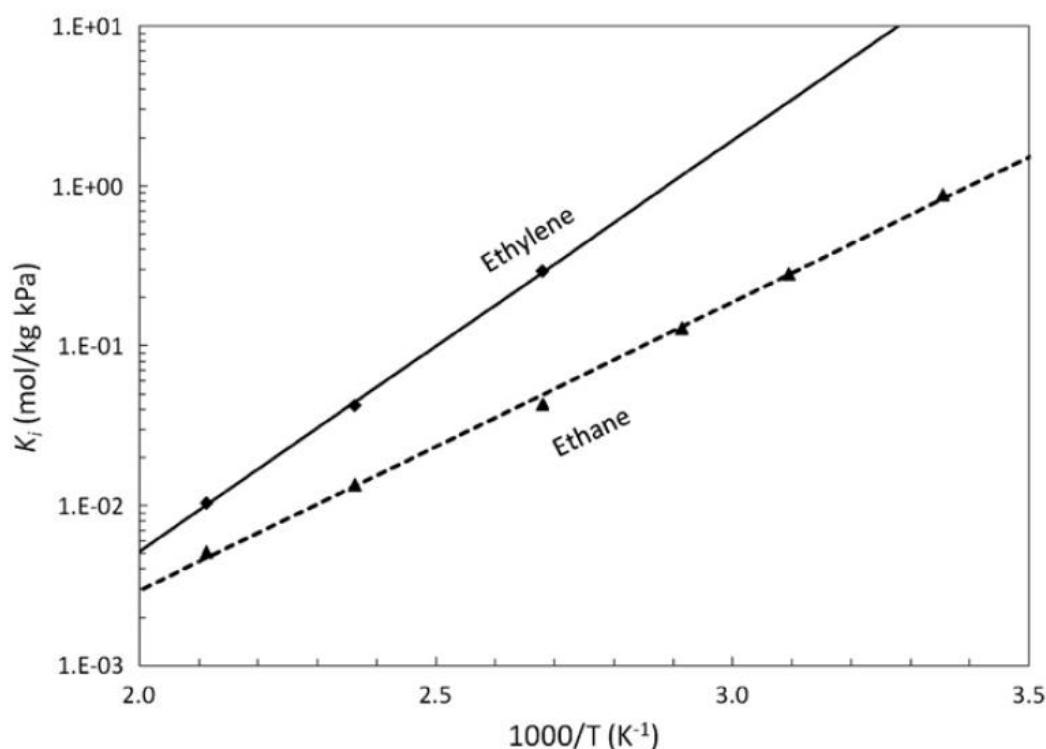


Figure 5-5. Henry's law constants for ethylene and ethane as a function of $1000/T$ for Na-ETS-10.

Figure 5-6 shows the isosteric heats of adsorption of ethylene and ethane as function of loading on Na-ETS-10. The isosteric heats for ethylene and ethane show an increasing trend as loading increases. The isosteric heat for ethylene increases from its lowest value of 49.7 kJ/mol (at zero loading) to 54.8 kJ/mol (0.6 loading). For ethane, the isosteric heat slightly increases from 34.8 kJ/mol (at zero loading) to an average value

of 37.0 kJ/mol (at loading above 0.2). At loadings higher than 0.2, the ethane isosteric heat remains essentially constant. This trend is different than expected for classical zeolites (such as zeolite 13X) and is consistent with the rising ethylene/ethane selectivities with rising total pressure reported in this work.

Table 5-2. Comparison of the experimental and literature reported isosteric heats of adsorption at zero loading for Na-ETS-10 and zeolite 13X.

Material	$(-\Delta H_{i,0})$ (kJ/mol)	
	Ethane	Ethylene
Zeolite 13X	23.0 ^[19]	32.6 ^[19]
	27-32 ^[21]	28-40 ^[21]
	-	38.4 ^[22]
	27.0 ^[23]	-
Na-ETS-10	33.0-36.0 ^[20]	34.0-43.0 ^[20]
	34.8	49.7

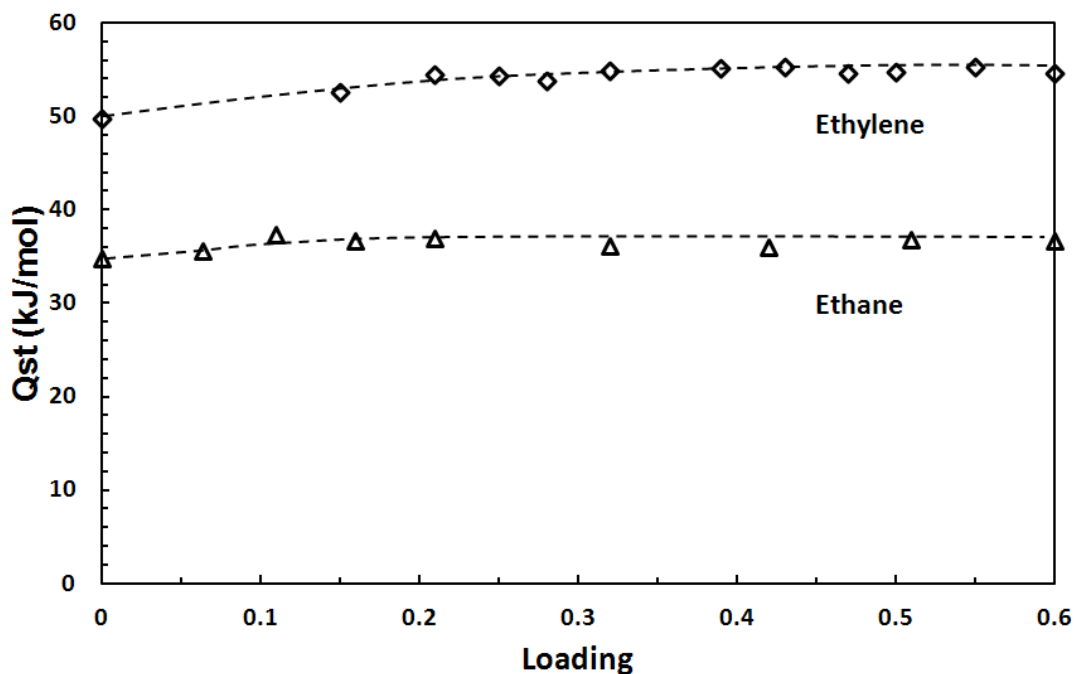


Figure 5-6. Calculated isosteric heats of adsorption for ethylene and ethane as a function of loading for Na-ETS-10.

5.4.2 Separation of a binary ethylene/ethane mixture

Breakthrough curves for ethylene and ethane on Na-ETS-10 at 298 K and 2,580 kPa are shown in Figure 5-7. The feed gas was composed of 59% ethylene and 41% ethane. The breakthrough concentration profiles are expressed as a function of the number of bed volumes of the feed gas mixture (at standard conditions: 298 K, 101 kPa) that flowed through the packed bed. During the first stage (up to 60 bed volumes), the adsorbent bed retained all the ethylene and the outlet stream (raffinate stream) was composed of pure ethane. After ~115 bed volumes, the concentration of the outlet gas reflected the inlet (feed gas) composition, indicating that the Na-ETS-10 had reached the adsorption equilibrium. Based on these data it is possible to design cycle times to optimize the recovery of pure ethane and enriched ethylene using Na-ETS-10 as the adsorbent at high pressure.

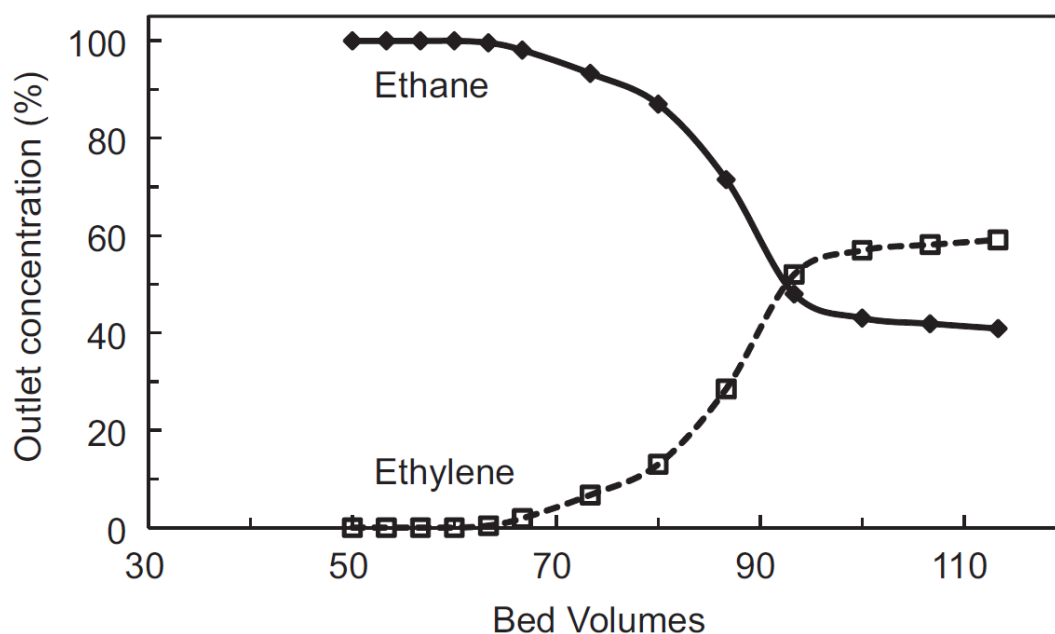


Figure 5-7. Breakthrough curves for ethylene and ethane as a function of bed volume on a fixed bed column composed of Na-ETS-10. Feed mixture: 59/41 ethylene/ethane. Feed rate: 150 sccm (298 K, 101.3 kPa). Column temperature: 298 K. Column pressure: 2,580 kPa.

The feed gas (59% ethylene/ 41% ethane mixture) flowed onto the packed bed column at different column pressures until the adsorbent within the column and the feed gas mixture approached equilibrium. Next, the column pressure was released against ambient pressure and the adsorbed phase on the bed was desorbed using steam. From here on we will refer to the desorbed phase as the extract stream or extract phase. The mole fractions of ethylene in the extract stream are shown in Table 5-3 as a function of the packed bed column pressure. As the adsorption column pressure increased so did the ethylene extract composition reaching up to 94% at 2580 kPa.

Table 5-3. Volume and composition of the extract stream (desorbed phase) for different column pressures. Adsorbent: Na-ETS-10. Temperature: 298 K.

Column Pressure kPa	Volume ml (STP) ^a	Composition % C ₂ H ₄	Adsorbent capacity mole C ₂ H ₄ /Kg ETS-10
101	1122	88.0	1.44
930	1207	91.6	1.61
1760	1233	92.1	1.66
2580	1344	94.0	1.84

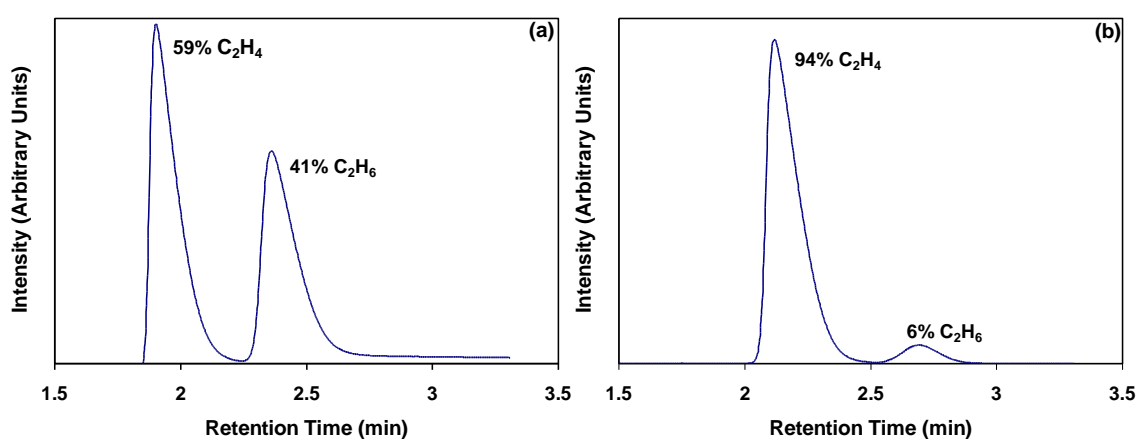


Figure 5-8. Gas chromatography analysis of feed gas (left) and extract composition (right) under 2,580 kPa at 298 K.

Gas chromatography analysis of feed gas and the extract composition is shown in Figure 5-8. The increasing trend of the ethylene mole fraction in the extract phase is consistent with the predicted behaviour of the equilibrium mole fraction based on the IAST model (Figure 5-9). However, the predicted values for ethylene mole fraction are higher than the experimental values in this study, particularly at low pressures. We speculate this could be due to the non-ideal adsorption behaviour of ethylene in comparison to that of ethane as previously suggested elsewhere [12].

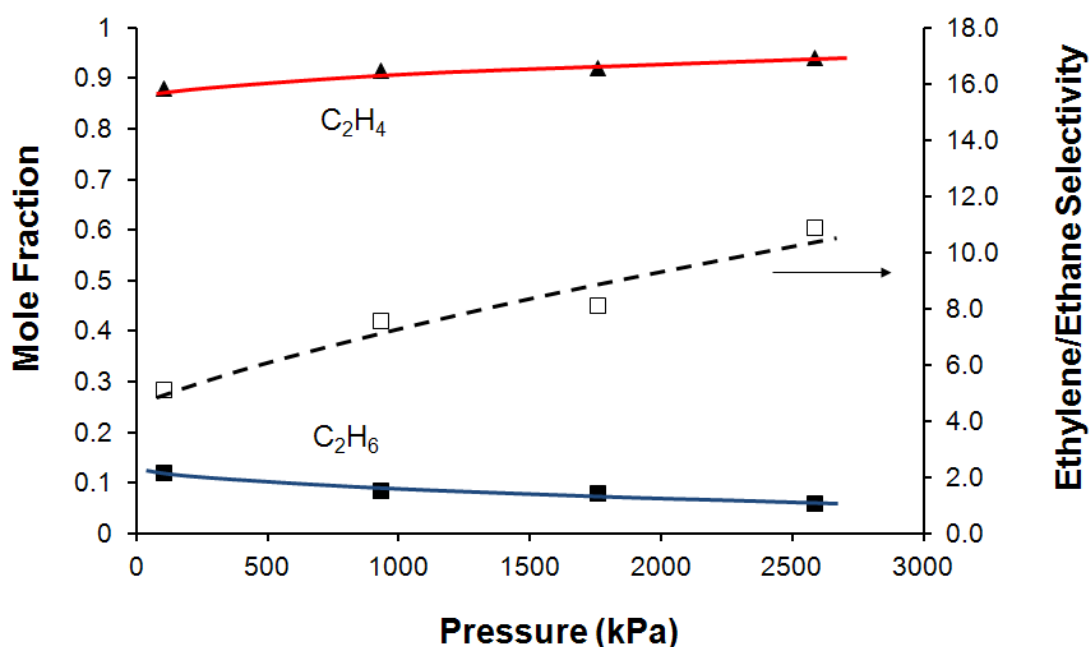


Figure 5-9. Mole fractions of ethylene and ethane in the extract stream (closed symbols, solid line) and ethylene/ethane selectivity from a Na-ETS-10 adsorption column at 298 K (open symbols) as a function of pressure. Predicted mole fractions are based on the IAST mixture adsorption model using single gas adsorption isotherm values from ethylene and ethane on NaETS-10 crystals at 298 K (dotted line).

In addition, the observed ethylene/ethane selectivity for this separation increased with the column pressure showing a value of ~11 at pressures (2580 kPa) similar to the ones in industrial streams (Table 5-4). Higher selectivities were obtained when the temperature was lowered to 273 K for almost all the entire pressure range. The only exception was at the highest tested pressure (2580 kPa), where we observed no change in low temperature selectivity. The results reflect the difference in isosteric heats for ethylene and ethane as shown in Figure 5-6. It is important to point out that the increasing trend of ethylene/ethane selectivity with pressure is consistent with that of the predicted equilibrium values based on the IAST model even though the predicted values are higher than those observed.

Table 5-4. Observed ethylene/ethane selectivities in the extract stream at 298 K and 273 K from a Na-ETS-10 adsorption column and those predicted by Ideal Adsorbed Solution Theory, as compared to previously reported equilibrium adsorbed fractions at 280 K.

Pressure	Ethylene/ethane selectivity			
	Observed		Equilibrium Ref. ^a	Equilibrium predicted
	298 K	273 K	280 K	298K
kPa				
101	5.1	6.3	-	12.4
150	-	-	7.0	12.9
500	-	-	7.8	15.0
930	7.6	9.1	-	15.9
1,760	8.1	9.8	-	17.2
2,580	10.9	10.5	-	17.9

Table 5-3 also shows the volumes of desorbed gas, ethylene extract composition and the amount of ethylene obtained per unit of adsorbent under different column pressures. At 2580 kPa, the volume of desorbed gas was 1344 mL (STP, 298 K, 101.3 kPa), which corresponds to 1.84 mole of ethylene per kg of adsorbent in the extract stream. Thus, a single step adsorption-desorption process was able to split a 59/41 ethylene/ethane feed mixture into an ethylene-rich extract stream and an ethane-rich raffinate stream that would require minimal recompression work. These results suggest that a stream containing 59% ethylene and 41% ethane can be enriched with up to 94% ethylene at high pressure using common adsorption-desorption steps. Na-ETS-10 adsorbent improves the performance of the ethylene/ethane separations as the adsorption column pressures increase (up to 2600 kPa).

5.5 Conclusions

This study demonstrates that Na-ETS-10 can be used as an effective adsorptive material to separate ethylene from ethane in a binary mixture under high pressure conditions. A 59/41 mixture of C_2H_4 and C_2H_6 was separated on Na-ETS-10 at 360 psi and 298 K over a pressure range of 101-2580 kPa. At the highest pressure tested (2580 kPa), an ethylene/ethane bed selectivity of ~ 11 was achieved, which is more than double the previously reported selectivity ($S = 5$) under low pressure. Although these are laboratory-scale results the potential use of Na-ETS-10 as an adsorbent that allows efficient separation of olefin/paraffin at industrial stream pressures is very promising and requires further investigation.

5.6 References

- [1] Kniel, L., Winter, O., Stork, K., 1980. *Ethylene: Keystone to the petrochemical industry*. Marcel Dekker Inc., New York and Basel.
- [2] Global Industry Analysts, Inc., 2008. *Ethylene: A global strategic business report*.
- [3] Eldrige, R.B., 1993. *Industrial & Engineering Chemistry Research* 32, 2208-2212.
- [4] Anson, A., Wang, Y., Lin, C.C.H., Kuznicki, T.M., Kuznicki, S.M., 2008. *Chemical Engineering Science* 63, 4171-4175.
- [5] Miltenburg, A. V., Gascon, J., Zhu, W., Kapteijn, F., Moulijn, J. A., 2008. *Adsorption* 14, 309-321.
- [6] Silva, F. A. D., Rodrigues, A.E., 2001. *AIChE Journal* 47, 341-357.
- [7] Gomes, P. S., Lamia, N., Rodrigues, A. E., 2009. *Chemical Engineering Science* 64, 1336-1357.
- [8] Lamia, N., Wolff, L., Leflaive, P., Gomes, P. S., Grande, C. A., Rodrigues, A. E., 2007. *Separation Science and Technology* 42, 2539-2566.
- [9] Kuznicki, S.M., 1991. *Large-pored crystalline titanium molecular sieve zeolites*. US Patent No. 5,011,591.
- [10] Anderson, M.W., Terasaki, O., Ohsuna, T., Philippou, A., Mackay, S.P., Ferreira, A., Rocha, J., Lidin, S., 1994. *Nature* 367, 347-351.
- [11] Sircar, S., Myers, A. L., 2003. *Handbook of Zeolite Science and Technology (Gas Separation by Zeolites)*. Marcel Dekker Inc., New York.
- [12] Al-Baghli, N.A., Loughlin, K.F., 2006. *Journal of Chemical and Engineering*

Data 51, 248-254.

- [13]Kuznicki, S.M., Ansón, A., Segin, T., Lin, C.C.H., 2009. *Modified ETS-10 Zeolites for Olefin Separation*. US Patent Application No. 20090187053.
- [14]Shi, M., Lin, C.C.H., Kuznicki, T.M., Hashisho, Z., Kuznicki, S.M., 2010. *Chemical Engineering Science* 65, 3494-3498.
- [15]Do, D. D., 1998. *Adsorption analysis: equilibria and kinetics*. Imperial College Press, London.
- [16]Myers, A. L., 2002. *AIChE Journal* 48, 145-160.
- [17]Myers, A.L., Prausnitz, J.M., 1965. *AIChE Journal* 11, 121-127.
- [18]Yang, R.T., 1987. *Gas separation by adsorption process*. Imperial College Press.
- [19]Ruthven, D. M., Reyes, S. C., 2007. *Microporous and Mesoporous Materials* 10, 59-66.
- [20]Al-Baghli, N. A., Loughlin, K. F., 2005. *Journal of Chemical and Engineering Data* 50, 843-848.
- [21]Hyun, S. H. Danner, R. P., 1982. *Journal of Chemical Engineering Data* 27, 196-200.
- [22]Triebe, R.W., Tezel, F.H., Knulbe, K.C., 1996. *Gas Separation and Purification* 10, 81-84.
- [23]Dunne, J. A., Rao, M., Sircar, S., Gorte, R. J., Myers, A. L., 1996. *Langmuir* 12, 5896-5904.

Chapter 6

Extraction of Ethane from Natural Gas at High Pressure by Adsorption on Na-ETS-10

A revised version of this chapter has been published. Reproduced with permission from Avila, A.M., Yang, F., Shi, M., Kuznicki, S.M., 2011. *Chemical Engineering Science* 66, 2991-2996.

6.1 Summary

Methane/ethane separation was achieved using Na-ETS-10 as a packed bed adsorbent over a pressure range of 450-5600 kPa at 298 K. At these pressures, pure methane gas raffinate streams were obtained prior to ethane breakthrough. The extract phase obtained following desorption from the packed bed column was enriched in ethane. Extract phases containing up to 75% ethane were achieved following separations of a 93/7 methane/ethane feed mixture. Separation performance did not deteriorate as adsorption column pressures increased. Selective adsorption of a synthetic natural gas mixture using a Na-ETS-10 packed bed column resulted in hydrocarbon outlet compositions ranging from pure methane (up to ~60 bed volumes at standard temperature and pressure) to ~93% methane, ~5% ethane and ~2% propane (~150 to ~850 bed volumes at standard temperature and pressure). In all cases, following desorption, the extract phase was highly enriched in the larger and more valuable hydrocarbons.

6.2 Introduction

Natural gas (NG) is one of the most important energy resources worldwide. Modern NG transport technologies ensure that large reserves of this high energy, clean burning fuel are available at a low overall cost. Since NG is a commodity, however, NG producers are constrained by the narrow operating margins between processing cost and market price.

NG must be conditioned before it is fed to pipelines for distribution; processing costs for treating NG are associated with both contaminant removal and liquid recovery [1]. Dehydration prevents corrosion, hydrate formation and freezing in the pipeline. Reducing the concentration of acid gases, including H₂S and CO₂, prevents corrosion and increases the NG energy content per unit volume. Removal of inert gases with no heating value (such as N₂) also increases energy density. Hydrocarbons heavier than methane, commonly known as natural gas liquids (NGL), can contribute to the energy content of NG, but heavier hydrocarbons generally have a higher product value when used as separate fuels or as chemical feedstocks, rather than as components of natural gas. For example, ethane (C₂) is a key feedstock in industrial ethylene production and, as such, efficient recovery of ethane (C₂) from NGL can control operating costs for ethylene plants [2]. In addition, heavy hydrocarbons (C₃+) are commonly removed from NG to prevent fouling of downstream valves, pipes and other equipment.

NGL and C₂ recoveries from NG, predominantly through cryogenic expansion, are both energy intensive processes [3, 4]. A conventional cryogenic expansion process, also known as a turbo-expander process, is outlined in Figure 6-1. After pretreatment, the gas mixture is cooled by heat exchangers and partially condensed, followed by separation into liquid and vapour streams in a flash separator. The vapor stream, which contains the more volatile species, is expanded through a turbo-expander into a distillation column (demethanizer), resulting in additional liquid condensation. The

liquid stream is injected into the same column for recovery of the heavy hydrocarbon components. The bottom product, containing C₂ and C₃+ (NGL) species, can be further fractionated to produce feedstocks for polyethylene plants (C₂) or incorporated into high heating value fuels such as Liquefied Petroleum Gas (LPG). The top product of the demethanizer column (residue gas) must be recompressed from approximately 100-450 psi (700 to 3100 kPa) up to common pipeline pressures (800 to 1000 psi/5500 to 6800 kPa) in order to be delivered as sales gas.

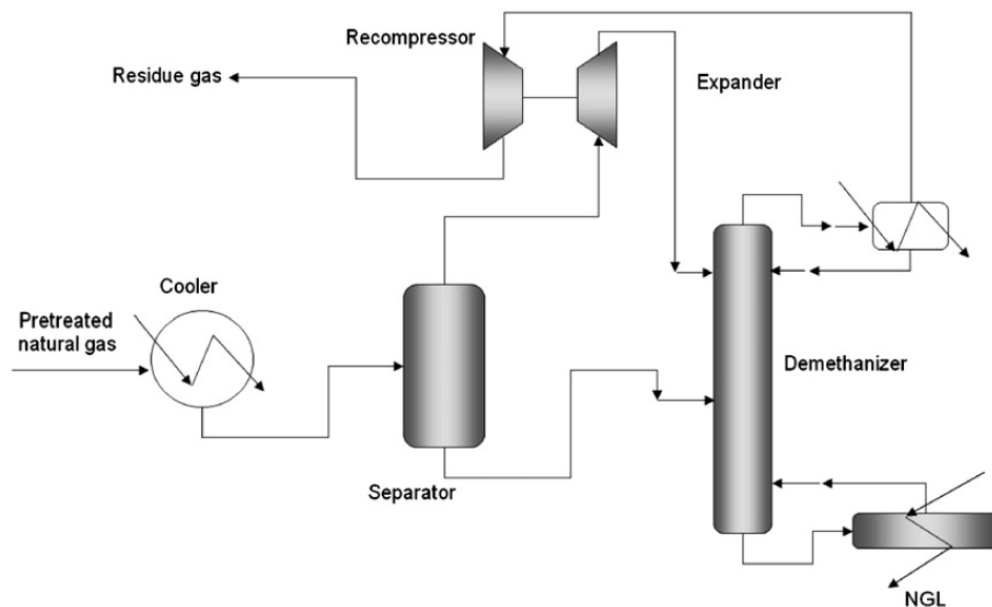


Figure 6-1. Conventional NGL recovery process. Basic turbo-expander process.

Adsorptive separation based on cation-exchanged ETS-10-type adsorbents has been proposed as a process that could decrease the energy consumption associated with ethane/methane separation and NGL recovery [5], reducing process costs and contributing to environmental sustainability. ETS-10 is a large-pored, mixed octahedral/tetrahedral titanium silicate with a framework composed of a three-dimensional network of interconnecting channels and cavities whose adsorption characteristics can be manipulated through cation exchange [6-8]. When Na-ETS-10,

Ba-ETS-10 and Ba/H-ETS-10 were applied to the separation of ethane from methane under low pressure conditions, Na-ETS-10 showed the most promising performance in terms of both adsorbent capacity and selectivity [5]. It is important to note that, since the average kinetic diameter of molecules that can enter the pores of ETS-10 (~8 Å) is much larger than either methane or ethane, this separation is likely achieved through equilibrium competitive adsorption [6].

NG feedstocks for the NGL recovery process are generally high pressure streams, occasionally at pressures as high as 10^4 kPa. Hence, any potential adsorption process related to natural gas treatment should contemplate materials and engineering designs with efficient separation performance at higher pressures [1]. Working at high pressures would minimize the re-compression work required before materials are introduced into the downstream pipeline. However, as is the case for previous studies of Na-ETS-10, adsorbent materials are generally evaluated at low pressures in the laboratory, far from the conditions found in natural gas pipelines. In fact, some previous work which examined the ethane/methane selectivity with as-synthesized (non-cation-exchanged) ETS-10 showed that for a given temperature, the selectivity of ethane/methane separation decreases as the pressure is increased, as is typical for molecular sieve separations [9, 10]. These results are silent, however, to ETS-10 performance at pressures above 500 kPa (72.5 psia) and to the effects of cation exchange on ETS-10 performance.

The use of a packed bed column with Na-ETS-10 pellets for treating the NG feedstock at high pressures could be a promising alternative to strip paraffinic hydrocarbons from NG by selective adsorption, if the adsorbent is able to support efficient separation at high pressures. Similarly, a packed bed column with Na-ETS-10 pellets could be used to extract the 1-2% ethane commonly present in the residue gas from demethanizer units in order to supply feedstock for ethylene plants. In both cases, adsorption at high pressure would minimize recompression work and address the difficulties associated with the separation of ethane as an intermediate

between methane and propane. High pressure adsorptive separation could provide clear advantages relative to energy intensification in natural gas treatment processes.

The objective of the current study was to evaluate Na-ETS-10 as an adsorbent material capable of separating C1/C2 and C1/NGL at conditions approximating natural gas pipeline pressures. Adsorption isotherms were measured for methane and ethane at high pressures and used to estimate the mixture adsorption equilibrium on Na-ETS-10 crystals as a function of pressure. The separation performance of Na-ETS-10 within packed-bed columns was analyzed based on the raffinate and extract streams produced from C1/C2 and C1/NGL feed mixtures at room temperature and high pressures (up to 5600 kPa).

6.3 Experimental

6.3.1 Material synthesis

Hydrothermal synthesis of ETS-10 was carried out as previously described [6]. A mixture of 50 g of sodium silicate (28.8% SiO₂, 9.14% Na₂O, Fisher), 3.2 g of sodium hydroxide (97% NaOH, Fisher), 3.8 g of KF (anhydrous, Fisher), 4 g of HCl (1M, Fisher), and 16.3 g of TiCl₃ solution (Fisher) was stirred in a blender for 1 h. The mixture was then transferred to a Teflon-lined autoclave and reacted for 64 h at 488 K. The product was washed with deionized water and dried at 373 K. Following drying, ETS-10 was reduced to a fine powder (<150 μm; 100 mesh). Samples to be used for breakthrough analysis were pelletized by mixing 2.5 g of Ludox HS-40 colloidal silica (Aldrich) with 6 g of dried ETS-10, homogenizing with mortar and pestle, and compressing in a pellet press. The resulting discs were ground and sieved to 20-50 mesh (297-841 μm).

6.3.2 Adsorption isotherms

The ethane and methane adsorption isotherms on Na-ETS-10 at high pressures (0-1800 kPa) were measured at 298 K, 323 K and 373 K with an HPVA-100 High Pressure Volumetric Analyzer adsorption unit from VTI instruments (Hialeah, FL) using a static volumetric method. Low pressure isotherms (up to 10 kPa) were obtained at 298 K with an Autosorb-1MP volumetric system from Quantachrome Instruments (Boynton Beach, FL). Na-ETS-10 materials in crystalline powder form (with no added binders or diluents) were dried at 523 K for 12 h under a vacuum of greater than 10^{-4} Torr prior to adsorption tests.

6.3.3 Breakthrough experiments

Breakthrough experiments were performed using 30 g samples of pelletized, ground and sieved test adsorbent. The adsorbent was packed into a 50 cc cylindrical stainless steel chamber with an outer diameter of 38 mm and a length of 95 mm. Following adsorbent loading, columns were activated at 473 K for 10 h under 30 sccm of helium flow. Two feed gas mixture compositions were used: i) a binary methane/ethane mixture (93.00 CH₄: 7.00 C₂H₆) and ii) a multicomponent mixture that approximates raw natural gas (90.99 CH₄: 5.60 C₂H₆: 1.63 C₃H₈: 0.69 CO₂: 0.50 N₂: 0.49 C₄H₁₀: 0.10 C₅H₁₂). Each feed mixture was introduced into the fixed-bed column at a flow rate of 250 sccm (298 K, 101.3 kPa). The column pressure ranged from 450 to 5600 kPa and column temperature was maintained at 298 K. Outlet gas composition was analyzed using a Varian 3800 gas chromatograph (GC) equipped with an HAYESEP Q column and a thermal conductivity detector. The adsorbed phase was extracted by steam desorption as described below and analyzed by GC. Methane (C1), ethane (C2) and propane (C3) were quantified in the sample, but also the fraction of heavier hydrocarbons (C4+: butanes, pentanes) were qualitatively detected.

6.3.4 Desorption experiments

The adsorbed phase was extracted and the column regenerated by steam desorption as previously described [11]. When the adsorbent within the column approached

equilibrium with the feed gas mixture, the column pressure was released against ambient conditions. Next, steam at 473 K was passed over the adsorbent bed and the gas desorbed from the adsorbent (the adsorbed phase) flowed into a downstream flask, displacing a volume of water equal to the volume of outlet gas. Outlet gas was sampled and analyzed by GC and, after desorption was complete, the sorbent was thermally re-activated at 473 K for 10 h prior to initiation of further adsorption/desorption cycles.

6.3.5 Theoretical background

Experimental isotherms were fitted to the Langmuir adsorption isotherm:

$$\frac{q_i}{q_{i,m}} = \frac{b_i P_i}{1 + b_i P_i} \quad (6.1)$$

For each hydrocarbon, q_i is the amount adsorbed on the solid, P_i represents the pressure in the gas phase, $q_{i,m}$ is the saturation or maximum adsorption capacity, and b_i is the Langmuir (equilibrium) constant. The Henry's Law constants $K_i = q_{i,m} b_i$, for each hydrocarbon were used to calculate the limiting C2/C1 selectivity (α):

$$\alpha = \frac{K_{C_2H_6}}{K_{CH_4}} \quad (6.2)$$

The Ideal Adsorbed Solution Theory (IAST) was used to estimate binary isotherms based on single component data [12]. Analogous to Raoult's law for vapour-liquid equilibrium, the IAST equation can be expressed as follows:

$$P y_i = P_i^*(\pi) x_i \quad i = 1, 2, \dots, n \quad (6.3)$$

where the mole fraction in the adsorbed phase is x_i

$$x_i = \frac{\theta_i}{\sum_i^n \theta_i} \quad (6.4)$$

and $P_i^*(\pi)$ is the sorption pressure for each pure component i , which yields the same spreading pressure, π , as that of the mixture. The Gibbs adsorption isotherm defines the spreading pressure as follows [13]:

$$\pi = \frac{RT}{A} \int_0^{P_i^*} \frac{n_i^0(P)}{P} dP \quad (\text{constant } T) \quad (6.5)$$

The observed C1/C2 separation selectivity for Na-ETS-10 was defined in terms of the extract composition and the feed mixture fractions:

$$S_{C2/C1} = \frac{X_{C2}Y_{C1}}{X_{C1}Y_{C2}} \quad (6.6)$$

where X and Y are the mole fractions of methane (C1) and ethane (C2) in the extract and feed gas, respectively.

6.4 Results and discussion

6.4.1 Single-gas isotherms at high pressure

Natural gas is commonly transported at high pipeline pressures, and adsorptive separations that extract ethane from natural gas at high pressure could increase the energy efficiency of NG conditioning. To investigate the suitability of Na-ETS-10 for the separation of ethane from methane in industrial natural gas streams, the evaluation of single gas adsorption isotherms should include a pressure range far from diluted conditions. Figure 6-2 depicts single gas adsorption isotherms of CH₄ and C₂H₆ on Na-ETS-10 crystals at 298 K for pressures up to 1800 kPa. C₂H₆ adsorbs more strongly than CH₄ on this material, resulting in a more rectangular isotherm that approaches saturation at much lower pressures.

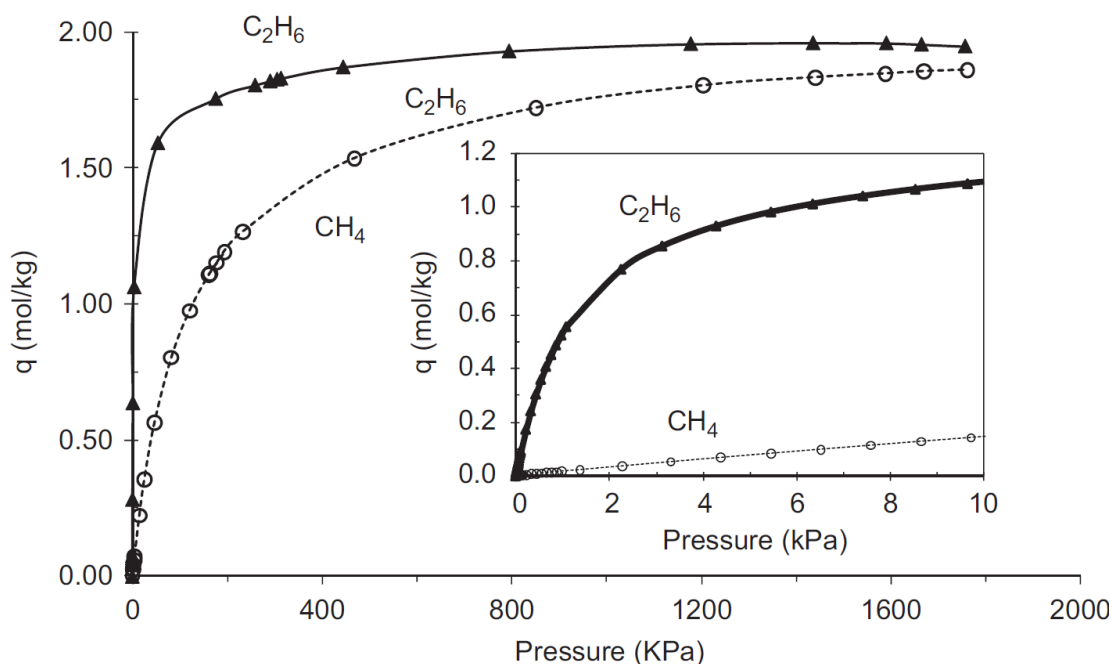


Figure 6-2. Adsorption isotherms for methane and ethane on Na-ETS-10 at 298 K. Insert: low pressure adsorption isotherms at 0-10 kPa.

Table 6-1. Adsorption parameters for ethane and methane on Na-ETS-10 materials at 298 K

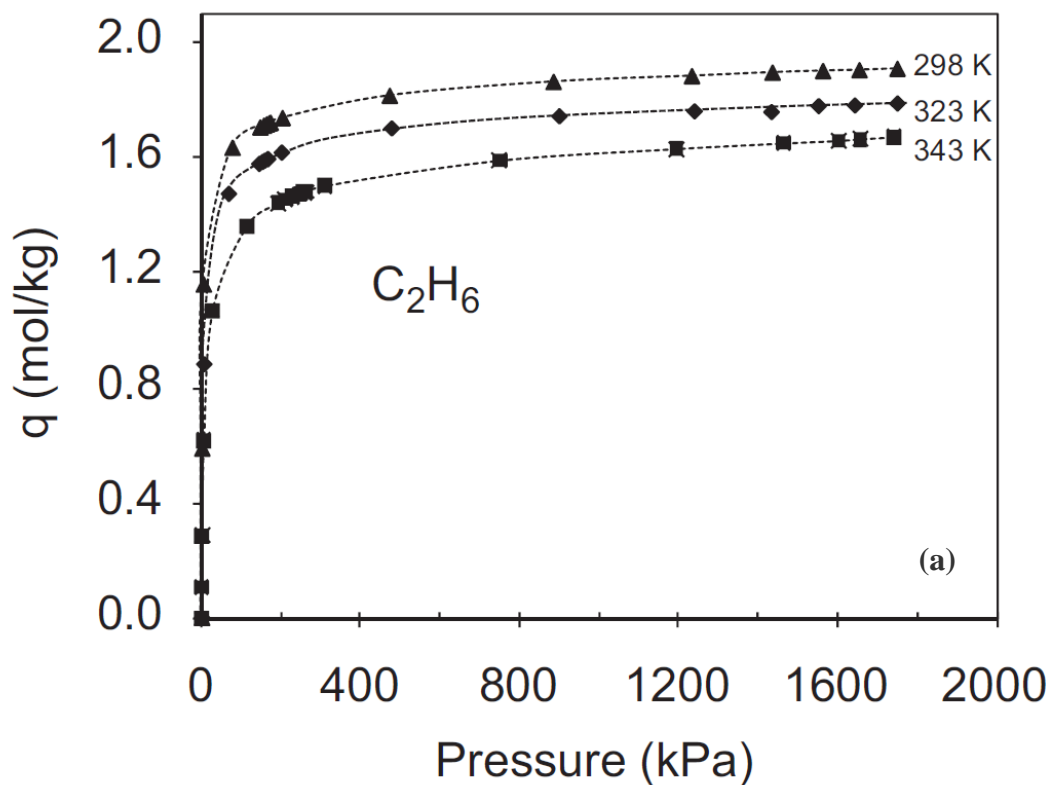
Gas	Adsorbent	$q_{i,m}$ (mol/kg)	b_i (kPa ⁻¹)	K_i (mol/kg kPa)	$\alpha_{CH_4}^{C_2H_6}$ (0-1800 kPa)	$\alpha_{CH_4}^{C_2H_6}$ (0-10 kPa)
CH ₄	Na-ETS-10	1.98	0.008	0.016	-	-
C ₂ H ₆	Na-ETS-10	1.88	0.369	0.693	44	52

The adsorption data were fitted with a Langmuir model and the adsorption parameters are shown in Table 6-1. Based on the high pressure data, the corresponding Henry's law constant (K_i) was estimated and the limiting or Henry's law selectivity for C2/C1 was determined to be $\alpha=44$. However, while adsorption capacities are expected to be more accurate when taken at high pressures, limiting selectivity is best determined at

low pressure. A more accurate value for limiting selectivity for C_2H_6/CH_4 on Na-ETS-10 at 298 K was measured in a low pressure range (0-10 kPa). In this case, the value for the Henry's law selectivity was determined to be $\alpha=52$, in agreement with previous results [5].

Figure 6-3 presents the adsorption isotherms for ethane and methane on Na-ETS-10 samples (using the same synthesis technique) at elevated temperatures of 323 K and 343 K. The values of the Henry's constants (K_i) and the corresponding ethane/methane selectivities ($\alpha_{CH_4}^{C_2H_6}$) at different temperatures are shown in Table 6-2.

As the temperature increases, $\alpha_{CH_4}^{C_2H_6}$ decreases according to the higher adsorption heat for ethane in comparison to methane. However, $\alpha_{CH_4}^{C_2H_6}$ is still higher than 20 at temperature of 343 K.



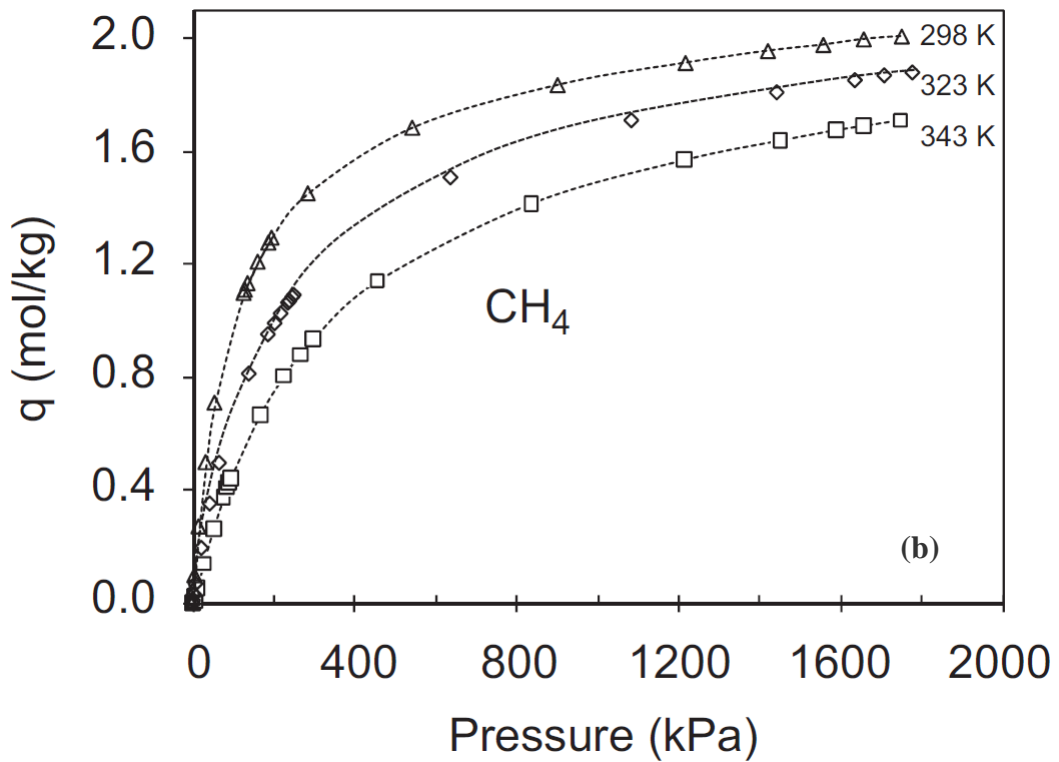


Figure 6-3. Adsorption isotherms of ethane (a) and methane (b) on Na-ETS-10 at temperatures 298 K, 323 K and 343 K.

Table 6-2. Henry's law constants for methane and ethane for Na-ETS-10 at temperatures 298 K, 323 K and 343 K and corresponding ethane/methane selectivities.

Temperature (K)	K_i (mol/kg kPa)		$\alpha_{CH_4}^{C_2H_6}$
	CH ₄	C ₂ H ₆	
298	0.0180	0.88	49
323	0.0092	0.28	30
343	0.0059	0.13	22

6.4.2 Separation of a binary methane/ethane (C1/C2) mixture

Breakthrough curves for ethane (C2) and methane (C1) on Na-ETS-10 at 298 K and 3200 kPa are shown in Figure 6-4. The feed gas was composed of 93% methane and 7% ethane. The breakthrough concentration profiles are expressed as a function of the number of bed volumes of the feed gas mixture (at standard conditions) that flowed through the packed bed. During the first stage (up to 230 bed volumes), the adsorbent bed retained ethane and the raffinate was composed of pure methane, free of ethane content.

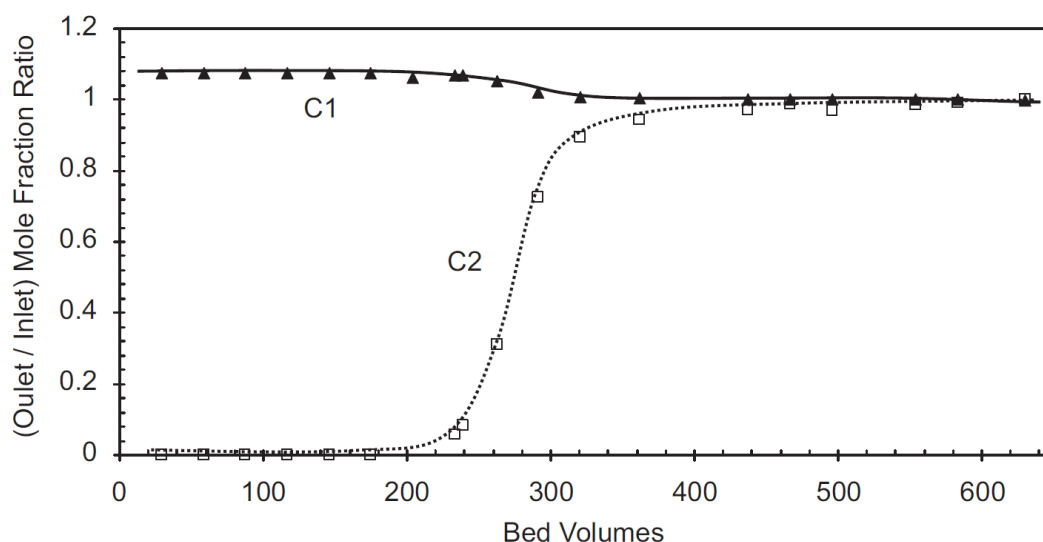


Figure 6-4. Breakthrough curves for methane (C1) and ethane (C2) as a function of bed volume on a fixed bed column composed of Na-ETS-10. Feed mixture: 93/7 methane/ethane. Feed rate: 250 sccm. Column temperature: 298 K. Column pressure: 3200 kPa.

For methane/ethane (93/7) mixtures on Na-ETS-10, the feed gas was flowed onto the packed bed column (at a range of column pressures) until the adsorbent within the column approached equilibrium with the feed gas mixture. Next, the column pressure was released against ambient conditions and the adsorbed phase on the bed was desorbed using steam. For the purposes of this discussion, the desorbed phase represents the extract stream. The mole fractions of methane and ethane in the extract

stream are shown in Figure 6-5 as a function of the packed bed column pressure.

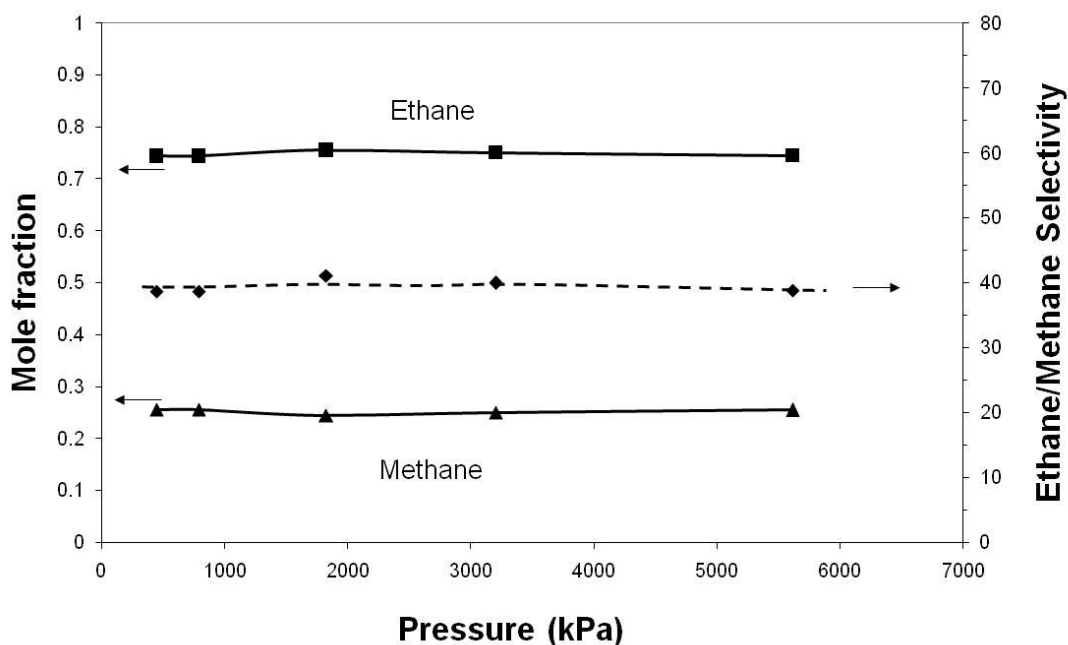


Figure 6-5. Mole fractions of methane and ethane (solid lines) and ethane/methane selectivity (dotted line) in the desorbed extract stream as a function of Na-ETS-10 adsorption column operating pressure. Feed mixture: 93/7 methane/ethane. Feed rate: 250 sccm. Column temperature: 298 K.

The extract composition was essentially unchanged over the entire range of column pressures (450-5600 kPa). Similarly, the extract mole fractions were ~75% for C₂H₆ and ~25% for CH₄ in all samples measured, representing a >10-fold increase in ethane in the extract stream, compared to the feed gas. In addition, the ethane/methane selectivity for this separation remained near 40 at all pressures tested, even at pressures similar to typical natural gas pipeline pressures (5600 kPa; Figure 6-5). For the separation performed at a column pressure of 3200 kPa, the volume of desorbed gas was 1035 cm³ (298 K, 101.3 kPa), which corresponds to ~1.1 mole of ethane per kg of adsorbent (0.77 mol per dm³ of adsorbent) in the extract stream. Similar amounts of extracted ethane were observed at all pressures tested. Thus, a single step

adsorption-desorption process was able to split a 93/7 C1/C2 feed mixture into an ethane-rich extract stream and a methane-rich raffinate stream that would require minimal recompression work. These results suggest that a methane stream containing only 7% ethane can be enriched up to 75% ethane at high pressure using common adsorption-desorption steps.

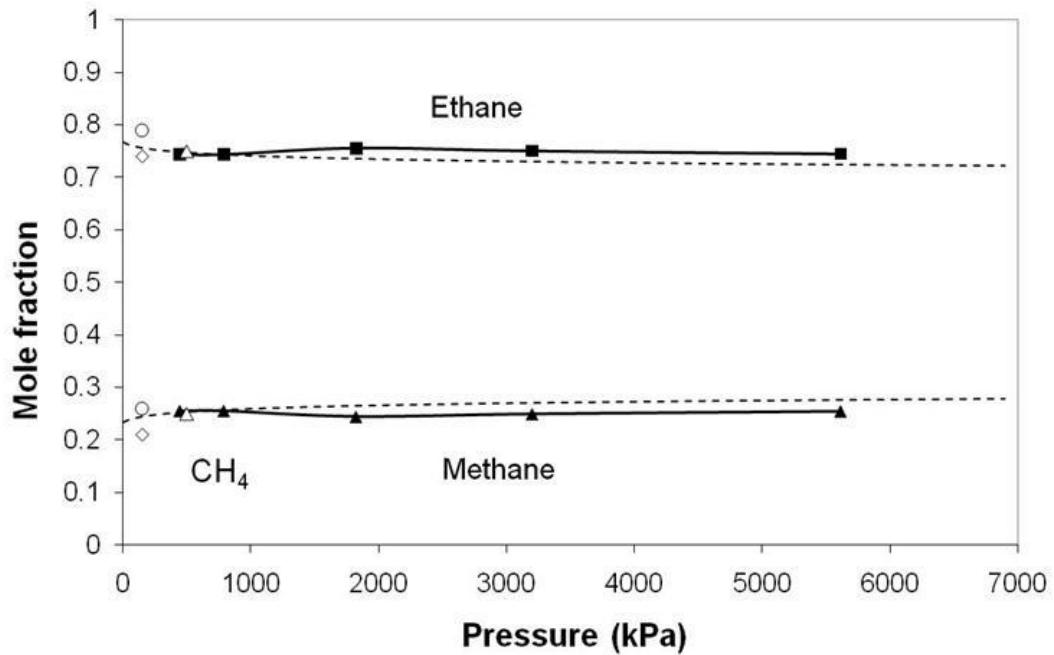


Figure 6-6. Observed mole fractions of methane and ethane in the extract stream (closed symbols, solid line) from an Na-ETS-10 adsorption column and those predicted by Ideal Adsorbed Solution Theory (dotted line), as compared to previously reported equilibrium adsorbed fractions from a 91/9 C1/C2 mixture at: (○)150 kPa, 280 K; (△)500 kPa, 280 K; (◇)150 kPa, 325 K. Predicted mole fractions are based on the IAST mixture adsorption model using single gas adsorption isotherm values from methane and ethane on NaETS-10 crystals at 298 K (dotted line).

Figure 6-6 shows observed extract mole fractions of methane and ethane as a function of pressure. IAST was used to predict mixture adsorption equilibria for a 93/7 methane/ethane mixture on Na-ETS-10 crystals, based on the single gas adsorption parameters from Table 6-1. IAST predicted values (Figure 6-6; dotted line) are shown as a reference for comparison to the observed values (Figure 6-6; closed symbols,

solid line). Published experimental extract mole fraction values are scarce for the adsorptive separation of methane and ethane, particularly at high pressures. Al-Baghli and Loughlin have reported low pressure (below 500 kPa) equilibrium adsorbate fractions for binary methane/ethane mixtures on Na-ETS-10, but did not address methane/ethane adsorption behavior at pressures similar to natural gas pipeline pressures [10]. At lower pressures, the previously reported fractions (open symbols) are in agreement with the observed and predicted equilibrium mole fractions on Na-ETS-10 reported here.

6.4.3 Separation of methane and natural gas liquids

The methane/NGL separation performance of Na-ETS-10 was evaluated through breakthrough curves obtained from a synthetic natural gas feed at 298 K and 3200 kPa. Under these conditions, the Na-ETS-10 adsorption column was able to separate the mixture (90.99 CH₄: 5.60 C₂H₆: 1.63 C₃H₈: 0.69 CO₂: 0.50 N₂: 0.49 C₄H₁₀: 0.10 C₅H₁₂) into three successive raffinate streams that were classified according to outlet gas composition. Three different zones, corresponding to the proposed raffinate streams, can be observed in the breakthrough profile (Figure 6-7).

In the Zone A, all hydrocarbons other than C1 are completely retained on the adsorbent bed. During this period, the raffinate is a methane stream, free of C2+ content, which could be merged into a pipeline network without any recompression work. The capacity of this Na-ETS-10 adsorbent for providing a methane-only stream at high pressures is approximately 60 bed volumes. In Zone B (~60 to 150 bed volumes), the only hydrocarbons present in the raffinate are methane and ethane and the C1/C2 ratio averages ~97/3 (similar to the mixture separated in Figures 6-4, 6-5 and 6-6, above). Propane and larger hydrocarbons are still being adsorbed on the Na-ETS-10 during this period. The Zone B stream could be recycled and reextracted

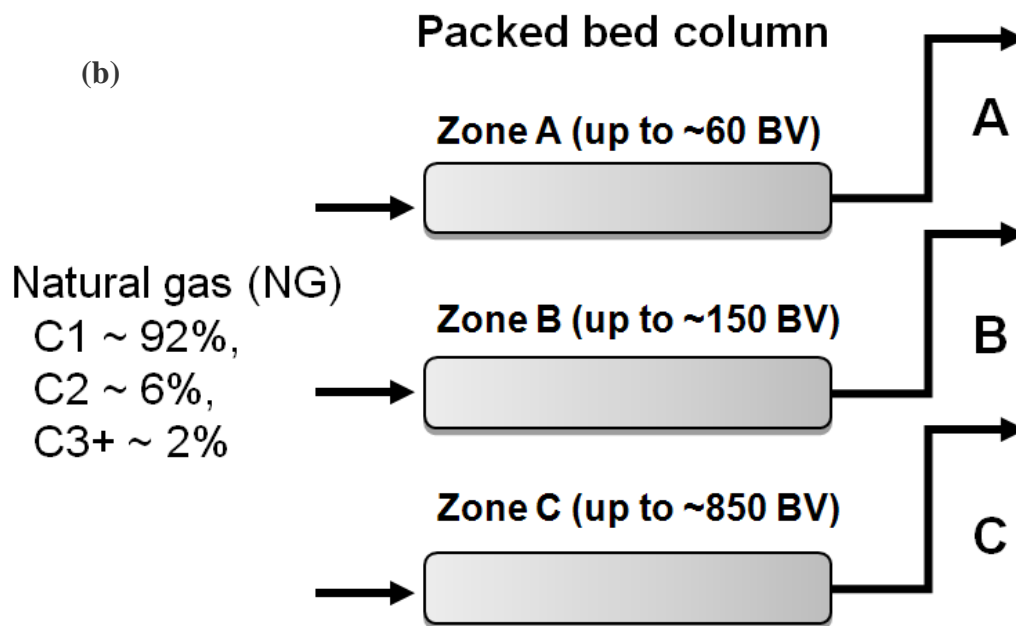
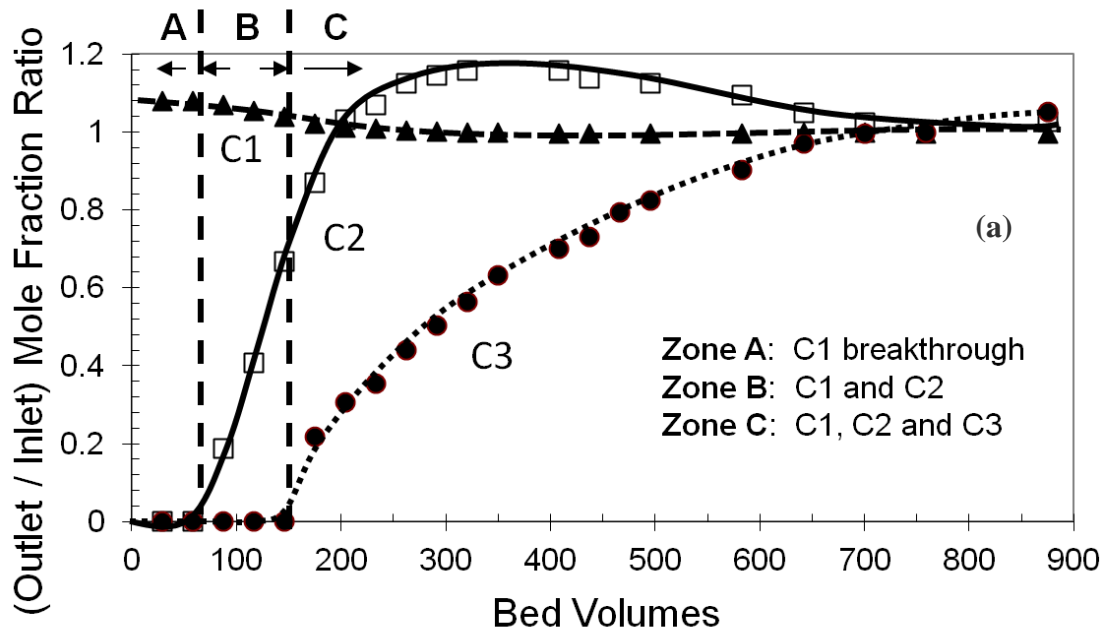


Figure 6-7. (a): Breakthrough curves for methane (C1), ethane (C2) and propane (C3) as a function of bed volumes on a fixed bed column composed of Na-ETS-10. (b): A packed bed column composed of Na-ETS-10 producing three successive raffinate streams (A, B and C) from classified according to their outlet compositions. Feed gas composition: 90.99 CH₄: 5.60 C₂H₆: 1.63 C₃H₈: 0.69 CO₂: 0.50 N₂: 0.49 C₄H₁₀: 0.10 C₅H₁₂. Feed rate: 250 sccm. Column temperature: 298 K. Column pressure: 3200 kPa.

on Na-ETS-10, to obtain an extract with higher ethane content. The Zone C stream includes methane, ethane and propane, but larger hydrocarbons such as butane and isobutane are not present. The hydrocarbon composition in the stream is approximately: C1:93%:C2:5%:C3:2%. The Zone C raffinate could be recycled into any convenient node of the natural gas conditioning process.

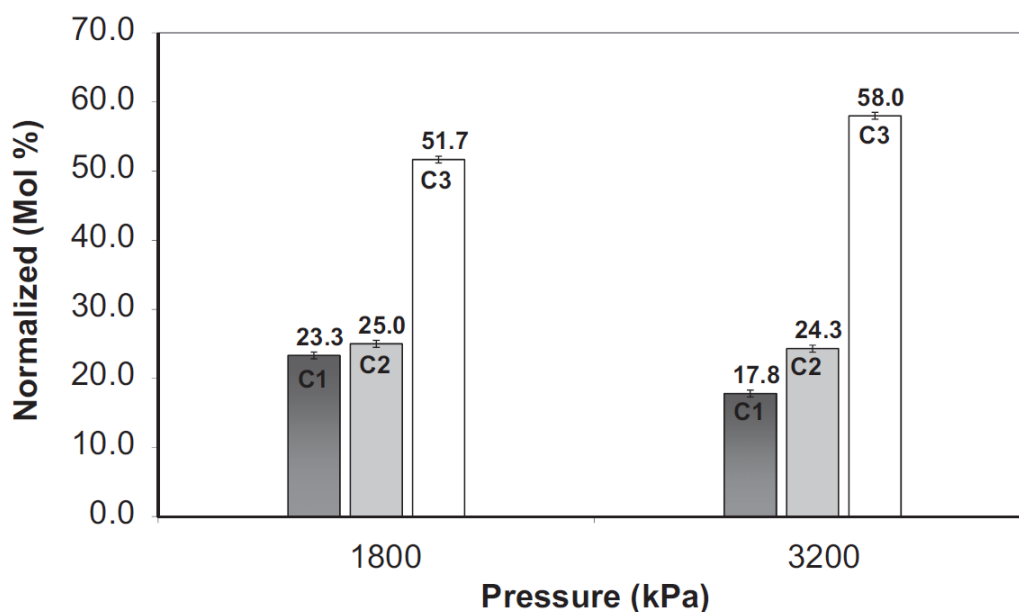


Figure 6-8. Fractions of methane (C1), ethane (C2) and propane (C3) in the desorbed extract stream following steam desorption from a fixed bed column composed of Na-ETS-10. Fractions were desorbed after the column had been exposed to ~850 bed volumes of the feed gas mixture at one of two different column pressures. Feed mixture: 90.99 CH₄: 5.60 C₂H₆: 1.63 C₃H₈: 0.69 CO₂: 0.50 N₂: 0.49 C₄H₁₀: 0.10 C₅H₁₂. Feed rate: 250 sccm. Column temperature: 298 K. Column pressures: 1800 or 3200 kPa.

6.4.4 Increase in NGL/C1 ratio with increasing column pressure

After approximately 850 bed volumes of gas flow, the Na-ETS-10 adsorbent column approaches equilibrium with the feed mixture (Figure 6-7) and the adsorbate phase is composed of larger, more valuable hydrocarbons including propane, butane, isobutane and pentane. When the column pressure is released against ambient conditions and the

adsorbed phase on the bed is desorbed using steam, the desorbed phase represents the extract stream. When the extract compositions from separations performed at two different column pressures (1800 and 3200 kPa) were compared, the C₂₊/C₁ molar ratio in the extract was found to increase with column pressure (Figure 6-8). At 1800 kPa, the ratio is equal to 3.3, while at 3200 kPa, the ratio is equal to 4.6. However, higher C₂₊/C₁ molar ratios are expected since C₄₊ were not quantified as mentioned in the experimental section. Based on these results, NGL/C₁ ratios are predicted to increase as the column pressure increases.

6.5 Conclusions

In the current work, the separation of ethane from methane was achieved using a Na-ETS-10 adsorbent at pressures approximating natural gas pipeline pressures (up to 5600 kPa). A packed-bed Na-ETS-10 adsorbent column was used to split a 93/7 methane/ethane gas mixture into a raffinate stream composed of ethane-free methane and an extract stream containing 75% ethane. The extract composition was virtually independent of the packed-bed column pressure (0-5600 kPa). The Na-ETS-10 adsorbent was also able to separate the components of a synthetic natural gas mixture (90.99 CH₄: 5.60 C₂H₆: 1.63 C₃H₈: 0.69 CO₂: 0.50 N₂: 0.49 C₄H₁₀: 0.10 C₅H₁₂) at high pressure. The breakthrough profile for this separation showed three distinct zones based on outlet composition: C₁, C₁/C₂, and C₁/C₂/C₃. We propose that these zones could be treated as separate raffinate streams that could also be recycled into appropriate nodes of the natural gas treatment process. The adsorbed phase could be recovered as an extract stream enriched in larger and more valuable hydrocarbons including propane, butane, isobutene and pentane. Taken together, these results indicate that ethane can be extracted from natural gas feedstocks at pipeline pressures up to 5600 kPa by selective adsorption on an ETS-10-type material.

6.6 References

- [1] Tagliabue, M., Farrusseng, D., Valencia, S., Aguado, S., Ravon, U., Rizzo, C., Corma, A., Mirodatos, C., 2009. *Chemical Engineering Journal* 155, 553-566.
- [2] Ren, T., Patel, M., Blok K., 2006. *Energy* 31, 425-451.
- [3] Pitman, R.N., Hudson, H.M., Wilkinson, J.D., Cuellar K.T., 1998. *Next generation processes for NGL/LPG recovery*, In: Proceedings of the Seventy-seventh Annual GPA Convention Dallas.
- [4] Chebbi, R., Al-Amoodi, N.S., Abdel Jabbar, N.M., Hussein, G.A., Al Mazroui, K.A., 2010. *Chemical Engineering Research and Design* 88, 779-787.
- [5] Magnowski, N.B.K., Avila, A.M., Lin, C.C.H., Shi, M., Kuznicki, S.M., 2011. *Chemical Engineering Science* 66, 1697-1701.
- [6] Kuznicki, S.M., 1991. *Large-pored crystalline titanium molecular sieve zeolites*. US Patent No. 5,011,591.
- [7] Anderson, M.W., Terasaki, O., Ohsuna, T., Philippou, A., Mackay, S.P., Ferreira, A., Rocha, J., Lidin, S., 1994. *Nature* 367, 347-351.
- [8] Anson, A., Wang, Y., Lin, C.C.H., Kuznicki, T.M., Kuznicki, S.M., 2008. *Chemical Engineering Science* 63, 4171-4175.
- [9] Al-Baghli, N. A., Loughlin, K. F., 2005. *Journal of Chemical and Engineering Data* 50, 843-848.
- [10] Al-Baghli, N.A., Loughlin, K.F., 2006. *Journal of Chemical and Engineering Data* 51, 248-254.
- [11] Shi, M., Lin, C.C.H., Kuznicki, T.M., Hashisho, Z., Kuznicki, S.M., 2010. *Chemical Engineering Science* 65, 3494-3498.

[12] Myers, A.L., Prausnitz, J.M., 1965. *AIChE Journal* 11, 121-127.

[13] Yang, R.T., 1987. *Gas separation by adsorption process*. Imperial College Press.

Chapter 7

Removal of CO₂ from a Binary Mixture of Carbon Dioxide and Methane by Na-ETS-10

A revised version of this chapter will be submitted to Chemical Engineering Science. Reproduced with permission from Shi, M., Avila, A.M., Sawada, J.A., Wu, L., Kuznicki, S.M. 2011.

7.1 Summary

Adsorption of carbon dioxide and methane in Na-ETS-10 was measured by elution chromatography over a temperature range of 30-130 °C. Limiting selectivity and isosteric heat of adsorption at zero loading were obtained through these inverse-phase gas chromatography analyses. The adsorption equilibria of carbon dioxide and methane on ETS-10 were measured by a static volumetric method at 25 °C and pressure up to 100 kPa. The equilibrium isotherms were modeled using Toth equation which was applied in the IAST model. IAST was used to predict the separation performance. A mixture of 10% carbon dioxide and 90% methane obtained from an industrial process stream was run through 150 mL Na-ETS-10 bed. Breakthrough data was obtained through this single bed separation system. Experimental adsorbed phase composition was investigated by water desorption and was verified with the data predicted by the IAST model.

7.2 Introduction

The increasing global economy is faced with a continuous demand for natural gas. Depending on the source, raw natural gas is composed mainly of methane (typically 80-95%), and impurities such as CO₂, nitrogen, and heavier hydrocarbons (C₂+). Natural gas must be liquefied at a very low temperature before being fed to pipelines for transportation. The presence of the acidic carbon dioxide will cause pipeline corrosion and reduce transportation efficiency [1, 2]. Therefore separation of carbon dioxide from methane is one of the most important separations in the chemical and petrochemical industries.

Many available methods exist for removal of CO₂ from natural gas in order to meet the pipeline requirements. They include adsorptive separation [3, 4, 5], chemical absorption [6, 7], membrane separation [8, 9], and cryogenic distillation [10]. Among the adsorptive separation methods pressure-swing adsorption (PSA) removes CO₂ from natural gas by using zeolite adsorbents that preferentially adsorb CO₂ to methane. PSA has low energy requirements and low capital costs, and therefore has been extensively applied in separation industry [11, 12].

The key to the success of adsorptive separation is finding an adsorbent with a high CO₂ over CH₄ selectivity and a high CO₂ capacity. A classical aluminum silicate zeolite known as 13X has been widely studied and applied in the field of gas separation. A VSA-PSA system using zeolite 13X as the adsorbent has been investigated for removal of CO₂ from a CH₄/CO₂/N₂ mixture to achieve fuel grade methane [2]. Another example of using 13X to separate a CH₄/CO₂ mixture by layered pressure swing adsorption for natural gas upgrade was also reported [14]. Natural chabazite, mordenite, and Linde 4A have also been screened for CH₄/CO₂ separation [15]. Amorphous silica molecular sieve has been shown to be a promising candidate for the adsorption and separation of CO₂/CH₄ [16]. As a new family of

porous crystalline materials, metal-organic frameworks (MOF) are also reported as potential adsorbents for separation of CO₂ and CH₄. It is reported that, a copper-based metal-organic-framework processing apertures of ($\sim 3.5 \times 3.5$ Å), favors the kinetically controlled separation of CO₂ and CH₄. The kinetic selectivity is found to be 26 at 298 K [17].

Recently, Engelhard titanosilicate-10 (ETS-10), a mixed coordinate titanosilicate zeolite, has been shown in laboratory-scale studies great potential in binary gas separations of mixtures such as ethylene/ethane [18] and ethane/methane [19]. The pore size of ETS-10 has an average kinetic diameter of ~ 8 Å, which allows both CO₂ (3.3 Å) and CH₄ (3.8 Å) molecules to enter into the cages and channels of ETS-10. Previous work on equilibrium isotherms suggests the possibility of separating a CO₂/CH₄ mixture on ETS-10 based on the differences in thermodynamic equilibrium between the gases [20, 21].

In this work, adsorption of a carbon dioxide-methane mixture in Na-ETS-10 was characterized by elution chromatography at different temperatures (25-140 °C). Both limiting selectivity and heat of adsorption at zero loading were calculated. Experimental single-adsorption isotherms data for carbon dioxide over methane were obtained at 25 °C and pressures up to 100 kPa. A gas mixture, with a composition commonly found in industrial processes (10% CO₂-90% CH₄) was separated by a laboratory-scale demonstration unit which contained 100 g samples of pelletized Na-ETS-10 adsorbent. 100% purity methane was obtained at the outlet stream. A desorption experiment was carried out to verify the prediction of the Ideal Adsorbed Solution theory model.

7.3 Experimental

7.3.1 Sample preparation

Na-ETS-10 was synthesized using conventional hydrothermal synthesis [21]. Preparation involved thoroughly mixing 50 g of sodium silicate (28.8% SiO₂, 9.14% Na₂O, Fisher), 3.2 g of sodium hydroxide (97+% NaOH, Fisher), 3.8 g of KF (anhydrous, Fisher), 4 g of HCl (1 M), and 16.3 g of TiCl₃ solution (Fisher), in a Waring blender for 1 h. The mixture was then transferred to a 125 cm³ sealed, teflon-lined autoclave (PARR Instruments) and heated at 215 °C for 64 h. The material was then thoroughly washed with de-ionized water, and dried at 100 °C. Na-ETS-10 materials were pelletized by mixing 6 g of the molecular sieve with 2.5 g of Ludox HS-40 colloidal silica (Aldrich). The mixture was homogenized using a mortar and pestle and compressed in a pellet press at 69,000 kPa for 3 min. The resulting cakes were crushed and sieved to obtain particles ranging in size between 0.85-1.68 mm. The pelletized, crushed and sieved materials were used in both gas chromatographic and column separation experiments.

7.3.2 Characterization

Inverse-phase gas chromatography (IGC) analysis was performed on a Varian 3800 gas chromatograph (GC) equipped with a thermal conductivity detector (TCD). Test adsorbents were packed into 10-inch copper columns with an OD of 0.25 inches. The columns were filled with 3.5 g pelletized adsorbent, which was activated at 200 °C for 10 h under a helium flow of 30 mL/min. Gas (single-phase and mixtures) was introduced by 1 mL pulse injections into the column. Experiments were conducted at temperatures range of 30-130 °C.

Low-pressure adsorption isotherms (up to 100 kPa) for carbon dioxide, and methane on crystalline adsorbent powders were measured volumetrically at 25 °C using an AUTOSORB-1-MP (Quantachrome Instruments, Boynton Beach, FL). No binders or

diluents were added to the adsorbent samples. Samples were activated at 200 °C for 10 h under vacuum (<0.00005 kPa).

Breakthrough experiments were performed using 28 g samples of pelletized, ground and sieved test adsorbent. The adsorbent was packed into a 150 mL cylindrical stainless steel chamber with an outer diameter of 38 mm and a length of 95 mm. Following adsorbent loading, columns were activated at 473 K for 10 h under 10 mL/min of helium flow. The feed gas mixture composition was: a binary carbon dioxide/methane mixture (10% CO₂: 90% CH₄). The gas mixture was prepared by Praxair to mimic the process gas composition in natural gas plants. The feed mixture was introduced into the fixed-bed column at a flow rate of 300 mL/min (298 K, 101.3 kPa). The column pressure was 100 kPa and column temperature was maintained at 298 K. Outlet gas composition was analyzed using a Varian 3800 gas chromatograph (GC) equipped with an HAYESEP Q column and a thermal conductivity detector. The system reaches equilibrium when the gas-phase outlet concentration is equal to the inlet gas concentration. GC analysis of the outlet composition was used to confirm that equilibrium was reached.

To analyze the composition of the adsorbed phase gases, another small scale adsorption experiment was carried out. The 150 mL bed was replaced by a 50 mL bed which was packed with 30 g of Na-ETS-10 adsorbent. The bed was saturated until equilibrium as illustrated in the breakthrough experiment section. After the bed reached equilibrium, we injected pure water directly into the chamber, after which the adsorbed gases (a mixture of CO₂ and CH₄) were desorbed by water and collected by the gas collection unit. After the complete desorption the desorbed gas was sampled by a syringe and the composition was analyzed by GC analysis.

7.3.3 Theoretical background

The inverse gas chromatography method used for the determination of sorption properties of gases is described in detail elsewhere. The values of retention times after

correction of dead time were used to calculate net retention volume, V_N , and specific retention volume, V_m , using the following equation:

$$V_N = \frac{F t_{Rj} \left(1 - \frac{P_w}{P_o}\right) T}{T_R} \quad (7.1)$$

Where $V_m = \frac{V_N}{w_s}$ and $j = \left(\frac{3}{2}\right) \left[\frac{\left(\frac{P_i}{P_o}\right)^2 - 1}{\left(\frac{P_i}{P_o}\right)^3 - 1} \right]$, and F is the carrier gas flow rate. t_R is the corrected retention time, P_i and P_o are the column inlet and outlet pressures, P_w is the water vapor pressure at room temperature T_R , T is the column temperature and w_s is the weight of adsorbent in the column [22].

V_m can be correlated to Henry's constant by using the ideal gas law. Then the limiting selectivity of carbon dioxide over methane $\alpha(A/B)$ and the heat of adsorption at zero coverage, ΔH_o , could be calculated using the corrected retention time (Equation 7.2 and 7.3).

$$\alpha_B^A = \frac{V_{m(A)}}{V_{m(B)}} = \frac{t_R(A)}{t_R(B)} \quad (7.2)$$

$$\Delta H_o = R \frac{d \ln(t_R)}{d(1/T)} \quad (7.3)$$

Where R is the gas constant and T is the GC column temperature in Kelvin.

Experimental isotherms were fitted to a popular empirical equation proposed by Toth (Equation 7.4):

$$q_i = q_{i,m} \frac{b_i P}{[1 + (b_i P)^\epsilon]^{1/\epsilon}} \quad (7.4)$$

with the standard deviations (σ Equation 7.5):

$$\sigma = \sqrt{\frac{\sum(n_{exp} - n_{calc})^2}{N - 2}} \quad (7.5)$$

where q_i is the amount adsorbed on the solid, P represents the pressure in the gas phase, $q_{i,m}$ is the saturation or maximum adsorption capacity, and b_i is the equilibrium constant. t is a parameter which is usually less than unity. n_{exp} is the experimentally measured adsorption at pressure P , n_{calc} is the adsorption calculated from the Toth equation at the same pressure. N is the number of measured experimental points. When $t = 1$, the Toth equation reduces to the famous Langmuir equation.

As was pointed out by Do, t is a parameter that characterizes the system's heterogeneity. The more the parameter t deviates from unity, the more heterogeneous the system is [23]. Based on hundreds of verifications and comparisons, the Toth equation is recommended as the first choice of isotherm fitting for adsorption of hydrocarbons, carbon dioxide, hydrogen sulfide on zeolitic adsorbents.

Ideal adsorbed solution theory (IAST) is on the basis of solution thermodynamics [24]. The mixed adsorbates are assumed in equilibrium with the gas phase, and the adsorbed mixture is treated as a two-dimensional phase. IAST can be expressed as an analogue of Raoult's law for vapor-liquid equilibrium:

$$Py_i = P_i^0(\pi)x_i \quad (\text{constant } T) \quad (7.6)$$

where P is the total pressure of the gas-phase mixture, y_i is the composition of component i in the gas phase, x_i is the composition of component i in the adsorbed phase, and $P_i^0(\pi)$ is the pure component hypothetical pressure which yields the same

spreading pressure as that of the mixture.

From the Gibbs isotherm, the spreading pressure π can be calculated based on its pure isotherm [25].

$$\pi_i = \frac{RT}{A} \int_0^{P_i^0} \frac{n_i^0(P)}{P} dP \quad (\text{constant } T) \quad (7.7)$$

where $n_i^0(P)$ is the adsorption isotherm for pure component i , A is the area, R is the ideal gas constant, and T is the temperature.

The basic assumption of IAST is that spreading pressures are equal for all components at the adsorption equilibrium, which is:

$$\pi_1 = \pi_2 = \dots = \pi_N \quad (7.8)$$

For a binary system, the IAST model consists of the following set of equations.

$$Py_1 = P_1^0(\pi)x_1 \quad (7.9)$$

$$Py_2 = P_2^0(\pi)x_2 \quad (7.10)$$

$$x_1 + x_2 = 1 \quad (7.11)$$

$$y_1 + y_2 = 1 \quad (7.12)$$

$$\int_0^{P_1^0} \frac{n_1^0(P)}{P} dP = \int_0^{P_2^0} \frac{n_2^0(P)}{P} dP \quad (7.13)$$

$$\frac{1}{n_t} = \frac{x_1}{n_1^0(P_1^0)} + \frac{x_2}{n_2^0(P_2^0)} \quad (7.14)$$

The observed carbon dioxide/methane separation selectivity for Na-ETS-10 was defined in terms of the extract composition and the feed mixture fractions (Equation 7.15):

$$S = \frac{X_C/X_M}{Y_C/Y_M} \quad (7.15)$$

where X_C , X_M and Y_C , Y_M are the mole fractions of carbon dioxide (C) and methane (M) in the extract and feed gas respectively.

7.4 Results and discussion

7.4.1 Inverse phase GC

Retention times for carbon dioxide and methane on Na-ETS-10 at different temperatures (CO_2 was measured at 100 °C, 120 °C and 140 °C; CH_4 was measured at 25 °C, 30 °C, 40 °C and 100 °C) are shown in Figure 7-1, 7-2, and 7-3 and Table 7-1. Based on the equation 1, limiting selectivity of carbon dioxide over methane on Na-ETS-10 can be calculated and a selectivity of 31.5 was obtained at 100 °C. Extrapolating the limiting selectivity at various temperatures it can be shown that selectivity decreases as temperature increases, and the limiting selectivity of CO_2 over CH_4 at 25 °C could reach up to 293. The Arrhenius plot of the low coverage isosteric heat of adsorption for CH_4 and CO_2 on Na-ETS-10 is shown in Figure 7-4. The heats of adsorption for carbon dioxide and methane at zero coverage, calculated based on equation 3, are 42.1 kJ/mol and 23.3 kJ/mol respectively. Both the limiting selectivity and the zero loading heat of adsorption indicate that Na-ETS-10 has a stronger interaction with CO_2 than CH_4 .

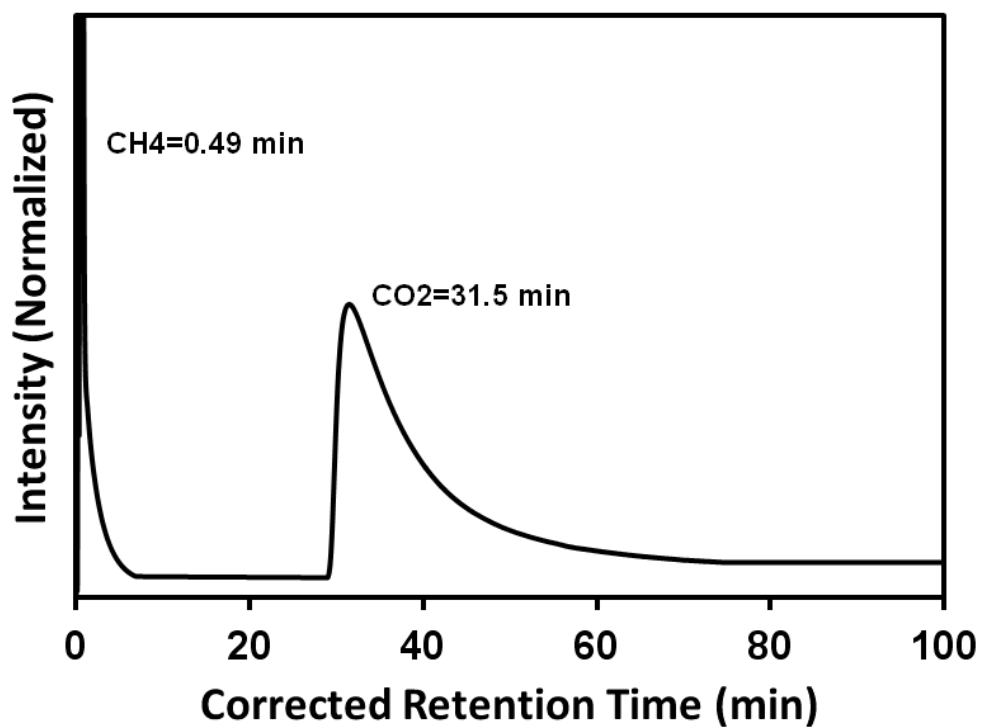


Figure 7-1. A typical separation of CO₂ and CH₄ on Na-ETS-10 at 100 °C. A mixture of 50% CH₄ and 50% CO₂ was injected into a Na-ETS-10 column and retention times were determined by IGC analysis.

Table 7-1. Corrected Retention time for CH₄ and CO₂ on Na-ETS-10 at temperature range from 25 to 140 °C. The value in () are extrapolated through Van't Hoff Equation.

T(°C)	T(K)	Corrected Retention Time (min)		Selectivity CO ₂ /CH ₄
		CH ₄	CO ₂	
25	298	3.26	(957)	(294)
30	303	2.83	(723)	(255)
40	313	2.08	(423)	(203)
100	373	0.49	31.5	64
120	393	(0.34)	15.18	(45)
140	413	(0.24)	8.44	(35)

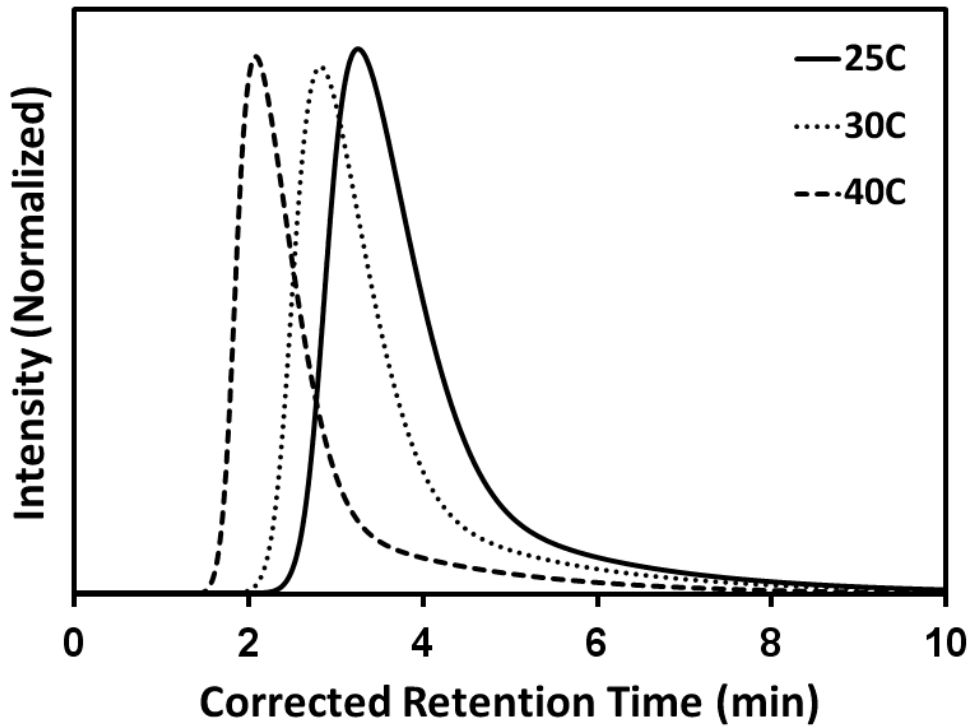


Figure 7-2. IGC analysis of methane on Na-ETS-10 at 25, 30, and 40 °C.

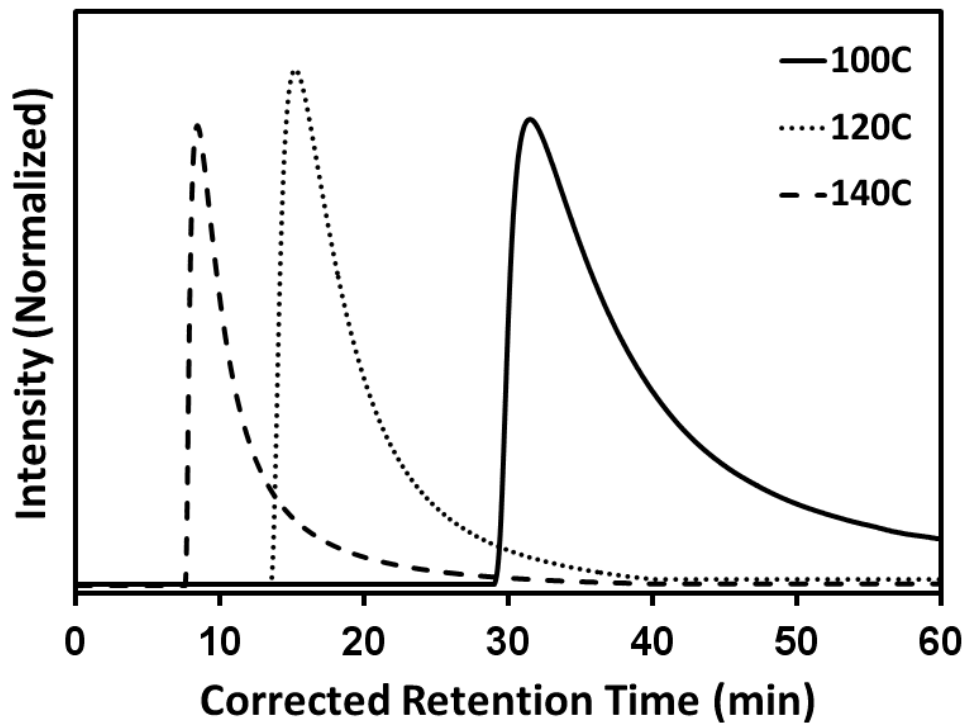


Figure 7-3. IGC analysis of Carbon dioxide on Na-ETS-10 at 100, 120, and 140 °C.

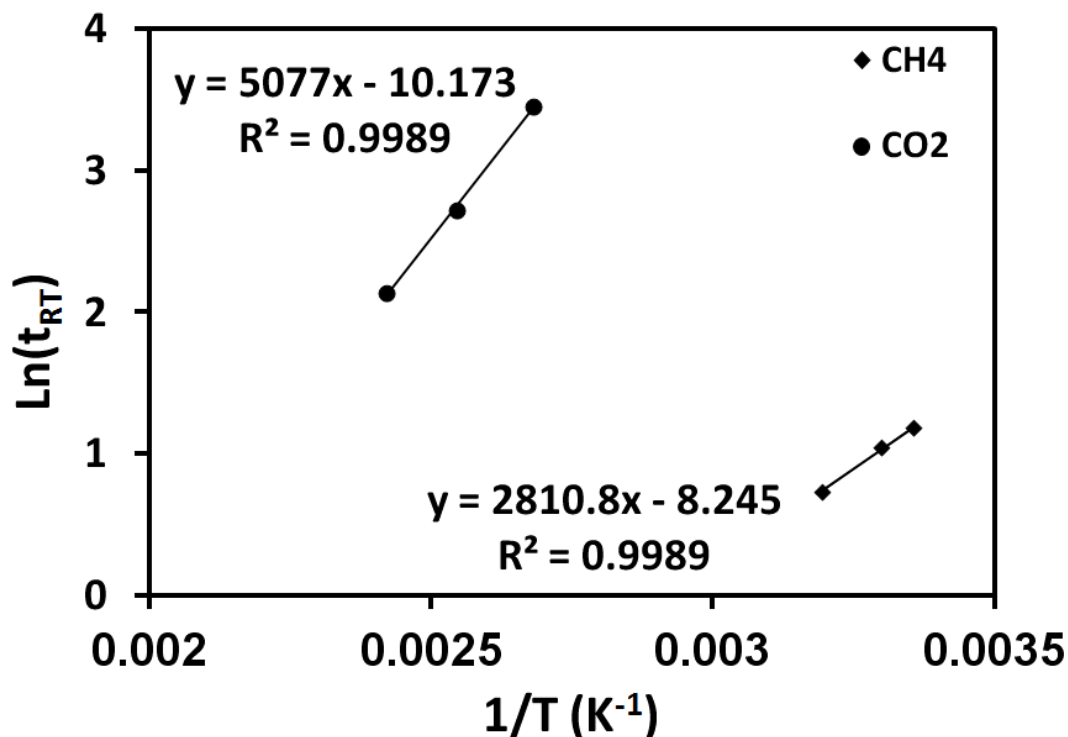


Figure 7-4. Arrhenius plot of the low coverage isosteric heat of adsorption for CH₄ and CO₂ on Na-ETS-10. CH₄, 23.3 kJ/mol; CO₂, 42.1 kJ/mol.

7.4.2 Equilibrium isotherms

The isotherms for CO₂ and CH₄ adsorbed on Na-ETS-10 at 25 °C and pressures up to 100 kPa are shown in Figure 7-5. The curve for carbon dioxide is more rectangular than the curve for methane, indicating that Na-ETS-10 has a stronger interaction with carbon dioxide than methane. The equilibrium isotherms also show that Na-ETS-10 possesses a higher capacity for carbon dioxide (2 mmol/g) than for methane (0.77 mmol/g) at ambient temperature. The Toth equation was used to fit the isotherms for carbon dioxide and methane. The adsorption parameters obtained from the Toth fits are listed in Table 7-2. Judging from the standard deviation the Toth model appears to provide a good description of the equilibrium isotherms.

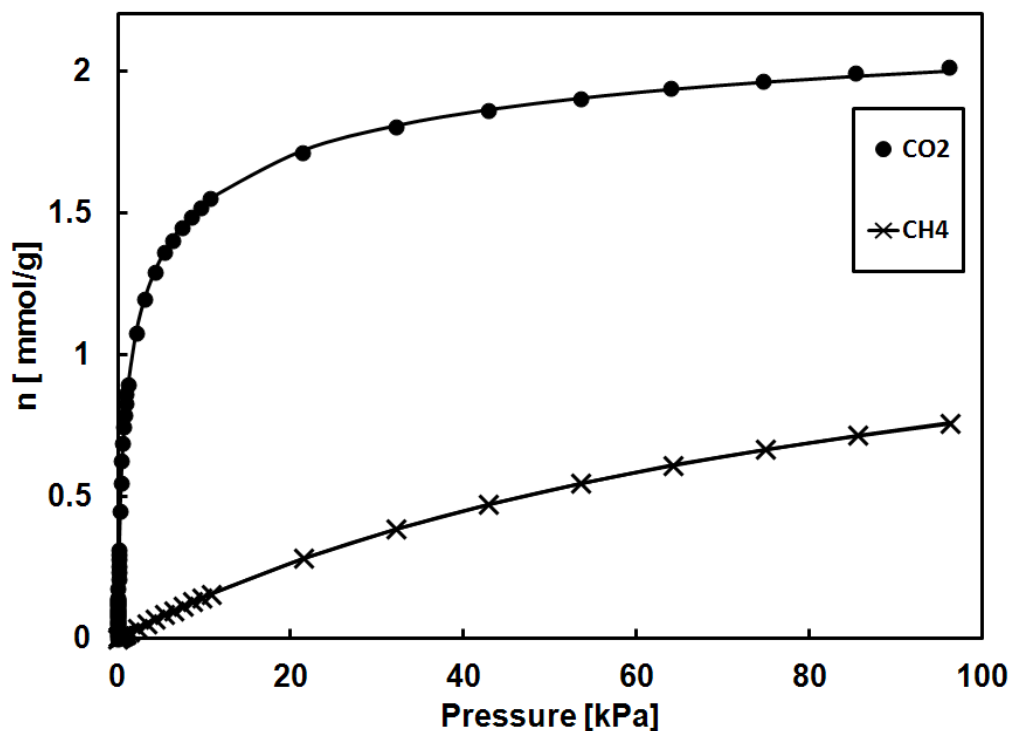


Figure 7-5. Equilibrium adsorption isotherms with Toth equation fitting for CO₂ and CH₄ on Na-ETS-10 at 25 °C and pressure up to 100 kPa.

Table 7-2. Constrained Toth parameters for adsorption data in the range of 0-100 kPa at 25 °C

Adsorbate	Toth equation parameters			
	$q_{i,m}$ (mmol g ⁻¹)	b_i (kPa ⁻¹)	t	SD
CO ₂	2.40875	4.51385	0.4152	0.0088
CH ₄	1.46665	0.01110	1.00	0.002

7.4.3 Lab-scale demonstration

The carbon dioxide/methane separation performance of Na-ETS-10 was evaluated in a lab-scale demonstration. Figure 7-6 depicts a breakthrough curve for CH₄ and CO₂ on Na-ETS-10 at 25 °C and 100 kPa. With a continuous flow of feed gas (90% CH₄-10% CO₂) at 300 mL/min, a pure methane product was detected after 2.5 bed volumes. The bed continued to produce pure methane for 270 bed volumes of continuous flow until the carbon dioxide front started to breakthrough. After 300 bed

volumes of continuous flow the concentration of CO₂ and CH₄ in the outlet gas begins to reflect the inlet (feed gas) composition, indicating that the Na-ETS-10 adsorbent has reached saturation.

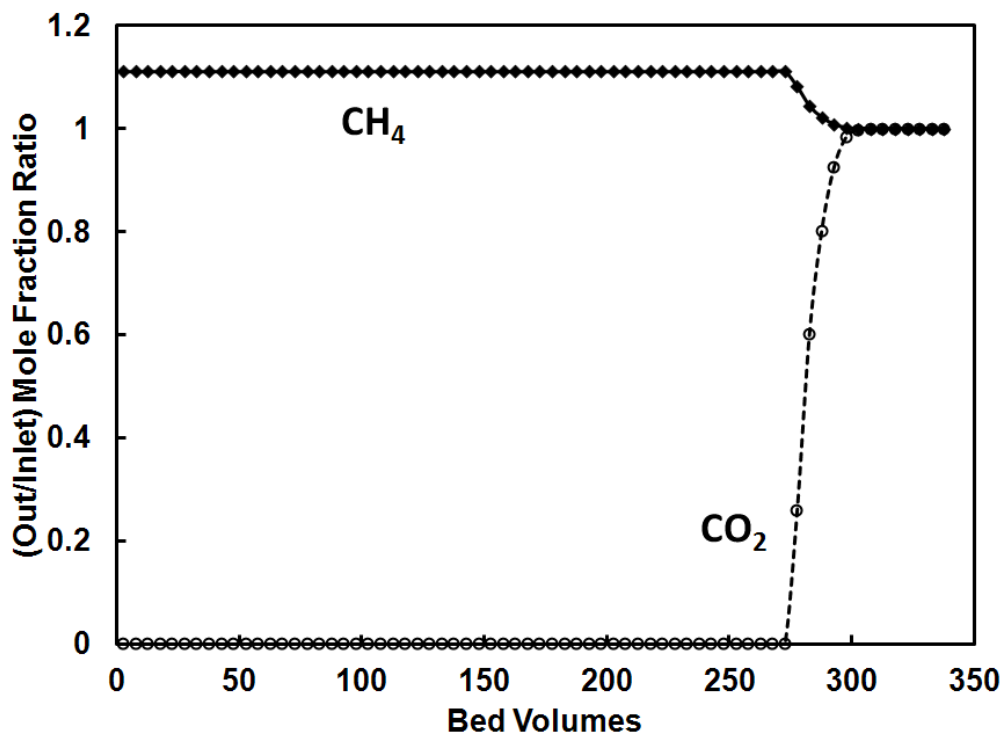


Figure 7-6. CH₄/CO₂ breakthrough curve on Na-ETS-10 at ambient Condition. Feed gas (a mixture of 10% CO₂ and 90% CH₄) was introduced into a column containing 120 g of pelletized Na-ETS-10 (10-20 mesh) at a flow rate of 300 mL/min (bed volume 150 mL). Column temperature 25 °C, column pressure 1 bar. Hydrocarbon content of the outlet gas was determined by GC analysis

Figure 7-7 shows the outlet gas flow rate monitored by an Agilent ADM 1000. The Agilent flow meter was calibrated using a Bronkhorst mini CORI-FLOW™ to ensure accuracy of the measured volumetric flow rates. With the breakthrough information for methane and carbon dioxide, the outlet flow rate profile can be properly explained. It shows that helium from the dead volume came out at the first 2 min. Pure methane can be detected at 2.5 min but with a relative slow flow rate of 20 mL/min, which could be due to the initial adsorption of both CO₂ and CH₄. The outlet continued to produce pure methane with a flow rate reaching up to 270 mL/min at 12.5 min. At this point the adsorbent bed is starting to saturate with methane. During the next 125 min,

the outlet stream produces pure methane maintaining the same flow rate (270 mL/min) while the CO₂ is removed from the feed gas. After this point CO₂ becomes detectable and the outlet flow rate starts to increase, explained by the fact that the bed is nearing complete saturation with CO₂. When the outlet stream flow rate increased to 300 mL/min, the same as the feed flow rate, the system reached equilibrium and the bed was saturated with both CH₄ and CO₂.

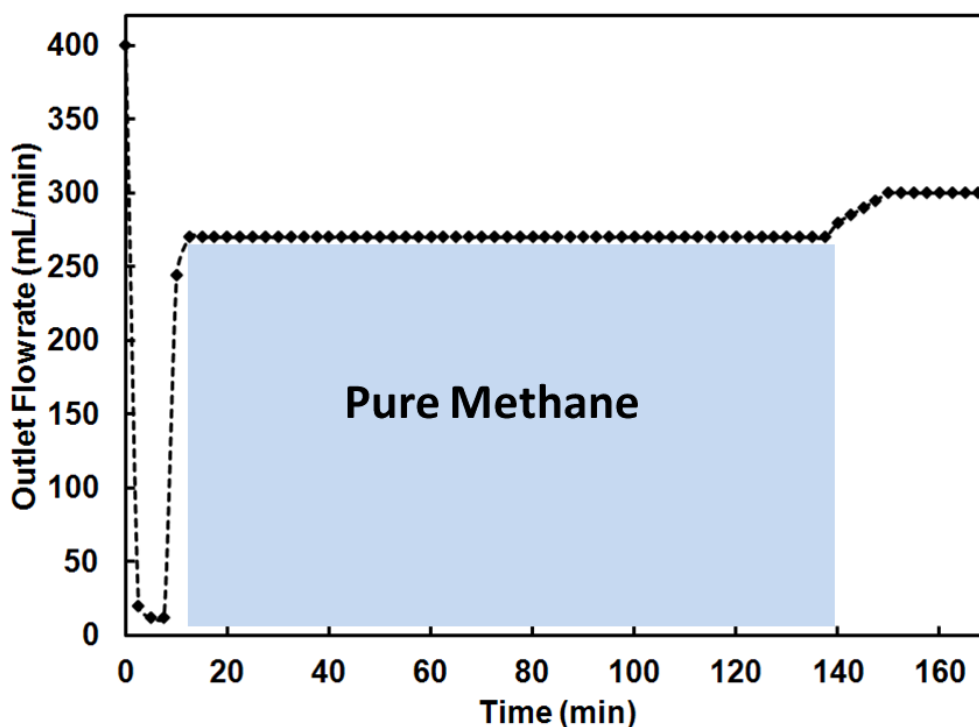


Figure 7-7. Outlet flow rate monitored by Agilent ADM 1000 in adsorption procedure

7.4.4 Desorption

Given the single gas equilibrium isotherms of CO₂ and CH₄, we can predict the adsorption performance of a binary mixture system (adsorption capacity and composition in the adsorbed phase gas) by ideal adsorbed solution theory model. The Toth modeling of both CO₂ and CH₄ on Na-ETS-10, was applied. The feed composition used was 90% CH₄ and 10% CO₂. The amounts of adsorbed CO₂ and methane calculated by IAST modeling are given in Table 7-3. These predicted numbers are compared with the experimental desorption data.

Table 7-3. Comparison of IAST, and lab-scale separation demonstration at 25 °C and 100 kPa.

Method	Capacity (mmol/g)		Adsorbed Phase Composition
	CO ₂	CH ₄	
Single Isotherm	2	0.77	N/A
IAST	1.467	0.073	95.27% CO ₂ , 4.73% CH ₄
Lab-scale Demo	1.526	0.151	91% CO ₂ , 9% CH ₄

Through the mass action displacement mechanism, adsorbed gas can be desorbed by water desorption. The saturated Na-ETS-10 was flushed with water and the desorbed gas was collected in a gas collection container. Desorption started immediately after water injection. A total of 1230 mL gas was collected from approximately 30 g of Na-ETS-10 pellets through water desorption; therefore the adsorption capacity is 41 mL/g Na-ETS-10. Based on GC-TCD analysis, the desorbed gas consisted of 91% CO₂ and 9% CH₄, indicating that a measured binary bed selectivity for carbon dioxide over methane could reach up to 91. Adsorption capacity and composition confirmed from the experimental tests are close to modeling prediction. This suggests that IAST could be a modeling tool to quickly predict equilibrium adsorption of gas mixture.

The lab-scale breakthrough demonstration suggests that Na-ETS-10 can be a potential candidate as adsorbent for CO₂ removal from natural gas steams.

7.5 Conclusions

In this work, removal of CO₂ from a binary mixture (90%CH₄-10%CO₂) was achieved using a Na-ETS-10 adsorbent at ambient condition. Inverse phase gas chromatography and volumetric isotherm measurements indicate that Na-ETS-10 processes a strong adsorptive selectivity (up to 300) for carbon dioxide over methane. Elution chromatography shows that the heats of adsorption at zero loading for carbon dioxide and methane on Na-ETS-10 are 37 kJ/mol, 25 kJ/mol respectively. A

packed-bed Na-ETS-10 adsorbent column was used to split a 90/10 methane/carbon dioxide gas mixture into a raffinate stream composed of pure methane and an extract stream containing 91% CO₂. Desorbed gas analysis shows that Na-ETS-10 possesses a binary bed selectivity for carbon dioxide over methane of approximately 91. These results together indicate that Na-ETS-10 would be a good candidate as adsorbent for removal of CO₂ from a 90%CH₄-10% CO₂ mixture system.

7.6 References

- [1] Gerasimov, V.E., Peredel'skii, V.A., Lyapin, A.I., Darbinyan, R.V., Dovbish. A.L., 2004. *Chemical and Petroleum Engineering* 40, 339-343.
- [2] Cavenati, S., Grande, C.A., Rodrigues, A.E., 2006. *Energy & Fuels* 20, 2648-2659.
- [3] Kapoor, A., Yang, R.T., 1989. *Chemical Engineering Science* 44, 1723-1733.
- [4] Himeno, S., Komatsu, T., Fujita, S., 2005. *Journal of Chemical & Engineering Data* 50, 369-376
- [5] Chaudhary, V.R., Mayadevi, S., 1996. *Zeolites* 17, 501-507.
- [6] Leal, O., Bolivar, C., Ovalles, C., Garcia, J.J., Espidel, Y., 1995. *Inorganica Chimica Acta* 240, 183-189.
- [7] Gupta, H., Fan, L.S., 2002. *Industrial & Engineering Chemistry Research* 41, 4035-4042.
- [8] Sandstrom, L., Sjoberg, E., Hedlund, J., 2011. *Journal of Membrane Science* 380, 232-240.
- [9] Scholes, C.A., Stevens, G.W., Kentish, S.E., 2012. *Fuel* 96, 15-28.
- [10] Fieler, E.R., 2010. *Controlled freeze zone tower*. US Patent No. 2010/0018248 A1
- [11] Sircar, S., 1988. *Separation Science and Technology* 23, 519-529.
- [12] Ruthven, D.M., Farooq, S., Knaebel, K.S., 1994. *Pressure Swing Adsorption*, VCH Publishers: New York.
- [13] Cavenati, S., Grande, C.A., Rodrigues, A.E., 2006. *Chemical Engineering Science* 61, 3893-3906.

- [14]Jensen, N.K., Rufford, T.E., Watson, G., Zhang, D.K., Chan, K.I., May, E.F., 2012. *Journal of Chemical & Engineering Data* 57, 106-113.
- [15]Morishige, K., 2011. *The Journal of Physical Chemistry C* 115, 9713-9718.
- [16]Bao, Z., Alnemrat, S., Yu, L., Vasiliev, I., Ren, Q., Lu, X., Deng, S., 2011. *Journal of Colloid and Interface Science* 357, 504-509.
- [17]Shi, M., Lin, C.C.H., Kuznicki, T.M., Hashisho, Z., Kuznicki, S.M., 2010. *Chemical Engineering Science* 65, 3494-3498.
- [18]Magnowski, N.B.K., Avila, A.M., Lin, C.C.H., Shi, M., Kuznicki, S.M., 2011. *Chemical Engineering Science* 66, 1697-1701.
- [19]Kuznicki, S.M., 2010. *Removal of carbon dioxide from paraffins*. US Patent No. 2010/0228069 A1.
- [20]Anson, A., Lin, C.C.H., Kuznicki, S.M., Sawada, J.A., 2009. *Chemical Engineering Science* 64, 3683-3687
- [21]Kuznicki, S.M., 1991. *Large-pored crystalline titanium molecular sieve zeolites*. US Patent No. 5,011,591.
- [22]Choudary, V.N., Jasra, R.V., Bhat, T.S.G., 1993. *Industrial & Engineering Chemistry Research* 32, 548-552.
- [23]Do, D. D., 1998. *Adsorption analysis: equilibria and kinetics*. Imperial College Press, London.
- [24]Myers, A.L., Prausnitz, J.M., 1965. *AIChE Journal* 11, 121-127.
- [25]Yang, R.T., 1987. *Gas separation by adsorption process*. Imperial College Press.

Chapter 8

Regeneration of Na-ETS-10 Using Microwave and Conductive Heating

A version of this chapter has been published. Reproduced with permission from Chowdhury, T., Shi, M., Hashisho, Z., Sawada, J.A., Kuznicki, S.M., 2012. *Chemical Engineering Science* 75, 282-288.

8.1 Summary

Desorption of ethylene/ethane and carbon dioxide/methane mixtures was performed by microwave heating and conductive heating on Na-ETS-10. Gas recovery, Na-ETS-10 regeneration efficiency and swing capacity were compared between the two methods. Na-ETS-10 regeneration occurred within 8 minutes for microwave heating and 22 minutes for conductive heating. For microwave heating the energy consumption was 0.7 kJ/g Na-ETS-10 and the gas recovery was 94% for C₂H₄/C₂H₆ and 70% for CO₂/CH₄. Conductive heating had an energy consumption of 7.7~7.9 kJ/g Na-ETS-10 and resulted in 71% gas recovery for C₂H₄/C₂H₆ and 57% for CO₂/CH₄. The adsorption capacity of Na-ETS-10 did not change over 5 adsorption-regeneration cycles for both heating techniques. Microwave desorption provided a faster heating rate and desorption rate, higher desorption and gas recovery and lower energy consumption compared to conductive heating. Hence, microwave heating can be used as a more efficient and energy saving regeneration technique for Na-ETS-10 for adsorptive separation of binary mixtures such as C₂H₄/C₂H₆ and CO₂/CH₄.

8.2 Introduction

High purity ethylene (C_2H_4) is required for the production of polymers, rubber, fibre and various organic chemicals [1]. Generally, C_2H_4 is prepared through steam cracking or thermal decomposition of ethane (C_2H_6). The gas product of cracking contains un-cracked C_2H_6 . Separation of un-cracked C_2H_6 from C_2H_4 is crucial in the polymer manufacturing production chain [2]. Cryogenic distillation is the most reliable and commonly used technique for C_2H_4/C_2H_6 separation but it is extremely energy intensive [3].

Currently, natural gas provides one fourth of the world's energy needs for homes, vehicles and industries [4]. Typically natural gas contains 80-95% methane; the rest is made of C_2^+ hydrocarbons, nitrogen, and carbon-dioxide impurities. High concentration of carbon dioxide in methane can lead to pipeline and equipment corrosion and therefore, reducing it to trace levels is necessary to achieve the pipeline quality methane (no more than 2% CO_2) [5]. Typically the separation of CO_2 is accomplished by chemical absorption with amines which is energy intensive and requires high reagent costs [6].

Adsorptive separation is an effective alternative to cryogenic distillation or chemical absorption as it requires less energy and capital cost [2]. Preliminary studies and model predictions suggest that Engelhard Titanosilicate-10 (Na-ETS-10) has great potential as an adsorbent in the separation of C_2H_4/C_2H_6 and CO_2/CH_4 mixtures [7-8]. It has been reported that the adsorption separation of the binary mixture of C_2H_4/C_2H_6 using Na-ETS-10 can achieve a bed selectivity of 5 at ambient pressure and up to 11 at 2580 kPa [3, 9].

ETS-10 is a large pored, mixed octahedral/tetrahedral titanium silicate molecular sieve possessing an inherent three dimensional network of interconnecting channels

[10, 11]. The average pore size of ETS-10 has a kinetic diameter of ~ 8 Å. Hence C_2H_4 , C_2H_6 , CO_2 and CH_4 can enter the crystalline lattice as the pore size is larger than the molecular diameter of all four species stated [9]. Therefore, separation selectivity of C_2H_4 over C_2H_6 or CO_2 over CH_4 would be based on the equilibrium competitive adsorption. Na-ETS-10 could preferentially adsorb ethylene in the binary mixture of C_2H_4 and C_2H_6 [9] and preferentially adsorb CO_2 in the binary mixture of CH_4 and CO_2 [7].

Despite Na-ETS-10's great potential in adsorptive separation of C_2H_4 , C_2H_6 , CO_2 and CH_4 , its regeneration cost presents a challenge because of the high heats of adsorption of the gases to be separated [9, 12]. In this context, microwave heating can be a promising alternative to the conventional pressure swing and temperature swing regeneration methods that are currently used in separation industry [13, 14]. Although microwave heating was initially used for rapid heating of food, its unique selectivity and fast heating rate proved to be useful in other applications such as industrial drying [15]. In a conventional thermal regeneration process, the thermal energy is transferred from the surface to the bulk of the material. By contrast in microwave heating the energy is transferred from the inside to the outside of the material as microwaves propagate through molecular interactions between the material and the electromagnetic field [16].

Microwave heating has been reported for the regeneration of zeolite 13X [13], DAY [17, 18], zeolite 3A, 4A, 5A [19], and Na-X and Ca-X [20, 21]. A preliminary study of microwave regeneration of Na-ETS-10 was recently completed using a kitchen microwave and showed that microwave heating is capable of regenerating Na-ETS-10 over several adsorption/desorption cycles [9].

Conventional thermal regeneration, known as temperature swing regeneration, is another widely used method for adsorbent regeneration in separation and purification industries. During temperature swing regeneration a hot gas stream or steam is used

for bed heating and a cold gas stream is used for bed cooling [22]. There have been several reports of using temperature swing to regenerate zeolite 13X [23], 4A and 5A [24] as well as an extensive review on temperature swing regeneration which can be found elsewhere [25-27].

The objective of this study is to investigate the performance of both conductive heating and microwave heating for the regeneration of Na-ETS-10. Two gas mixtures, ethylene/ethane (C_2H_4/C_2H_6) and carbon dioxide/methane (CO_2/CH_4), commonly used in industry, were separated on Na-ETS-10 in packed bed columns which were later regenerated by microwave heating and conductive heating. The Na-ETS-10 swing capacity, regeneration efficiency and energy consumption were determined and compared between microwave heating and conductive heating. The recovery and purity of the desorbed gases were also determined.

8.3 Experimental

8.3.1 Sample preparation

Na-ETS-10 was synthesized using the hydrothermal technique as described elsewhere [10]. A typical sample was prepared by thorough mixing of 50 g of sodium silicate (28.8% SiO_2 , 9.14% Na_2O), 3.2 g of sodium hydroxide (97+% NaOH), 3.8 g of anhydrous KF, 4 g of HCl (1M), and 16.3 g of $TiCl_3$ solution. The mixture was stirred in a blender (Waring) for 1h. Then it was transferred to a 125 mL sealed autoclave (PARR instruments) and heated at 215 °C for 64 h. The resultant material was carefully washed with de-ionized water and then dried in an oven at 100 °C. The material was reduced to fine powder ($< 150 \mu m$) and pelletized by mixing 6 g of the material (equilibrated at 100 °C) with 2 g of Ludox HS-40 colloidal silica (Aldrich). Mortar and pestle were used to homogenize the mixture. Then the mixture was compressed using a pellet press at 10,000 psi for 3 min. The resulting cake was crushed and sieved to acquire 16-20 mesh particles. The prepared pellets were used in

the adsorption-desorption experiments.

8.3.2 Adsorption-desorption experiments

Adsorption-desorption experiments were performed by saturating 10 g of pelletized Na-ETS-10 (16-20 mesh) in a double-ended cylindrical quartz column. The adsorbent bed height was 3.75 cm and its diameter was 2.9 cm. The sample was activated at 200 °C in a laboratory oven for 16 h under 120 mL/min helium gas flow. During adsorption, feed gas flow was maintained at 22 °C and 101.325 kPa. Feed gas consisted of either 59% C₂H₄/ 41% C₂H₆ mixture or 10% CO₂/ 90% CH₄. The feed gas mixtures were introduced to the fixed bed adsorbent column at a flow rate of 180 mL/min (C₂H₄/C₂H₆) and 300 mL/min (CO₂/CH₄). The feed gases (Praxair) were surrogate mixtures for the process gas streams of ethylene cracking and natural gas purification units. Outlet gas was sampled using 5 mL syringe at 5 minute intervals. Outlet gas composition was analysed using a 5890A Agilent Gas Chromatograph (GC) equipped with thermal conductivity detector (TCD) and a Supelco matrix Haysep Q column (well suited for hydrocarbon analysis). 0.5 mL samples were pulse injected and analysed with the GC-TCD. A continuous flow of feed gas was maintained until the outlet composition became the same as the inlet composition which occurred after approximately 16 minutes for C₂H₄/ C₂H₆ mixture and 90 minutes for CO₂/CH₄ mixture.

The microwave generation and propagation system consisted of a 2 kW switch-mode power supply (SM745G.1, Alter), a 2 kW microwave source (MH2.0W-S, National Electronics) equipped with a 2.45 GHz magnetron, an isolator (National Electronics), a three-stub tuner (National Electronics) and a waveguide applicator connected to a sliding short (IBF Electronic GmbH & Co. KG). The tuner and the sliding short were manually adjusted at the beginning of the experiment to improve the energy transfer to the adsorbent. The isolator was used to protect the microwave head by conducting reflected power into a water load. The power was monitored with a dual directional coupler with 60 db attenuation (Mega Industries), two power sensors (8481A, Agilent)

and a dual channel microwave power meter (E4419B, Agilent). The temperature of the material was monitored using a fiber optic temperature sensor and a signal conditioner (Reflex signal conditioner, Neoptix). The temperature sensor, power meter and power supply were connected to a data acquisition and control (DAC) system (Compact DAC, National Instruments) equipped with a Labview program (National Instruments) to record the data and control power application. Labview program was used to monitor and control heating during desorption. After saturation, the microwave generation system was turned on and the heating was initiated using Labview program. The desorbed gas was flown to a downstream flask and was collected by water displacement. The volume of the displaced water was equal to the volume of the gas that was collected at the outlet. The desorption experiment was continued until no gas evolution was observed. After desorption, the adsorbent was cooled to room temperature by purging with nitrogen at 120 mL/min. Once the bed reached ambient temperature, further adsorption/microwave desorption cycles were initiated.

In conductive heating technique, a double ended cylindrical steel column with an inner diameter of 1 cm and bed height of 7 cm was used as a reactor. Following saturation of the adsorbent bed, the column was wrapped with a heating tape (Omegalux™) followed by an additional insulation tape. The heating tape was connected to a 120 V AC power source through a solid state relay interfaced to a DAC system. A Labview program was used to initiate and control the heating. The bed temperature was maintained at 190 °C. A shielded type K thermocouple (Omega) was used to measure the bed temperature. Data were recorded using a DAC and a Labview program as described in the microwave desorption experiments. Desorbed gas collection system and post desorption adsorbent cooling system were analogous to those used in the microwave desorption experiments. Heating was continued until no gas evolution was observed. A block diagram for adsorption and regeneration by microwave heating and conductive heating process is illustrated in Figure 8-1.

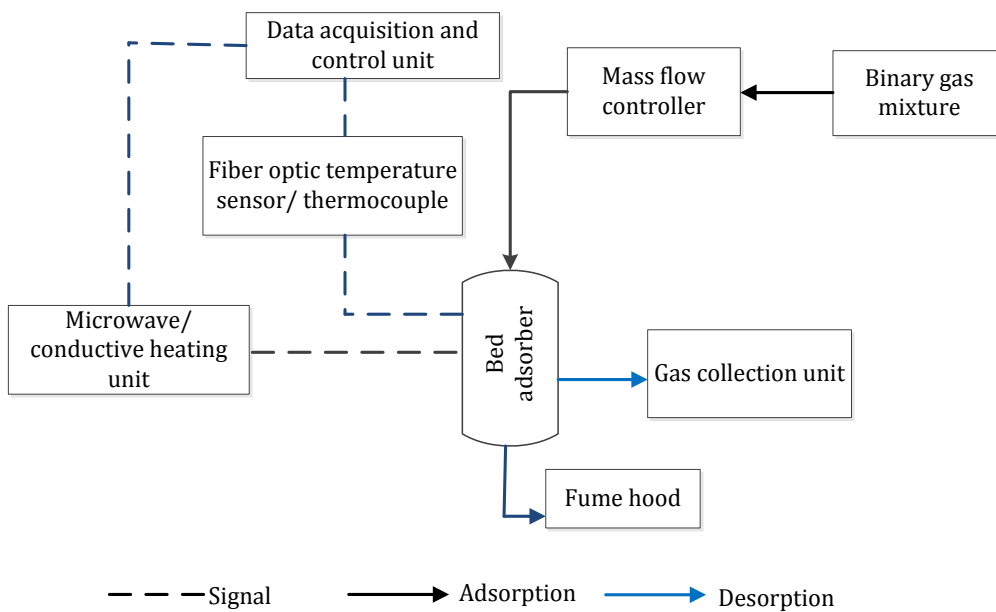


Figure 8-1. Block diagram showing adsorption and regeneration of Na-ETS-10 using microwave and conductive heating.

Swing capacity is generally defined as the adsorption capacity or working capacity of an adsorbent between two extreme states of the swing force [7]. In this work, swing capacity of Na-ETS-10 is defined as the amount of gas desorbed during heating from 22 °C to 190 °C. The maximum swing capacity was achieved by water desorption [3]. Gas recovery was calculated based on the Equation 7.1.

$$Gas\ recovery\ (\%) = \frac{V_{M/C}}{V_W} \times 100\% \quad (7.1)$$

Where, $V_{M/C}$ = volume of gas desorbed by microwave (M) or conductive (C) heating and V_W = the volume of gas desorbed by water desorption.

8.4 Results and discussion

8.4.1 Ethylene/ethane (C_2H_4/C_2H_6) desorption from Na-ETS-10

Desorption achieved by water desorption is considered as complete (100%) through the mass action displacement mechanism [9]. Therefore, the saturated Na-ETS-10 was flushed with water and the desorbed gas was collected in a gas collection container. Desorption started immediately after water injection and lasted for 7-8 minutes. A total of 320 mL gas was collected from approximately 10 g of Na-ETS-10 through water desorption; therefore the maximum adsorption capacity is 30 mL/g Na-ETS-10 or 1.24 mmol/g Na-ETS-10. Based on GC-TCD analysis, the desorbed gas consisted of 88% C_2H_4 and 12% C_2H_6 which is equal to the reported data elsewhere [9].

A comparison of the temperature profiles for microwave heating and conductive heating is provided in Figure 8-2(a). The temperature profile of microwave heating shows a steep heating rate of 64 °C/min compared to only 13 °C/min for conductive heating. The difference in heating duration is because heating was stopped when gas evolution stopped.

The two heating techniques were also compared by power consumption as function of temperature in Figure 8-2(b). During microwave heating, power consumption fluctuates between 0-25 W before it stabilizes around 12 W, while temperature becomes stable around 190 °C. During conductive heating, power consumption fluctuates between 0 and 112 W and finally stabilizes around 50 W, which is four times higher than that of microwave heating.

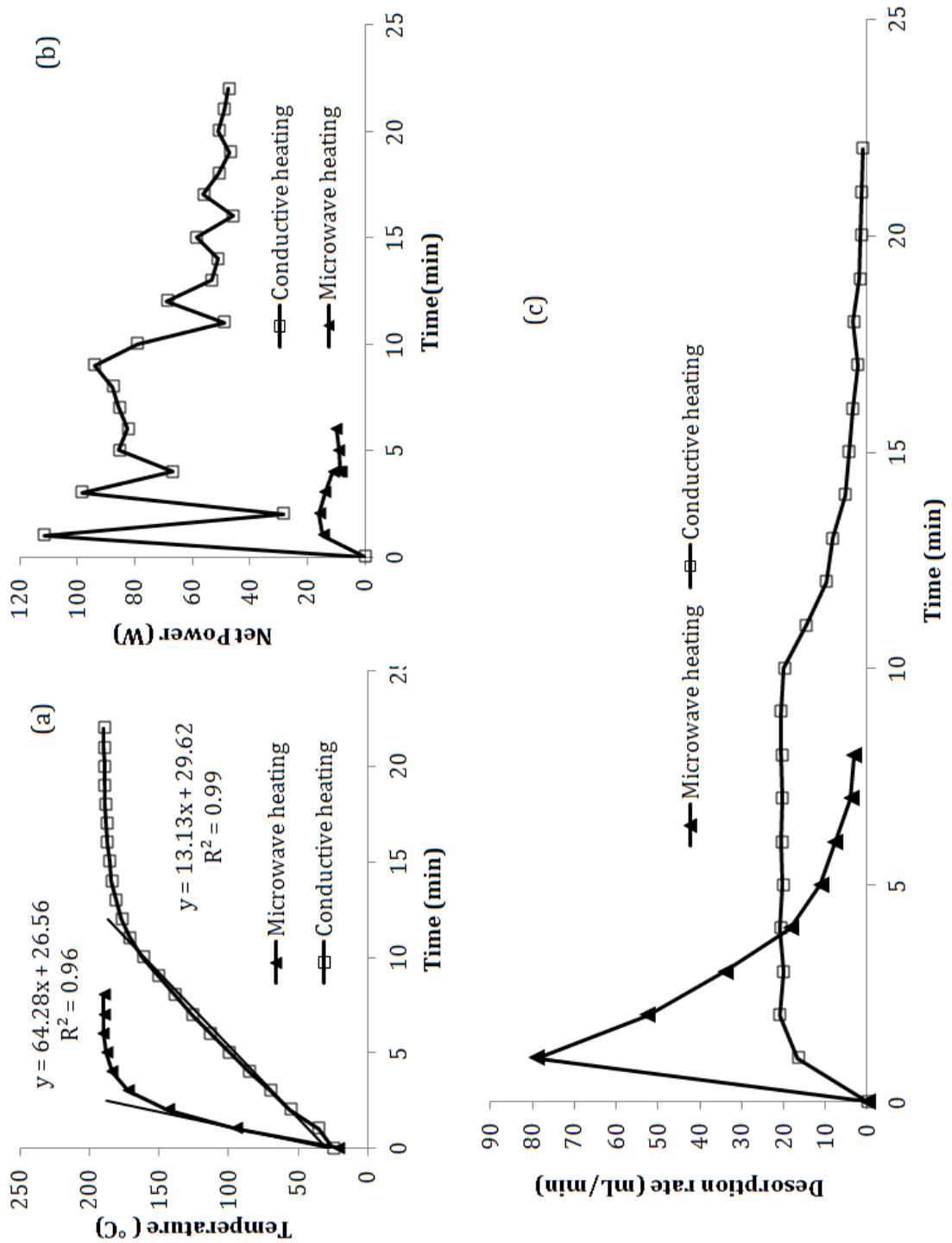


Figure 8-2. Desorption of C_2H_4/C_2H_6 saturated Na-ETS-10 with microwave heating and conductive heating: a) temperature; b) net power consumption; and c) desorption rate.

The comparison of desorption rates of adsorbed C_2H_4/C_2H_6 during microwave heating and conductive heating is shown in Figure 8-2(c). Although net power requirement is higher for conductive heating, the desorption rate is higher for microwave heating. During microwave regeneration, desorption starts immediately and reaches a maximum rate of 79 mL/min (3.25 mmol/min) within one minute. The rate decreases to 3 mL/min as the temperature stabilizes at 190 °C. In conductive heating on the other hand, desorption starts within the first minute and reaches a maximum rate of 20 mL/min (0.82 mmol/min) during the second minute of heating and maintains it up to the tenth minute. Then the rate decreases as the power decreases until the temperature stabilizes at 190 °C at which point the rate remains at 1 mL/min. Figure 8-2 illustrates that microwave heating performs better and quicker than conductive heating in terms of heating rate, net energy consumption and gas desorption rate for adsorptive separation of C_2H_4/C_2H_6 .

The microwave desorption took 8 minutes and 28 mL gas was recovered from 1 gram of Na-ETS-10 (1.16 mmol/g). Based on GC-TCD analysis, the desorbed gas contained 87% C_2H_4 and 13% C_2H_6 , which is consistent with adsorbed phase composition data reported elsewhere (Shi et al., 2010). When conductive heating was applied to regenerate the Na-ETS-10 saturated with the C_2H_4/C_2H_6 mixture, it took 22 minutes to evolve 21 mL/g Na-ETS-10 of gas (0.87 mmol/g).

A total of five adsorption/desorption cycles for the C_2H_4/C_2H_6 mixture were completed on Na-ETS-10 for both microwave and conductive heating. No mass loss of the adsorbent was observed after each adsorption-desorption cycles, and the refreshed adsorbent bed has the same weight as the starting adsorbent. A comparison of microwave heating and conductive heating techniques over these five cycles is presented in Figure 8-3 and Table 8-1. The swing capacity of Na-ETS-10 during microwave heating and conductive heating was stable; 1.16 mmol/g Na-ETS-10 and 0.87 mmol/g Na-ETS-10 respectively over five cycles of adsorption/desorption (Figure 8-3). The results indicate that swing capacity of microwave heating is 1.33

times larger than that of conductive heating. The swing capacity also indicates that the adsorption capacity of Na-ETS-10 is not influenced by successive microwave/conductive heating cycles.

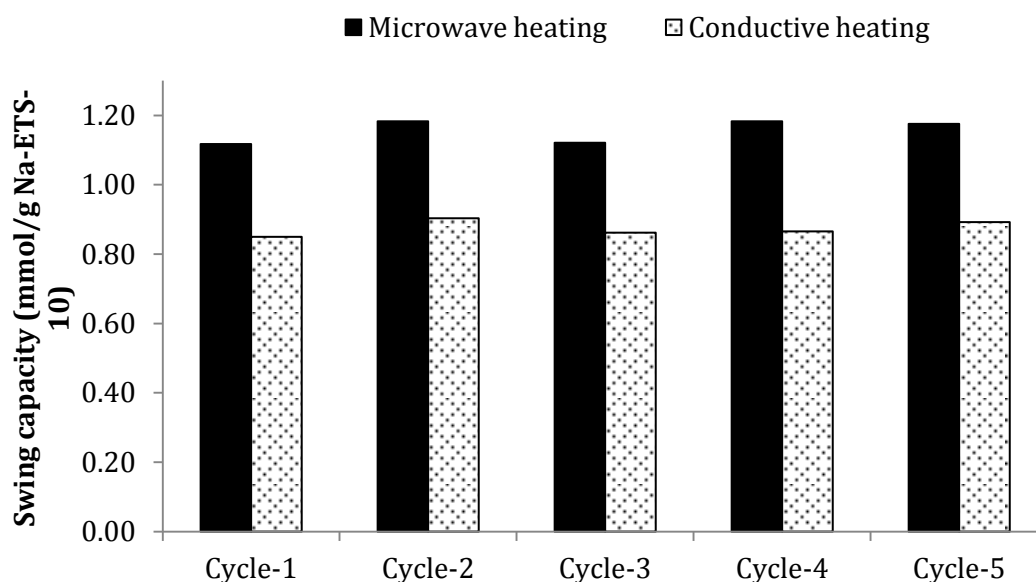


Figure 8-3. Swing capacity of Na-ETS-10 over 5 cycles remains unchanged under microwave heating and conductive heating of C_2H_4/C_2H_6 at $190\text{ }^\circ\text{C}$.

Table 8-1 shows that on average 94% of the adsorbed gas was recovered with microwave desorption while only 71% was recovered with conductive heating. However, with both techniques, the adsorption capacity remained steady over repeated adsorption-regeneration cycles. In microwave desorption, an average net energy of 0.73 kJ/g was consumed to achieve such desorption, however, approximately 7.9 kJ/g was consumed in the case of conductive heating.

Table 8-1. Comparison of microwave and conductive heating techniques for desorbing C₂H₄/C₂H₆ from Na-ETS-10

	Desorption temperature (°C)	Heating time (min)	Cooling time (min)	Gas recovered (%)					Applied energy (kJ/g Na-ETS-10)				
				Cycles					Cycles				
				1	2	3	4	5	1	2	3	4	5
				Microwave heating	190	8	20	90	96	91	96	95	0.7
Conductive heating	190	22	60	69	74	70	71	73	7.6	7.7	8.1	8.1	8.2

Table 8-2. Summary of the desorbed gas purity measured for microwave heating and conductive heating for C₂H₄/C₂H₆

		Purity of the gas recovered (%)				
		Cycles				
		1	2	3	4	5
Microwave Heating	C ₂ H ₄	87.1	87	87.5	87	87.4
	C ₂ H ₆	12.9	13	12.5	13	12.6
Conductive Heating	C ₂ H ₄	85.5	85.1	85	85	85.5
	C ₂ H ₆	14.5	14.9	15	15	14.5

On average, 25 J microwave energy and 370 J conductive energy was needed to desorb 1mL of the adsorbed gas (mixture of ethylene/ethane) in each of the five cycles performed (Figure 8-4). While both systems display steady energy consumption during the five cycles of adsorption and desorption, the conductive heating requires 14.8 times more energy than microwave heating to desorb the same volume of gas. In the conductive heating experiments, the reactor was heated first and then the energy was transferred to the adsorbent through conductive heating. However, in microwave heating, the energy is transferred from the inside to the outside of the material as microwaves propagate through molecular interactions between the material and the electromagnetic field (Das et al., 2009). Hence, more energy loss occurred during the conductive heating, which explains why microwave heating is faster and consumes less energy.

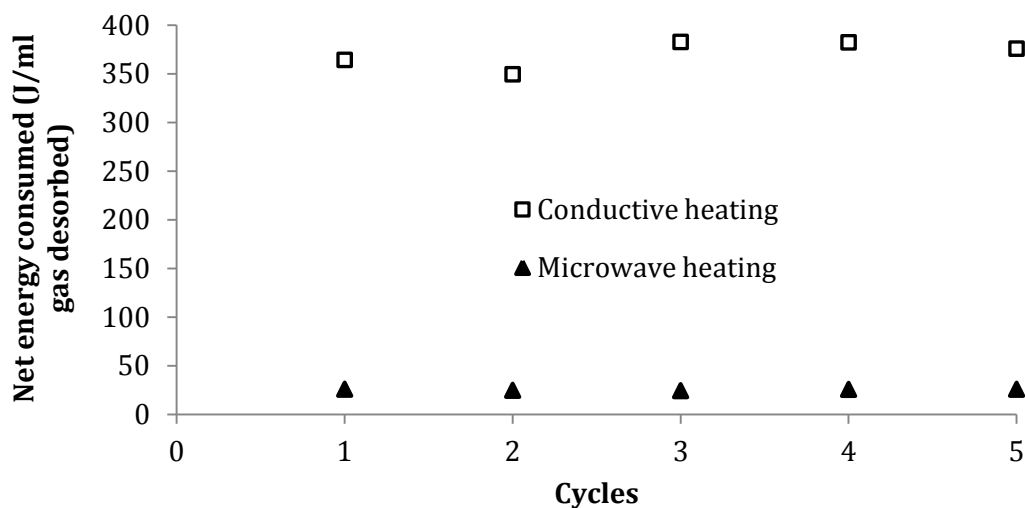


Figure 8-4. Variation in net energy consumption over 5 cycles was insignificant during microwave heating and conductive heating of C_2H_4/C_2H_6 on Na-ETS-10 at 190 °C.

Desorbed gas composition of each cycle was analyzed by GC-TCD which was presented in Table 8-2. It shows that 87~87.5% C₂H₄ and 12.5~13% C₂H₆ could be obtained during the microwave desorption and 85~85.5% C₂H₄ and 14.5~15% C₂H₆ could be obtained during the conductive heating. Both methods gave the similar desorbed gas composition as adsorbed phase gas.

8.4.2 Carbon dioxide/methane (CO₂/CH₄) desorption from Na-ETS-10

Complete (100%) desorption of CO₂/CH₄ from Na-ETS-10 was obtained by water desorption, generating a total of 407 mL of gas from 10 g of Na-ETS-10, indicating a maximum desorption capacity of 39 mL/g. Based on the GC-TCD analysis, the desorbed gas contained 89% CO₂ and 11% CH₄.

Comparisons of temperature profile, power consumption profile and desorption rate of adsorbed CO₂/CH₄ for both methods are shown in Figure 8-5. For microwave heating, power consumption fluctuated between 0-20 W and stabilized around 12 W while temperature stabilized at 190 °C. For conductive heating power consumption fluctuated between 0-101 W and stabilized around 44 W. Desorption rate for conductive heating is slower than for microwave heating and also net power requirement is higher. Desorption rate during microwave heating reached a maximum of 100 mL/min in the first minute then decreased reaching close to zero at the eighth minute. During conductive heating, the desorption rate reached a maximum of 26 mL/min in the seventh minute, remained constant up to the tenth minute and then decreased and stabilized at 1 mL/min at twenty second minute of heating time. Figure 8-5 illustrates that microwave heating is more efficient and faster than conductive heating in terms of heating rate, net energy consumption and gas desorption rate for adsorptive separation of CO₂/CH₄.

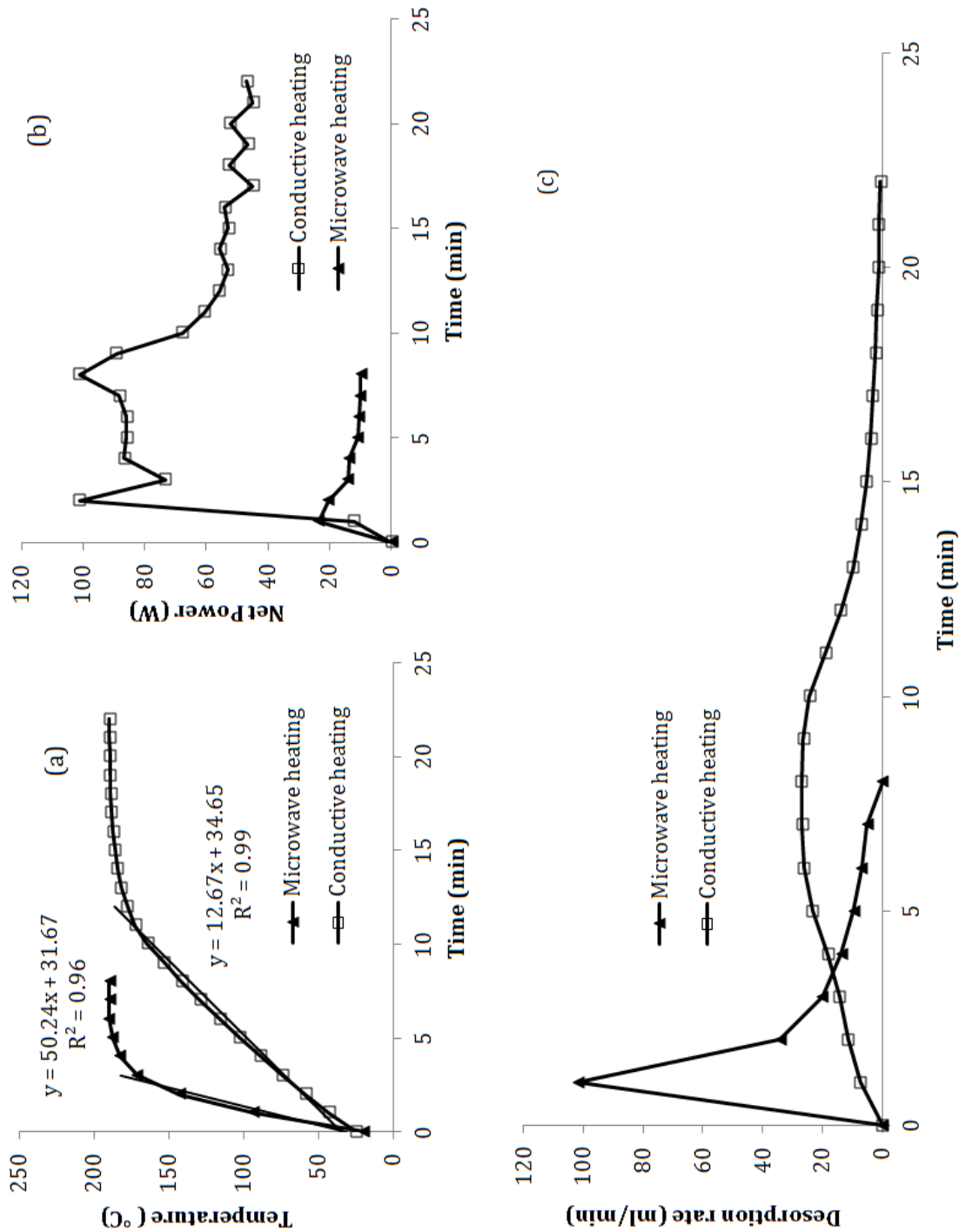


Figure 8-5. Desorption of CO₂/CH₄ saturated Na-ETS-10 with microwave heating and conductive heating: a) temperature; b) net power consumption; and c) desorption rate.

Microwave heating was successful in desorbing CO₂/CH₄ mixture from Na-ETS-10. 27 mL of desorbed gas per gram of Na-ETS-10 was recovered after 8 minutes of microwave heating. The desorbed gas consisted of 82% CO₂ and 18% CH₄ as determined by GC-TCD analysis. After heating, the bed was cooled under N₂ flow at 120 mL/min. Regeneration of CO₂/CH₄ saturated Na-ETS-10 with conductive heating took 22 minutes to evolve 22 mL/g of gas.

A total of five adsorption/desorption cycles for the CO₂/CH₄ mixture were completed on Na-ETS-10 for both microwave and conductive heating. A comparison of microwave heating and conductive heating over 5 cycles is presented in Figure 8-6 and Table 8-3.

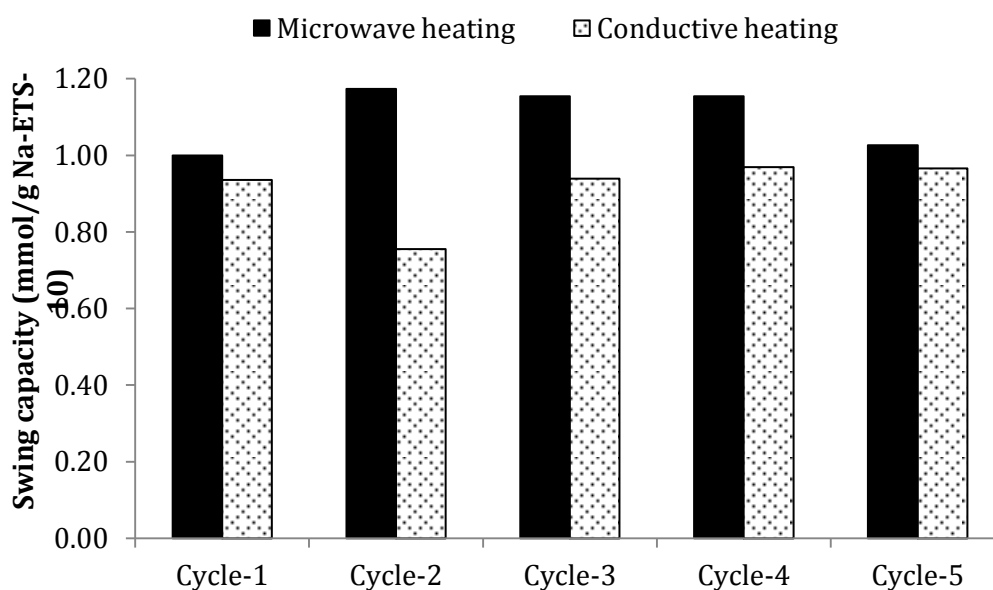


Figure 8-6. Swing capacity of Na-ETS-10 over 5 cycles remains unchanged under microwave heating and conductive heating of CO₂/CH₄ at 190 °C.

Based on the gas being recovered, the swing capacity of Na-ETS-10 over 5 adsorption-desorption cycles during microwave heating and conductive heating were stable around 1.10 mmol/g Na-ETS-10 and 0.91 mmol/g Na-ETS-10 (Figure 8-6). Figure 8-6 illustrates that the adsorption capacity of Na-ETS-10 was unchanged

during both microwave heating and conductive heating. The results also indicate that swing capacity of microwave is 1.21 times larger than that of conductive heating.

Table 8-3 shows that 70% of the adsorbed CO₂/CH₄ was recovered by microwave heating while only 57% by conductive heating. In microwave desorption, an average net energy of 0.67 kJ/g was consumed to achieve such desorption, however, approximately 7.7 kJ/g was consumed in the case of conductive heating.

On average 25 J of microwave energy and 348 J of conductive energy are needed to release 1 mL of gas adsorbed on Na-ETS-10. Throughout the five adsorption-regeneration cycles, conductive heating requires 14 times more energy than microwave heating in order to desorb the same volume of gas. The higher energy requirement in conductive heating is due to high heat loss as discussed in section 7.3.1. Figure 8-7 illustrates the consistency in energy consumption over 5 cycles of CO₂/CH₄ desorption for microwave heating and conductive heating.

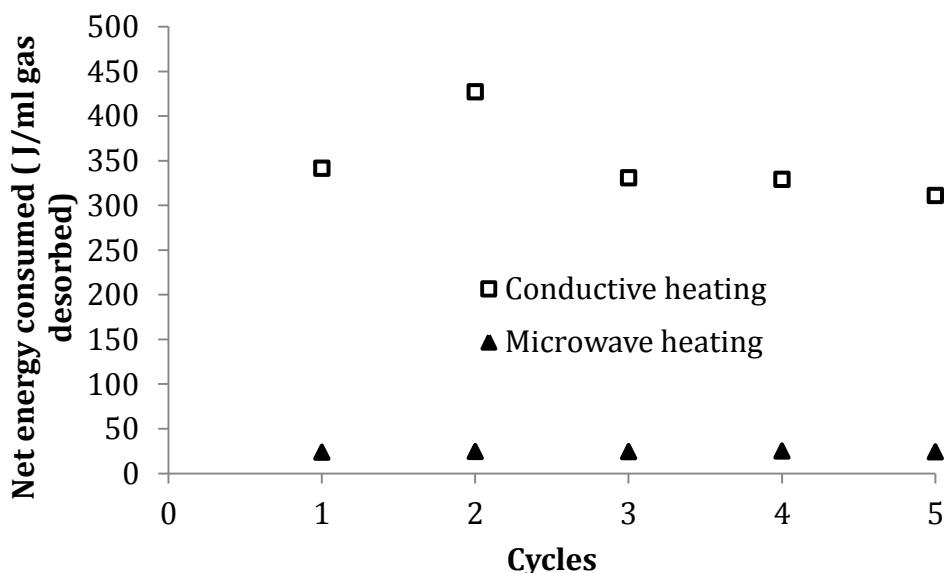


Figure 8-7. Variation in net energy consumption over 5 cycles was insignificant during microwave heating and conductive heating of CO₂/CH₄ on Na-ETS-10.

Table 8-3. Comparison of microwave and conductive heating techniques for desorbing CO₂/CH₄ from Na-ETS-10

	Desorption temperature (°C)	Heating time (min)	Cooling time (min)	Gas recovered (%)					Applied energy (kJ/g Na-ETS-10)				
				Cycles					Cycles				
				1	2	3	4	5	1	2	3	4	5
Microwave heating	190	8	20	63	74	73	73	65	0.6	0.7	0.7	0.7	0.6
Conductive heating	190	22	60	59	47	59	61	60	7.8	7.9	7.6	7.8	7.3

Table 8-4. Summary of the desorbed gas purity measured for microwave heating and conductive heating for CO₂/CH₄

		Purity of the gas recovered (%)				
		Cycles				
		1	2	3	4	5
Microwave Heating	CO ₂	82.1	83	82	82.5	82.7
	CH ₄	17.9	17	18	17.5	17.3
Conductive Heating	CO ₂	81.3	81	81.8	81	81.5
	CH ₄	18.7	19	18.2	19	18.5

Table 8-4 summarizes the purity of the recovered CO₂/CH₄ gas for these two heating techniques over five cycles of adsorption/desorption. Based on GC-TCD analysis, the purity of the gas desorbed by microwave heating consisted of 82~83% CO₂ and 17~18% CH₄ while the purity of the gas desorbed by conductive heating contained 81~81.8 % CO₂ and 18~19% CH₄.

Comparing these two different binary systems (C₂H₄/C₂H₆, CO₂/CH₄), the recovery percentage of C₂H₄/C₂H₆ was higher than CO₂/CH₄. In C₂H₄/C₂H₆ separation system, the adsorbed phase is highly enriched C₂H₄ which has a polarizability of $42.52 \times 10^{-25} \text{ cm}^3$, while in CO₂/CH₄ separation system, the adsorbed phase is highly enriched CO₂ which has a polarizability of $29.11 \times 10^{-25} \text{ cm}^3$ [28]. Considering in the case of physical adsorption, the adsorbed phase is in a liquid-like phase [29], so the adsorbed C₂H₄ consumed the microwave more efficiently than CO₂. By supplying the same amount of microwave energy, a higher recovery rate could be obtained in C₂H₄/C₂H₆ separation system.

8.5 Conclusions

In this work, two binary gas mixtures C₂H₄/C₂H₆ (59:41) and CO₂/CH₄ (10:90) were separated by adsorption on Na-ETS-10 at 22 °C and 101.325 kPa. Na-ETS-10 was regenerated using microwave and conductive heating desorption and the desorbed gas was collected. Results show that microwave desorption can regenerate Na-ETS-10 more efficiently than conventional temperature swing regeneration such as conductive heating. Swing capacity achieved in microwave heating is higher than that of conductive heating. For both heating techniques swing capacity is not affected by successive heating cycles. During microwave desorption, 94% of the adsorbed C₂H₄/C₂H₆ and 71% of the adsorbed CO₂/CH₄ mixture were recovered. On the other hand, during desorption with conductive heating, 71.4% C₂H₄/C₂H₆ and 57.2%

CO₂/CH₄ were recovered. Microwave desorption required an average of 0.7 kJ/g Na-ETS-10 during 8 minutes of heating while conductive heating required 7.7~7.9 kJ/g Na-ETS-10 during 22 minutes of heating. Results show that microwave desorption is characterized by faster heating, higher desorption rate, and lower energy consumption compared to desorption with conductive heating. Therefore, microwave heating can potentially be used as a cheaper energy source to regenerate Na-ETS-10 for adsorptive separation of binary gas mixtures such as C₂H₄/C₂H₆ and CO₂/CH₄.

The regeneration results can be further improved by using a sweep gas that can purge the adsorbent bed during heating. Using steam as purge gas can be a practical approach to enhance the heating both during microwave heating and conductive heating. Another approach can be using previously recovered C₂H₄/CO₂ to ensure purging without diluting the product gas. It is expected that using C₂H₄/CO₂ as purge gas would speed up the desorption process and would improve heating and therefore, requires further investigation.

8.6 References

- [1] Kniel, L., Winter, O., Stork, K., 1980. *Ethylene: Keystone to the Petrochemical Industry*, first ed. M. Dekker, New York.
- [2] Eldrige, R.B., 1993. *Industrial and Engineering Chemistry research* 32, 2208-2212.
- [3] Shi, M., Avila, A.M., Yang, F., Kuznicki, T.M., Kuznicki, S.M., 2011. *Chemical Engineering Science* 66, 2817-2822.
- [4] Cavenati, S., Grande, C.A., Rodrigues, A.E., 2004. *Journal of Chemical and Engineering Data* 49, 1095-1101.
- [5] Cavenati, S., Grande, C.A., Rodrigues, A.E., 2006. *Energy and Fuels* 20, 2648-2659.
- [6] Rao, A.B., Rubin, E.S., 2002. *Environmental Science and Technology* 36, 4467-4475.
- [7] Anson, A., Lin, C.C.H., Kuznicki, S.M., Sawada, J.A., 2009. *Chemical Engineering Science* 64, 3683-3687.
- [8] Anson, A., Wang, Y., Lin, C., Kuznicki, T.M., Kuznicki, S.M., 2008. *Chemical Engineering Science* 63, 4171-4175.
- [9] Shi, M., Lin, C.C.H., Kuznicki, T.M., Hashisho, Z., Kuznicki, S.M., 2010. *Chemical Engineering Science* 65, 3494-3498.
- [10] Kuznicki, S.M., 1991. *Large pored crystalline titanium molecular sieve zeolite*. US Patent No. 5, 011, 591.
- [11] Anderson, M.W., Terasaki, O., Ohsuna, T., Philippou, A., Mackay, S.P., Ferreira, A., Rocha, J., Lidin, S., 1994. *Nature* 367, 347-351.

- [12] Al-Baghli, N.A., Loughlin, K.F., 2005. *Journal of Chemical Engineering Data* 50, 843-848.
- [13] Roussy, G., Chenot, P., 1981. *Journal of Physical Chemistry* 85, 2199-2203.
- [14] Roussy, G., Juulalian, A., Charreyre, M., Thiebaut, J., 1984. *Journal of Physical Chemistry* 88, 5702-5708.
- [15] Tierney, J.P., Lidström, P., 2005. *Theoretical Aspects of Microwave dielectric heating: Microwave Assisted Organic Synthesis*, first ed. Blackwell Publishing, Oxford.
- [16] Das, S., Mukhopadhyay, A.K., Datta, S., Basu, D., 2009. *Bulletin of Material Science* 32, 1-13.
- [17] Reuß, J., Bathen, D., Schmidt-Traub, H., 2002. *Chemical Engineering and Technology* 25, 381-384.
- [18] Turner, M.D., Laurence, R.L., Conner, W.C., Yngvesson, K.S., 2000. *AIChE Journal* 46, 758-768.
- [19] Ohgushi, T., Komarneni, S., Bhalla, A.S., 2001. *Journal of Porous Materials* 8, 23-35.
- [20] Ohgushi, T., Nagae, M., 2003. *Journal of Porous Materials* 10, 139-143.
- [21] Ohgushi, T., Nagae, M., 2005. *Journal of Porous Materials* 12, 265-271.
- [22] Clause, M., Bonjour, J., Meunier, F., 2004. *Chemical Engineering Science* 59, 3657-3670.
- [23] Merel, J., Clause, M., Meunier, F., 2006. *Environmental Progress* 25, 327-333.
- [24] Siriwardane, R.V., Shen, M.S., Fisher, E.P., 2005. *Energy and Fuels* 19, 1153-1159.

- [25] Ruthven, D.M., 1984. *Principles of Adsorption and Adsorption Process*, first ed. J. Willy, New York.
- [26] Suzuki, M., 1990. *Adsorption Engineering*, first ed. Elsevier, Amsterdam.
- [27] Cherbanski, R., Komorowska-Durka, M., Stefanidis, G.D., Stankiewicz, A., 2011. *Industrial and Engineering Chemistry Research* 50, 8632-8644.
- [28] Li, J., Kuppler, R.J., Zhou, H., 2009. *Chemical Society Reviews* 28, 1477-1504.
- [29] Myers, A. L., Prausnitz, J.M., 1965. *AIChE Journal* 11, 121-127.

Chapter 9

Conclusions and Recommendations

9.1 Conclusions

Compared with the traditional cryogenic distillation process, adsorptive separation of gases is a viable alternative with a considerably lower energy requirement. In this dissertation, application of titanosilicate molecular sieve ETS-10 in different gas separation systems were demonstrated and evaluated, such as production of argon free oxygen from air, separation of ethylene and ethane at high pressure, extraction of ethane from natural gas at high pressure and removal of CO₂ from natural gas. We have found that ETS-10 is a promising adsorbent for the different adsorptive separation systems mentioned above.

Air separation has been used in industry for decades however, the purity of the oxygen produced is still limited at around 95%. It is still a challenge to produce argon free oxygen through adsorptive separation. In chapter three, adsorption measurements demonstrate that Ag-ETS-10 is selective for argon over oxygen and nitrogen over oxygen. Production of argon free oxygen has been achieved by Ag-ETS-10 through one-stage lab-scale demonstration. 99+% purity of oxygen has been produced and a recovery rate of 30% was reached at ambient condition. This suggests that Ag-ETS-10 could be an effective adsorbent in a PSA system designed for generating high purity O₂.

In chapter four the mathematical model that we designed predicts that enhancing the Ag-ETS-10 bed density will increase the recovery rate of oxygen in the air separation system. Two methods were used to increase the bed density: by changing the synthesis conditions high density Ag-ETS-10 could be produced; by packing the bed with different size granules increasing its bulk density. Through these two improvements, Ag-ETS-10 bed density could be increased by 34%. Using such high density Ag-ETS-10 we were able to demonstrate in one-stage lab-scale demonstration the production of argon free oxygen of 99+% purity with a recovery rate approaching

40% at ambient condition. This suggests that Ag-ETS-10 with enhanced density could improve the performance of generating high purity O₂.

Separation of ethylene and ethane and extraction of ethane from natural gas using adsorptive separation have been widely studied and reported. However such separations at high pressure were rarely reported before. To the best of our knowledge no investigation of separation by titanolate molecular sieve zeolites at high pressure has been reported. In chapter five, we demonstrate that Na-ETS-10 can be used as an effective adsorptive material to separate ethylene from ethane in a binary mixture under high-pressure conditions. A 59/41 mixture of C₂H₄ and C₂H₆ was separated on Na-ETS-10 at 360 psi and 298 K over a pressure range of 101-2580 kPa. At the highest pressure tested (2580 kPa) an ethylene/ethane bed selectivity of ~11 was achieved, which is more than double the previously reported selectivity (S = 5) under low pressure. Although these are laboratory-scale results the potential use of Na-ETS-10 as an adsorbent that allows efficient separation of olefin/paraffin at industrial stream pressures is very promising and requires further investigation.

In chapter six, the separation of ethane from methane was achieved using a Na-ETS-10 adsorbent at pressures approximating natural gas pipeline pressures (up to 5600 kPa). A packed-bed Na-ETS-10 adsorbent column was used to split a 93/7 methane/ethane gas mixture into a raffinate stream composed of ethane-free methane and an extract stream containing 75% ethane. The extract composition was virtually independent of the packed-bed column pressure (0-5600 kPa). The Na-ETS-10 adsorbent was also able to separate the components of a synthetic natural gas mixture (90.99 CH₄: 5.60 C₂H₆: 1.63 C₃H₈: 0.69 CO₂: 0.50 N₂: 0.49 C₄H₁₀: 0.10 C₅H₁₂) at high pressure. The breakthrough profile for this separation showed three distinct zones based on outlet composition: C1, C1/C2, and C1/C2/C3. We propose that these zones could be treated as separate raffinate streams that could also be recycled into appropriate nodes of the natural gas treatment process. The adsorbed phase could be recovered as an extract stream enriched in larger and more valuable hydrocarbons

including propane, butane, isobutene and pentane. Taken together, these results indicate that ethane can be extracted from natural gas feedstocks at pipeline pressures up to 5600 kPa by selective adsorption on an ETS-10-type material.

In chapter seven, the possibility of using ETS-10 to remove CO₂ from a binary mixture (90%CH₄-10%CO₂) was examined at ambient conditions. Inverse phase gas chromatography and volumetric isotherm measurements indicate that Na-ETS-10 possesses a strong adsorptive selectivity (up to 300) for carbon dioxide over methane. Elution chromatography shows that the heats of adsorption at zero loading for carbon dioxide and methane on Na-ETS-10 are 37 kJ/mol and 25 kJ/mol respectively. A packed-bed of Na-ETS-10 adsorbent column was used to split a 90/10 methane/carbon dioxide gas mixture into a raffinate stream composed of pure methane and an extract stream containing 91% CO₂. Desorbed gas analysis shows that Na-ETS-10 possesses a binary bed selectivity for carbon dioxide over methane of approximately 91. These results together indicate that Na-ETS-10 is a good adsorbent candidate for removal of CO₂ from a 90%CH₄-10% CO₂ mixture system.

The data reported in chapter five to seven shows there is a strong affinity between ethylene or CO₂ and ETS-10 adsorbent, which illustrated by a high heat of adsorption for ethylene and CO₂ on ETS-10. Following adsorption it becomes necessary to find an efficient method for the regeneration of the ETS-10 adsorbent. In chapter eight, two binary gas mixtures C₂H₄/C₂H₆ (59:41) and CO₂/CH₄ (10:90) were separated by adsorption on Na-ETS-10 at ambient conditions. Na-ETS-10 was regenerated using microwave and conductive heating desorption and the desorbed gas was collected. Results show that microwave desorption can regenerate Na-ETS-10 more efficiently than conventional temperature swing regeneration such as conductive heating. Microwave desorption is characterized by faster heating, higher desorption rate, and lower energy consumption compared to desorption with conductive heating. Therefore, microwave heating can potentially be used as a cheaper energy source to regenerate Na-ETS-10 for adsorptive separation of binary gas mixtures such as

C_2H_4/C_2H_6 and CO_2/CH_4 .

9.2 Recommendations

9.2.1 *Materials Aspect*

In chapter three and four, Ag-ETS-10 has been demonstrated to separate air and produce argon free oxygen. A simple three times silver ion exchange was preferred as an ion exchange standard. It is important to continue studying the silver ion exchange isotherm on ETS-10, in order to understand the capacity of Ag cation on ETS-10 and reduce the usage of the silver nitrate during the ion exchange procedure. Furthermore, finding a balance between the Ag loading and the optimal separation performance requires future studies.

ETS-10, as a mixed coordinate titanium silicate zeolite molecular sieve, has been demonstrated to efficiently separate ethane and ethylene, ethane and methane, CO_2 and methane. This opens up the possibility of using materials of similar structure and framework, such as ETAS-10 and vanadium silicate, in the same gas separation systems mentioned above.

ETAS-10 was invented by Kuznicki in 1990, and is a crystalline titanium-aluminum-silicate molecular sieve with a large pore size of approximately 9 Å units, having both aluminum and titanium in the framework structure. Although ETAS-10 is structurally related to ETS-10, the substantial quantities of highly polar mono-charged tetrahedral aluminum sites profoundly change the character of the sieve, and impact the adsorptive properties of the material. The incorporation of aluminum expands the lattice planes and pore openings. This in turn allows ETAS-10 to adsorb molecules somewhat larger than those adsorbed by ETS-10. Additionally, ETAS-10 is a stronger sorbent than ETS-10 [1]. These differences between ETAS-10 and ETS-10 would enable these materials to perform differently in applications such as separation

of ethylene and ethane, ethane and methane, CO₂ and methane, or even larger hydrocarbon gas mixture.

Another new class of microporous materials, vanadium silicates was reported after ETS-10 invention. In 1997, Rocha reported the first example of a large-pore vanadium silicate containing stoichiometric amounts of hexacoordinate vanadium (Si/V=5) [2]. This material, dubbed AM-6, is a structural analogue of titanium silicate ETS-10, where titanium has been fully replaced by vanadium. It is also possible to replace titanium with other transition metals such as Zirconium. Because of the different physical and chemical properties of these transition metals, a difference in adsorptive properties of the respective ETS-10 analogues is expected. There is little information in the literature on adsorption of vanadium silicate and zirconium silicate, so investigation on this area is a worthwhile effort that might produce interesting results.

9.2.2 Process Aspect

All the suggestions above are related to improvements on the material side. Future work should focus more the process aspect as well. All the experiments in this dissertation were carried out by one stage separation unit. If a two bed PSA process or a VSA process could be applied, it will be very helpful for practical application. At the same time diffusion simulation work will be also valuable for a real separation unit design. Future studies on mass balance and energy balance of the system could help to better understand the separation systems.

9.3 References

- [1] Kuznicki, S.M., Thrush, K.A., 1993. *Large-pored molecular sieves with charged octahedral titanium and charged tetrahedral aluminum sites*, US Patent No. 5,244,650.

- [2] Rocha, J. Brandao, P. Lin, Z., Anderson, M.W., Alfredsson, V., Terasaki, O., 1997. *Angewandte Chemie International Edition* 36, 100-102.